OUKA
The University of Osaka
Institutional Knowledge Archive

Title	Theoretical studies on CP violation in a two Higgs doublet model toward electroweak baryogenesis
Author(s)	久保田, 充紀
Citation	大阪大学, 2021, 博士論文
Version Type	VoR
URL	https://doi.org/10.18910/82002
rights	
Note	

The University of Osaka Institutional Knowledge Archive : OUKA

https://ir.library.osaka-u.ac.jp/

The University of Osaka

Ph. D. thesis

Theoretical studies on CP violation in a two Higgs doublet model toward electroweak baryogenesis

Mitsunori Kubota

Department of Physics, Osaka University

February 28, 2021

Abstract

In this thesis, we investigate the aligned two Higgs doublet model which has the CP-violating phases both in the Higgs potential and the Yukawa interaction as a concrete example for the electroweak baryogenesis. The Yukawa interaction terms are aligned to avoid flavor changing neutral currents at tree level, and the Higgs potential is also aligned such that the coupling constants of the lightest Higgs boson with the mass of 125 GeV to the standard model particles are the same as those of the standard model at tree level. We find that in this model effects on the EDM from the two sources of CP violation can be destructive, and consequently their total contribution can satisfy the EDM data even when each CP-violating phase is $\mathcal{O}(1)$. Stability of this kind of scenario is confirmed by using a renormalization-group-equation analysis. Such a large CP-violating phase can be tested at collider experiments even when the EDM data are satisfied. In particular, in the CP-violating model with the alignment, the collider phenomenology of the additional Higgs bosons play a role to test CP violation. We focus on the decay of the additional neutral Higgs boson into a tau lepton pair. By performing the simulation of production and decays of the additional Higgs bosons at future electron positron colliders, we investigate the angular distributions of hadronic decay products from the tau leptons. As the result of the analysis of the signal and the background, we find that the scenario with a finite CP-violating phase of the lepton Yukawa sector satisfying the EDM data can be distinguished from those without the CP-violating phase at the International Linear Collider with the consideration of the several plans of collision energies.

Acknowledgement

I would like to express my sincere gratitude to my supervisor, Prof. Shinya Kanemura for providing me a lot of instruction to research of particle physics. I am much obliged to Prof. Mayumi Aoki, Prof. Kei Yagyu, Dr. Hashino Katsuya and Mr. Daiki Kaneko for the fruitful collaborations. I would like to appreciate Prof. Tetsuya Onogi, Prof. Hajime Nanjo, Prof. Kinya Oda and Prof. Minoru Tanaka for the careful reading of my thesis. I am also grateful to faculty members of Particle Physics Theory group of Osaka university, Prof. Koji Hashimoto, Prof. Satoshi Yamaguchi, Prof. Hidenori Fukaya, Prof. Norihiro Iizuka and Prof. Yutaka Hosotani. I also thank to colleagues of the laboratory, Mr. Tetsuya Akutagawa, Mr. Toshihiro Ota, Mr. Masashi Aikou, Mr. Kazuki Enomoto and Mr. Masanori Tanaka.

Contents

1 Introduction **5**
- 1.1 Overview . . . 5
  - 1.1.1 Baryogenesis . . . 5
  - 1.1.2 Sakharov's conditions . . . 6
  - 1.1.3 Electroweak baryogenesis . . . 6
  - 1.1.4 Our reserches . . . 8
- 1.2 Oganaization . . . 9

2 Review of the standard model **10**
- 2.1 Higgs sector of the SM . . . 10
- 2.2 Kobayashi-Maskawa phase . . . 12
- 2.3 Elwctroweak baryogenesis in the SM . . . 13

3 CP violating observable **17**
- 3.1 Electric dipole moment data . . . 17
  - 3.1.1 Definition of the EDM . . . 17
  - 3.1.2 Current bound . . . 19
  - 3.1.3 Barr-Zee type contributions . . . 19
- 3.2 Angular distribution . . . 20

4 Aligned two Higgs doublet model **26**
- 4.1 Lagrangian . . . 27
  - 4.1.1 Higgs potential . . . 27
  - 4.1.2 Yukawa interaction term . . . 29
  - 4.1.3 Kinetic term of the scalar fields . . . 31
  - 4.1.4 Theoretical and experimental constraints . . . 31
- 4.2 Scenario cancelling the electric dipole moment . . . 32
  - 4.2.1 Constraint from the electric dipole moment data . . . 32
  - 4.2.2 Destructive interference between the Barr-Zee type contributions 33

4.2.3 Numerical analysis for the aligned two Higgs doublet model . . 34
4.2.4 Future experiment for the electric dipole moment 37
4.3 Renormalization group equation analysis 37
4.4 Collider signals 39
4.4.1 Production of the extra Higgs bosons 40
4.4.2 Decay of the extra Higgs bosons 42
4.4.3 Angular distribution 43
4.5 Simulation studies at future lepton colliders 46

5 Summary **56**
5.1 Conclusion 56
5.2 Future prospects 57
5.3 My contributions in the original papers 57

A Parameters of the scalar potential: relations between two bases **59**

B Exact formulae of the Barr-Zee type contributions **60**

C Decay of the heavy Higgs bosons **62**

D Beta functions **64**

E Other scenarios **67**

F Description for a spin of fermions **74**
F.1 Notation and convention 74
F.2 Solution of the Dirac equation 75

Chapter 1

Introduction

1.1 Overview

The standard model (SM) is successful in explaining the experimental data of the particle physics. In particular, by the discovery of the Higgs boson which are the last particle predicted[1, 2], the SM has been established as an effective theory for low energy scales below $\mathcal{O}(100)$ GeV. However, the dynamics behind the electroweak symmetry breaking is still unknown, and some phenomenological problems remain unsolved. For example, the SM do not have the mechanism getting the tiny neutrino mass and the candidate explaining the dark matter abundance. In addition, there are the problem of the baryon asymmetry of the Universe which cannot be realized in the framework of the SM.

The existence of these beyond the SM phenomena indicates that the SM should be replaced by more fundamental theory. However, it is difficult to treat these problems at the same time. In this thesis, we propose the one possibility of the effective theory for more higher scales by focusing the baryon asymmetry of the Universe.

1.1.1 Baryogenesis

The baryon asymmetry of the Universe is characterized by

$$\eta = \frac{n_b - n_{\bar{b}}}{n_\gamma}, \tag{1.1}$$

where n_b ($n_{\bar{b}}$) and n_γ are the number densities of the baryon (anti-baryon) and photon, respectively. This can be determined by the big-bang nucleosynthesis. The abundances of the light atomic nucleus, for example, ^{3}He, ^{4}He, D and ^{7}Li can be predicted once η is fixed. By these abundances observed by the cosmological experiments, the ratio

η is given as 5.8-6.5 $\times$ 10^{-10} (95% confidence level (CL))[3]. In addition, η can be independently determined by the cosmic microwave background. The energy density of the baryon affects the temperature fluctuations of the cosmic microwave background. By the observed energy density of the baryon, η is given as $(6.105 \pm 0.055) \times 10^{-10}$ (95% CL)[3] which is consistent with the value given by the abundances of the light atomic nucleus. It is shown us that when the inflation is considered in the early universe, η is needed to be given as $\mathcal{O}(10^{-10})$ from the baryon symmetric universe before the big-bang nucleosynthesis.

1.1.2 Sakharov's conditions

In order to create the baryon asymmetry from baryon symmetric early universe, the theory is required to satisfy the Sakharov's three conditions[4] which are given as

1. Baryon number violation,
2. C and CP violation,
3. Departure from thermal equilibrium.

The first condition is trivially required. The second one is needed in order to avoid the cancellation between the process increasing the baryon number and the process correspond to the transformed one by the C or CP transformation, which decrease the baryon number. Finally, in the theory in which the third condition is not satisfied, even if the first and second one are satisfied, the net number of the baryon number is washed out in the equilibrium by the inverses processes of the baryon number creating processes.

1.1.3 Electroweak baryogenesis

So far, the scenarios which satisfy the Sakharov's conditions are proposed to solve the baryon asymmetry problem. For example, there are the baryogenesis in the framework of the grand unification theory[5, 6], the leptogenesis[7], the electroweak baryogenesis[8] and so on. The electroweak baryogenesis satisfies the Sakharov's conditions as

1. Sphaleron process,
2. Weak interaction and CP violating phase,
3. First order electroweak phase transition.

The sphaleron transition rate which can change the baryon number is enhanced in the high temperature universe. The C symmetry is violated by weak interaction, and when the CP violating phase is finite in the theory, CP symmetry is not respected. If the electroweak phase transition is first order, the departure from equilibrium of the sphaleron process can be realized. The SM can qualitatively realize the electroweak baryogenesis scenario. However, the experimental results show that the Kobayashi-

Maskawa phase[9] cannot realize the observed baryon number asymmetry if electroweak phase transition is first order[10], and the first order electroweak phase transition cannot occur with the observed Higgs mass[11]

The electroweak baryogenesis scenario is closely related to the structure of the Higgs sector which involve the electroweak scale phenomena, while in the other scenarios such a leptogenesis, the typical energy scale is usually much higher than it. Therefore, it is interesting that the electroweak baryogenesis scenario might be tested by experiments in near future. In order to realize electroweak baryogenesis, the Higgs sector of the SM is needed to be extended so that the first order phase transition occur and also the new CP violating phase is needed to be introduced with sufficient value for the observed baryon asymmetry of the universe. So far, the electroweak baryogenesis scenarios in various extended Higgs models have been discussed. For example, there are the models which are composed of the SM contents and the additional scalar of the isospin singlet[12, 13, 14], doublets[15, 16, 17, 18, 19, 20, 21], triplets[22, 23] and so on.

The scenario of electroweak baryogenesis generally have distinguishable characteristics, which provide important clues for testing the scenario. The strong first-order phase transition is strongly associated with the Higgs 3-point coupling and leads its stronger coupling than the SM[24], for example, the multi-Higgs doublet model is discussed in Ref.[25]. The couplings may be measured at future collider experiments such as the high-luminosity upgrade of the Large Hadron Collider (HL-LHC) [26] and the International Linear Collider (ILC) [27, 28]. In addition, the strong first-order phase transitions may leave traces as background gravitational waves. Testing its spectrum with future space gravitational wave interferometers such as LISA[29], DECIGO[30] and BBO[31] have been studied[32, 33, 34, 35, 36, 37, 38, 39, 40].

The CP violation in the extended Higgs sector as the ingredient for baryogenesis which can be searched by electric dipole moment experiments[41, 42, 43, 44, 45, 46, 47, 48, 49] is also important characteristic. The high energy collider experiments are also important in which the couplings of ZZZ, ZWW[50, 51], and hff[52, 53, 54] can be tested by precisely measuring the deviation from the prediction of the SM. Many other methods have been studied[55, 56, 57, 58, 59]. In addition, CP violation in the extended Higgs sector can be also tested by measuring the angular distribution of SM-like Higgs boson decay and additional Higgs boson decays[60, 61, 62, 63, 64, 65, 66, 67]. However, the phase of the additional CP violation is strongly constrained by the EDM data which make it generally difficult to get a sufficient value of CP violating phase for baryogenesis. On the other hand, in recent years, 125 GeV Higgs bosons have been studied in some cases in which it is difficult to distinguish them from SM Higgs bosons due to alignment of the model[68]. Knowing the nature of such Higgs bosons is also important for testing CP violation.

1.1.4 Our reserches

The physics contents of this thesis is based on the two papers [69] and [70]. In the following, we shortly introduce the physics results of these papers.

In our work[69], we discussed the extended Higgs sector, which has multiple phases of CP violation. We investigated the possibility of scenarios in which each CP-violating phase has $\mathcal{O}(1)$, while those contributes to the EDM are in the destructive interference. As a simple example, we have focused on the two Higgs doublet model (THDM). In this model, the CP violation phase appears in the Higgs potential and Yukawa interaction. It is a new point of this study to take into account multiple independent CP-violating phases from different sectors and investigate the interference between effects from them. Since THDM in general leads to dangerous flavor changing neutral currents (FCNCs) mediated by the Higgs boson, the alignment is imposed on Yukawa interaction in order to avoid it[71]. In addition, another alignment of the Higgs potential is imposed so that the Higgs boson coupling with a mass of 125 GeV has the same coupling at the tree level as the SM Higgs boson found at LHC[72, 73]. As a result of the numerical analysis for the EDM, we have found that the Barr-Zee (BZ) type contributions of the fermion loops and the additional scalar boson loops, which give the dominant contributors, can destructively interfere, and then the $\mathcal{O}(1)$ CP-violating phases can allowed by the EDM bounds.[1] The conclusion that each CP-violating phase is allowed to have a certain size is important information for considering the feasibility of EWBG.

In our next study[70], we investigate the possibility of testing the CP violation in the models which do not derive large EDMs. In the case of the model we discussed in our previous study[69], the phenomenology of the collider experiment becomes important to test the CP violation. As pointed out in our paper[69], it may be possible to search for CP violation by investigating the decay of the additional neutral Higgs bosons into a tau lepton pair. There are studies to measure CP violation with this decay[60, 61, 62, 63, 64, 65, 66, 67], but there are not many studies measuring CP violation on the phenomenology of the additional Higgs bosons. In this study, by using the simulation tools such as MadGraph5[75] and TauDecay[61], we have performed the simulation of the production and the decay of the additional Higgs bosons, and discussed how to search for CP violation from the angular distribution of the decay products of the additional Higgs bosons. As a result of signal and background analysis assuming future ILC experiments with several collision energies, we have found that the effects of CP violation can appear on the angular distribution even if the EDM data is satisfied.

[1] In Ref. [74], in the general THDM without alignment in the Higgs potential and in the Yukawa interaction, the cancellation between the BZ contributions from the fermion loops and the gauge boson loops is discussed. In this paper, they focus on effects of CP violation from the Yukawa sector, and effects of CP violation from the Higgs potential are treat as negligibly small due to the heavy additional Higgs masses.

In addition, we have found that the EDM experiments and the test of the angular distribution complement each other in the search for the parameters of the CP-violating model.

1.2 Oganaization

This thesis is composed as follows. In Chapter 2, we give a brief review of the SM. In Chapter 3, before introducing the concert model with the CP-violating extension of the Higgs sector, we discuss the CP-violating observables such as the electric dipole moment and the angular distribution of the scalar boson which have the CP-violating phase in the interaction to the SM particles. Then, we introduce the CP-violating two Higgs doublet model with two alignments for the Higgs potential and for the Yukawa interaction in Chapter 4. In this Chapter, after a brief review of the model, we discuss numerical analysis for the electric dipole moment [69]. From section 4.4, we discuss the simulation of the production and the decay of the additional Higgs boson and the test of CP violation using the angular distributions [70]. Finally, we give a conclusion of this thesis in Chapter 5.

Chapter 2

Review of the standard model

In this chapter, we give the review of the SM. In particular, we focus on the Higgs sector which is extended in below discussion. In addition, we mention the electroweak baryogenesis in the framework of the SM.

In the SM, which respects the gauge symmetry $SU(3)_C \times SU(2)_L \times U(1)_Y$, the Lagrangian is given as

$$\begin{aligned}\mathcal{L} = &-\frac{1}{4}G^{\alpha}_{\mu\nu}G^{\mu\nu}_{\alpha} - \frac{1}{4}W^{a}_{\mu\nu}W^{\mu\nu}_{a} - \frac{1}{4}B_{\mu\nu}B^{\mu\nu} \\ &+ \bar{F}_L i\gamma_\mu D^\mu F_L + \bar{f}_R i\gamma_\mu D^\mu f_R \\ &+ \mathcal{L}_{scalar} + \mathcal{L}_{Yukawa},\end{aligned} \tag{2.1}$$

where $G^{\alpha}_{\mu\nu}$, $W^{a}_{\mu\nu}$ and $B_{\mu\nu}$ are the strength tensor of the $SU(3)_C$, $SU(2)_L$ and $U(1)_Y$ gauge fields, respectively. $F_L = Q_L, L_L$ and $f_R = u_R$, d_R, e_R are the fermion matter contents of the model and Q_L and L_L are parametrized as $Q_L = (u_L, d_L)^T$ and $L_L = (\nu_L, e_L)^T$, and these charge assignments are exhibited in Tab. 2.1. The covariant derivative D_μ is given as $D_\mu = \partial_\mu + ig_3\frac{\lambda^\alpha}{2}G^\alpha_\mu + ig_2\frac{\sigma^a}{2}W^a_\mu + ig_1 Y B_\mu$ with g_3, g_2 and g_1 being the $\mathrm{SU}(3)_C$, $\mathrm{SU}(2)_L$ and $\mathrm{U}(1)_Y$ gauge coupling constants, respectively. The Higgs sector $\mathcal{L}_{scalar}$ and the Yukawa interaction term $\mathcal{L}_{Yukawa}$ are discussed in below sections.

2.1 Higgs sector of the SM

The Higgs sector $\mathcal{L}_{scalar}$ is composed of the kinetic term and the potential term of the iso-spin doublet scaler field Φ as follows.

$$\mathcal{L}_{scalar} = |D_\mu \Phi|^2 - \mathcal{V}. \tag{2.2}$$

	Q_L	L_L	u_R	d_R	e_R	Φ
$SU(3)_C$	3	1	3	3	1	1
$SU(2)_L$	2	2	1	1	1	2
$U(1)_Y$	$\frac{1}{6}$	$\frac{2}{3}$	$-\frac{1}{3}$	$-\frac{1}{2}$	-1	$\frac{1}{2}$

Table 2.1: The charge assignment of the particle contents of the SM.

The potential term, $\mathcal{V}$ is given as

$$\mathcal{V} = -\mu^2|\Phi|^2 + \lambda(|\Phi|^2)^2, \tag{2.3}$$

where μ^2 and λ are real parameters. The doublet field are parametrized as

$$\Phi = \begin{pmatrix} G^+ \\ \frac{1}{\sqrt{2}}(v + h + iG^0) \end{pmatrix}, \tag{2.4}$$

where G^+ and G^0 are the Nambu-Goldstone bosons and $v \equiv \sqrt{v_1^2 + v_2^2} = (\sqrt{2}G_F)^{-1/2}$ with G_F being the Fermi constant.

The stationary conditions for the Higgs potential

$$0 = \left.\frac{\partial \mathcal{V}}{\partial h}\right|_{\Phi=\langle\Phi\rangle}, \tag{2.5}$$

lead to

$$\mu^2 = \frac{1}{2}\lambda v^2. \tag{2.6}$$

and the mass of the Higgs boson h is given as

$$m_h^2 = \lambda v^2. \tag{2.7}$$

On the other hand, the masses of the gauge bosons are also given by the kinetic term of scalar field as $m_W = g_2 v/2$ and $m_Z = \sqrt{g_2^2 + g_1^2}\ v/2$. Then, the interaction of the Higgs field and the gauge bosons are expressed as

$$|D_\mu \Phi|^2 \supset \left(\frac{2m_W^2}{v} W_\mu W^\mu + \frac{m_Z^2}{v} Z_\mu Z^\mu\right) h. \tag{2.8}$$

The couplings of hVV ($V = W,\ Z$) are proportional to the squared mass of the gauge boson.

In addition, the Yukawa interaction term is given by

$$\mathcal{L}_{Yukawa} = -y_u \bar{Q}_L (i\sigma_2 \Phi^*) u_R - y_d \bar{Q}_L \Phi d_R - y_e \bar{L}_L \Phi e_R + h.c., \tag{2.9}$$

where y_f $(f = u, d, e)$ are the 3×3 Yukawa coupling matrices. This term gives the coupling terms of hff as

$$\mathcal{L}_{Yukawa} \supset -\frac{m_f}{v} \bar{f} f h, \tag{2.10}$$

where the mass m_f of the fermions are given as $m_f = \frac{1}{\sqrt{2}} v y_f$.

2.2 Kobayashi-Maskawa phase

By assuming three generations of quarks, it is possible to introduce the observed CP violation[9] which appears in K, B meson physics and so on. Assuming three generations of the quarks, the Yukawa interaction term is as follows.

$$\mathcal{L}_{Yukawa} \xrightarrow{SSB} \sum_{i,j} \{ -\frac{1}{\sqrt{2}} v Y_u^{ij} u_L^i u_R^j - \frac{1}{\sqrt{2}} v Y_d^{ij} d_L^i d_R^j + h.c. \} + \ldots, \tag{2.11}$$

where i and j is indices for the generation and Y_q^{ij} are a complex matrix. We consider a unitary transformation on the generation indices to diagonalize as

$$u_L = U_L u_L^{(m)},\ u_R = U_R u_R^{(m)},\ d_L = D_L d_L^{(m)},\ d_R = D_R d_R^{(m)}. \tag{2.12}$$

When Y_q^{ij} is diagonalized by the matrices $U_{L,R}, D_{L,R}$ defined as above, the diagonal component is the mass of the quarks. Here, the subscript of m in the quark field indicates the mass eigenstate. Using this mass eigenstate of the quarks, we can express the interaction between weak boson $W^\pm$ and the quarks as

$$-\frac{g_2}{\sqrt{2}} \bar{u}_L \gamma^\mu d_L W_\mu^+ + h.c. = -\frac{g_2}{\sqrt{2}} \bar{u}_L^{(m)} (U_L^\dagger D_L) \gamma^\mu d_L^{(m)} W_\mu^+ + h.c.. \tag{2.13}$$

For the product of the matrices, we introduce V_{CKM} being Cabbibo-Kobayashi-Maskawa matrix defined as

$$V_{CKM} \equiv U_L^\dagger D_L. \tag{2.14}$$

When CP transformation is applied to the interaction term of weak boson $W^\pm$ and quarks, it becomes as follows. Hereafter, the subscript m representing the mass eigenstate is omitted.

$$-\frac{g_2}{\sqrt{2}} \bar{u}_L V_{CKM} \gamma^\mu d_L W_\mu^+ - \frac{g_2}{\sqrt{2}} \bar{d}_L V_{CKM}^\dagger \gamma^\mu u_L W_\mu^- \tag{2.15}$$

$$\xrightarrow{CP} -\frac{g_2}{\sqrt{2}}\bar{d}_L V_{CKM}^T \gamma^\mu u_L W_\mu^- - \frac{g_2}{\sqrt{2}}\bar{u}_L V_{CKM}^* \gamma^\mu d_L W_\mu^+. \tag{2.16}$$

From this equation, it is found that the interaction do not respect CP symmetry when the following condition is satisfied

$$V_{CKM}^* \neq V_{CKM}. \tag{2.17}$$

Then, we consider when does V_{CKM} satisfy the above equation, that is, why can CP be broken if there are three generations of quarks. It can be understood by counting the number of the parameters of V_{CKM}. Generally, the $N \times N$ unitary matrix has N^2 parameters. Of these, ${}_NC_2 = N(N-1)/2$ are parameters related to rotation between generations. Therefore, the remaining parameters represent the phase. However, when considering $2N$ quarks for the up type and down type, the phase $2N-1$ can be absorbed into the quark field by redefining the field. After all, the number of physical phases that V_{CKM} has is given as

$$N^2 - \frac{N(N-1)}{2} - (2N-1) = \frac{(N-1)(N-2)}{2}. \tag{2.18}$$

Therefore, it needs to be $N \geq 3$ to break the CP symmetry.

2.3 Elwctroweak baryogenesis in the SM

From the cosmological observations[3], the baryon number to photon number ratio in the universe is given as

$$\eta = \frac{n_b - n_{\bar{b}}}{n_\gamma} \sim 10^{-10}. \tag{2.19}$$

However, it is not known how the current asymmetry was born from the early universe where matter and antimatter existed symmetrically.

The condition for generating the baryon number from the symmetric universe is [4] proposed by Sakharov as follows.

1. Baryons number violation
2. C and CP violation
3. Departure from equilibrium

Condition 1 is indispensable for baryon number generation. Condition 2 prevents that the the baryon number increasing processes $X \to Y$ and decreasing one $\bar{X} \to \bar{Y}$ has the same probability. If it happens with the same probability, the baryon number will just be canceled. (Detailed below.) Condition 3 prevents that the process breaking the baryon number$X \to Y$(and $\bar{X} \to \bar{Y}$) and the inverses process $Y \to X$(and $\bar{Y} \to \bar{X}$)

have the same probability and canceling the baryon number, otherwise the baryon number is canceled. In particular, the proof of condition (2) are given as follows. The state of the universe is represented by the density operator $\hat{\rho}(t)$. Suppose you write a state as $|\psi_n(t)\rangle$.

$$\hat{\rho}(t) = \sum_n p_n |\psi_n(t)\rangle\langle\psi_n(t)|. \tag{2.20}$$

At this time, the expected value of a certain observable is given as

$$\langle\mathcal{O}\rangle = \mathrm{Tr}[\hat{\rho}(t)\hat{\mathcal{O}}]. \tag{2.21}$$

The time evolution of $\hat{\rho}(t)$ is given by the Liouville equation as

$$i\frac{\partial}{\partial t}\hat{\rho}(t) + [\hat{\rho}(t), \hat{H}] = 0, \tag{2.22}$$

with the baryon symmetric initial conditions

$$\langle n_B\rangle_0 = \mathrm{Tr}[\hat{\rho}_0\hat{n}_B] = 0, \tag{2.23}$$

where H is the Hamiltonian. From this, it is shown that C and CP violation is a necessary condition for baryon number creation.The baryon number $\hat{n}_B$ is transformed under C and CP of baryon number as

$$\mathcal{C}\hat{n}_B\mathcal{C}^{-1} = -\hat{n}_B \quad , \quad \mathcal{CP}\hat{n}_B(\mathcal{CP})^{-1} = -\hat{n}_B. \tag{2.24}$$

If $\hat{H}$ is C symmetric, because of $[\hat{H}, \mathcal{C}] = 0$,$\rho$ that starts with a symmetric ρ_0 is always symmetric. Therefore, $[\hat{\rho}(t), \mathcal{C}] = 0$lead to $\langle n_B\rangle$ given as

$$\langle n_B\rangle(t) = \mathrm{Tr}[\hat{\rho}(t)\hat{n}_B] = \mathrm{Tr}[\hat{\rho}(t)\mathcal{C}\hat{n}_B\mathcal{C}^{-1}] = -\mathrm{Tr}[\hat{\rho}(t)\hat{n}_B] = 0. \tag{2.25}$$

Similarly, it is shown that if $\hat{H}$ is CP symmetric, it does not produce baryon numbers. Therefore, it is necessary to break both C and CP in order to generate baryon numbers.

The SM had the potential to explain the baryon number asymmetry due to the electroweak baryogenesis scenario, but experiments ruled out that possibility. The electroweak baryogenesis is a scenario in which baryon number generation is realized during the electroweak phase transition. First, assume a hot universe with zero baryon number and $SU(2)_L \times U(1)_Y$ symmetry. When the temperature drops below about 100 GeV which is the electroweak scale, the symmetry spontaneously breaks to $U(1)_{EM}$ and the phase settles into a vacuum. It is during this transition that the mechanism of electroweak baryogenesis works. The electroweak baryogenesis in the SM was a theory that can satisfy Sakharov's conditions as follows. The violation of the baryon number

of the condition 1 is achieved by the sphaleron process at high temperature. For the condition 2 C is broken by chiral gauge interaction, and CP is broken by Kobayashi-Maskawa phase. The departure from the equilibrium of the condition 3 is achieved by a strong first order electroweak phase transition.

In EWBG scenario, the baryon number creation occurs n the vicinity of the expanding bubble walls. The process progress in the following flow[76, 77]. In first step, particles in the plasma scatter with the bubble walls. CP violation of the underlying theory affects this scattering, and CP asymmetries are generated in particle number densities in front of the bubble wall. In second step, these asymmetries diffuse into the symmetric phase ahead of the bubble wall, where they bias electroweak sphaleron transitions [78, 79] to produce more baryons than anti-baryons. In third step, some of the net number of the baryons created out side the bubble wall is swept up by the expanding wall into the broken phase. In this phase, the sphaleron transition rate is strongly suppressed, and can be small enough to avoid washing out the baryons created in the first two steps.

Unfortunately, the experiments have shown that CP violation by the Kobayashi-Masukawa phase is not sufficient to create baryon number asymmetry[10]. Also, if the SM is required in which a first-order electroweak phase transition be realized, the mass of the Higgs boson must be below about 70 GeV[11]. However, the mass of the Higgs boson found is 125 GeV. For these reason, the SM cannot explain the baryon number asymmetry of the universe. The SM has CP violation from the Kobayashi-Maskawa phase, but it raises the question of whether this can explain the number of baryons currently observed. The Kobayashi-Maskawa phase can be written anywhere in the matrix element by parameterizing the CKM matrix. Therefore, the degree of CP violation from the Kobayashi-Maskawa phase is discussed in an amount that does not depend on parameterization. Such an amount was proposed by Jarlskog [80]. It is made up of Cabibbo-Kobayashi-Maskawa matrix V_{CKM} and quark mass m_q as follows.

$$J = (m_t^2 - m_c^2)(m_t^2 - m_u^2)(m_c^2 - m_u^2)(m_b^2 - m_s^2)(m_b^2 - m_d^2)(m_s^2 - m_d^2)K, \tag{2.26}$$

where

$$K = |\mathrm{Im} V^{ii} V^{jj} (V^*)^{ij} (V^*)^{ji}| \quad (i \neq j). \tag{2.27}$$

By using this value, if the other Sakharov conditions satisfied, the baryon number to photon number ratio is estimated as

$$\eta \sim \frac{J}{T_{EW}^{12}} \sim 10^{-20} \quad (T_{EW} \sim 100\mathrm{GeV}), \tag{2.28}$$

where T_{EW}^{12} are taken to be a typical scale of the electroweak phase transition. This is too small to explain $\eta \sim 10^{-10}$.

Thus, we need the extended Higgs sector which has the sufficient CP violation and can realize the first order electroweak phase transition in order to the observed baryon asymmetry of the universe.

Chapter 3

CP violating observable

In this chapter, we give a review about the test of the CP violation. In particular, we focus on the electric dipole moment and the angular distribution as the CP violating observable leaded by the extended Higgs models with CP violation.

3.1 Electric dipole moment data

3.1.1 Definition of the EDM

The EDM d of particles are defined in similarly to the definition of the magnetic dipole moment.The non-relativistic particle with the spin $\vec{S}$ in the magnetic field $\vec{B}$ can be described by the following Hamiltonian

$$H = -d\,\frac{\vec{S}}{S}\cdot\vec{E}. \tag{3.1}$$

Under the transformation of time reversal, the Hamiltonian becomes [1]

$$H \to \mathcal{T}(H) = +d\,\frac{\vec{S}}{S}\cdot\vec{E}. \tag{3.3}$$

Thus, it is known if the EDM is non zero, time reversal invariance is broken, then the CPT theorem implies that CP symmetry is also broken. In terms of the Lagrangian,

[1]

$$\mathcal{T}(\vec{S}) = -\vec{S},\ \mathcal{T}(\vec{B}) = -\vec{B},\ \mathcal{T}(\vec{E}) = +\vec{E} \tag{3.2}$$

the EDM d_f of fermion can be written by the effective operator as

$$\mathcal{L}_{eff} = -\frac{d_f}{2}\bar{\psi}_f \sigma^{\mu\nu}(i\gamma^5)\psi_f F_{\mu\nu}, \tag{3.4}$$

where $F_{\mu\nu}$ is the electromagnetic field strength tensor and $\sigma^{\mu\nu} = \frac{i}{2}[\gamma^\mu, \gamma^\nu]$. Then we obtain the $\gamma f \bar{f}$ vertices as

$$i\Gamma^\mu = -ie\left[d_f \frac{2m_f}{e}\frac{i\sigma^{\mu\nu}q_\nu(i\gamma^5)}{2m_f}\right], \tag{3.5}$$

where q is the momentum of the photon whose direction is incoming. On the other hand, the vertices are generally written as

$$i\Gamma^\mu(q) = i\Gamma^\mu_V(q) + i\Gamma^\mu_A(q), \tag{3.6}$$

where the subscripts V and A mean the vector couplings and the axial vector couplings, respectively, and where they are given as

$$\Gamma^\mu_V = A_V \cdot \gamma^\mu + B_V \cdot (p' + p)^\mu + C_V \cdot q^\mu, \tag{3.7}$$
$$\Gamma^\mu_A = \left(A_A \cdot \gamma^\mu + B_A \cdot (p' + p)^\mu + C_A \cdot q^\mu\right)\gamma^5, \tag{3.8}$$

where p and p' are the momenta of the incoming fermion and outgoing fermion, and A, B and C are functions of q^2. By taking into account the gauge invariance $q_\mu\Gamma^\mu = 0$ and $q^2 = 0$, we find that the tensor structures are rewriten as

$$i\Gamma^\mu_V = -ie\left[F_1(q^2)\gamma^\mu + F_2(q^2)\frac{i\sigma^{\mu\nu}q_\nu}{2m_f}\right], \tag{3.9}$$
$$i\Gamma^\mu_A = -ie\left[F_3(q^2)\frac{i\sigma^{\mu\nu}q_\nu(i\gamma^5)}{2m_f}\right], \tag{3.10}$$

where the Gordon decomposition is used. Therefore, the EDM d_f can be calculated as

$$d_f = \frac{e}{2m_f}F_3(0). \tag{3.11}$$

We note that the $F_2(0)$ gives an anomalous magnetic dipole moment.

In addition, the neutron EDM receives the contribution from the chromo-EDM (CEDM) d^C_q for a quark q given as

$$\mathcal{L}_{\text{CEDM}} = -\frac{d^C_q}{2}\bar{q}\sigma^{\mu\nu}(i\gamma^5)qG_{\mu\nu}, \tag{3.12}$$

where the $G_{\mu\nu}$ is the QCD field strength tensor.

3.1.2 Current bound

The electron and neutron EDMs are constrained by various atomic and molecule experiments [45, 47] as follows. First, the ACME collaboration gave the upper limit $|d_e + kC_S| < 1.1 \times 10^{-29}$ e cm at the 90% confidence level (CL)[81] by using the thorium-monoxide EDM, where C_S is defined by the coefficient of the following dimension six operator

$$\mathcal{L} \supset C_S(\bar{e} i\gamma_5 e)(\bar{N}N), \tag{3.13}$$

with N being a nucleon. The coefficient k is given by $k \sim \mathcal{O}(10^{-15})$ GeV^2 e cm[47]. C_S are calculated when we consider the concrete model.

Second, The nEDM collaboration updated the constraint on the neutron EDM as $|d_n| < 1.8 \times 10^{-26}$ e cm (90% CL)[82]. There are several contributions to the neutron EDM from the EDM and CEDM of the light quarks such as up- and down-type quarks, the Weinberg operator $\mathcal{L} \supset \frac{1}{3} C_W G^a_{\mu\nu} \tilde{G}^{b\nu\sigma} G^c{}_\sigma{}^\mu$ and the four-fermi interaction $\mathcal{L} \supset C_{ff'}(\bar{f}f)(\bar{f}' i\gamma_5 f')$.

In the SM, although CP violation appears from the Kobayashi-Maskawa phase in the couplings between the quarks and the charged weak boson $W^\pm$, it is known the magnitude of the electron EDM is predicted as very small if we assume the QCD θ term is zero. For example, the d quark EDM is given from the 3-loop level. Contributions up to the two-loop level disappear completely due to the orthogonality of the CKM matrix when summing the internal quarks [42]. Because the electron EDM is induced via a diagram with a closed quark loop, its contribution appears at the four-loop level and thus it is rather suppressed as

$$d_e^{SM} \leq \mathcal{O}(10^{-38}) \text{e cm[83]}. \tag{3.14}$$

In extended Higgs model, CP violation can appear from the interaction between the additional and the fermions. It induce the electronic EDM significantly more larger than the contribution of SM. The dominant contribution to d_f given by the two-loop Barr-Zee(BZ) type diagrams[84]. We note that the one-loop contributions to d_f are negligibly smaller than those from the BZ diagrams, because the one-loop contribution has two additional powers of small Yukawa couplings for light fermions with respect to the BZ diagrams. In fact, we obtain d_e(1-loop) $\sim \mathcal{O}(10^{-34})$ e cm, while d_e(2-loop) $\sim \mathcal{O}(10^{-27})$ e cm in the typical input parameters with $\mathcal{O}(100)$ GeV of the masses of additional Higgs bosons and the $\mathcal{O}(1)$ coupling factors of the additional Higgs bosons to fermions[41].

3.1.3 Barr-Zee type contributions

The BZ diagrams are drawn by attaching the effective vertex $H_j^0 V^0 \gamma$ ($V^0 = \gamma, Z$) or $H^\pm W^\mp \gamma$ to the fermion line which are shown in Fig. 3.1. The BZ contribution to d_f

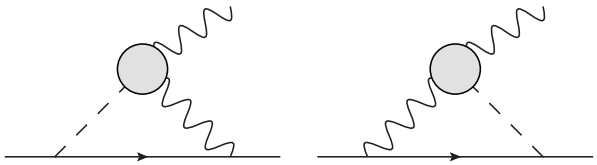


Figure 3.1: Barr-Zee diagrams. The figures are given by Ref. [69]

is decomposed into the contributions from fermion-loops, Higgs boson-loops and gauge bosom-loops as follows

$$d_f = d_f(\text{fermion}) + d_f(\text{Higgs}) + d_f(\text{gauge}). \tag{3.15}$$

Furthermore, each contribution can be classified as

$$d_f(X) = d_f^\gamma(X) + d_f^Z(X) + d_f^W(X), \tag{3.16}$$

where $d_f^\gamma(X)$, $d_f^Z(X)$ and $d_f^W(X)$ are the contributions from diagrams with γ, Z and W exchange, respectively. We note that the value of d_f, which consist of the BZ contribution, is not gauge invariant.

3.2 Angular distribution

The new CP-violating phase of the extended Higgs model can be measured from the Higgs-boson-decay products at collider experiments. The effects of the CP-violating phase of the Higgs-fermion-fermion couplings appear in the decays of the Higgs bosons into fermions. As discussed in Refs. [60, 85, 61, 62, 63], their decay into $\tau^+\tau^-$ pair with the hadronic decays of $\tau^\pm$ can be useful to see the CP-violating effects due to their simple kinematic structure. We thus focus on $H^0 \to \tau^-\tau^+ \to X^-\nu X^+\bar{\nu}$, where $X^\pm$ are hadrons, for example, $\pi^\pm$, $\rho^\pm$, $a_1^\pm$ mesons and so on. We consider $\rho^\pm$ ($a_1^\pm$) into $\pi^\pm\pi^0$ ($\pi^\pm\pi^0\pi^0$ or $\pi^\pm\pi^\pm\pi^\mp$) as the subsequent decay. The parent H^0 is a spin-0 boson, for example, the discovered Higgs boson or extra Higgs bosons which we introduce in below chapter. The CP-violating phase on the $H^0\tau^+\tau^-$ interaction affects the angular distribution of the pi mesons produced by the decays of tau leptons.

Here, we discuss the correlation between the CP-violating coupling on $H^0\tau\tau$ and the angular distribution of $H^0 \to \tau^-\tau^+$. We introduce the interaction of $H^0\tau\tau$ as

$$\mathcal{L}_{H^0\tau\tau} = -\frac{m_\tau}{v}|\kappa|\ \bar{\tau}(c_s + i\gamma_5 c_p)\tau H^0, \tag{3.17}$$

where κ is the complex coupling factor, and $c_s = \text{Re}(\kappa)/|\kappa| = \cos\theta_{\text{CP}}$ and $c_p = \text{Im}(\kappa)/|\kappa| = \sin\theta_{\text{CP}}$ whose subscripts s and p mean the scalar and pseudo coupling.

When the coupling factor $\kappa = 1$, the $H^0\tau\tau$ interaction is the same coupling as the Higgs boson of the SM. When CP $= n\pi$ or CP $= n\pi + \pi/2$ (n=0,1,2,...), H^0 is the CP-even or -odd state. Otherwise, H^0 cannot be defined as a CP eigenstate, and then there is CP violation on the $H^0\tau\tau$ interaction. From the above Lagrangian, the amplitude of $H^0 \to \tau^-\tau^+$ is given as

$$\mathcal{M}(H^0 \to \tau^-\tau^+) \propto \bar{u}(p_-)(c_s + i\gamma_5 c_p)v(p_+), \tag{3.18}$$

where $p^\mu_\pm$ are the momenta of $\tau^\pm$. The amplitude of $\tau^\pm \to X^\pm\nu(\bar{\nu})$ can be expressed as[60]

$$\mathcal{M}(\tau^- \to X^-\nu) \propto [\bar{u}(k_-)\gamma_\mu(1-\gamma_5)u(p_-)]J^\mu_-, \tag{3.19}$$
$$\mathcal{M}(\tau^+ \to X^+\bar{\nu}) \propto [\bar{v}(p_+)\gamma_\mu(1-\gamma_5)v(k_+)]J^{*\mu}_+, \tag{3.20}$$

where $k^\mu_\pm$ are the momenta of $\nu(\bar{\nu})$ and $J^\mu_\pm$ are the hadronic currents related to $X^\pm$. For $X^\pm = \pi^\pm$, the hadronic currents are expressed by the $\pi^\pm$ momenta $q^\mu_\pm$ as $J^\mu_\pm \propto q^\mu_\pm (= p^\mu_\pm - k^\mu_\pm)$[86]. The amplitude of $H^0 \to \tau^-\tau^+ \to X^-\nu X^+\bar{\nu}$ is given by the $\tau^\pm$ spin summation of the product fo Eqs. (3.18), (3.19) and (3.20) as[60]

$$\begin{aligned}
&\mathcal{M}(H^0 \to \tau^-\tau^+ \to \pi^-\nu\pi^+\bar{\nu}) \\
&= \sum_{\text{spin of } \tau^\pm} \mathcal{M}(\tau^- \to \pi^-\nu)\mathcal{M}(H^0 \to \tau^-\tau^+)\mathcal{M}(\tau^+ \to \pi^+\bar{\nu}) \\
&\propto \bar{u}(k_-)\not{J}_-(1-\gamma_5)(\not{p}_- + m_\tau)(c_s + i\gamma_5 c_p)(\not{p}_+ - m_\tau)\not{J}^*_+(1-\gamma_5)v(k_+).
\end{aligned} \tag{3.21}$$

In the above equation, we assume that the intermediate states of $\tau^\pm$ are on-shell. The $\nu(\bar{\nu})$ spin averaged squared amplitude is given as

$$\begin{aligned}
&\overline{|\mathcal{M}(H^0 \to \tau^-\tau^+ \to \pi^-\nu\pi^+\bar{\nu})|^2} \\
&\propto (c_s^2 + c_p^2)\big[(p_- \cdot k_+)(p_- \cdot k_-) + (p_+ \cdot k_-)(p_+ \cdot k_+) - m_\tau^2(k_- \cdot k_-)\big] \\
&+ (c_s^2 - c_p^2)\big[(p_- \cdot p_+)(k_- \cdot k_+) - (p_- \cdot k_-)(p_+ \cdot k_+) - (p_- \cdot k_+)(p_+ \cdot k_-)\big] \\
&- 2c_s c_p\ \epsilon_{\mu\nu\rho\sigma} p^\mu_- p^\nu_+ k^\rho_- k^\sigma_+,
\end{aligned} \tag{3.22}$$

where the convention $\epsilon_{0123} = 1$, and $\not{k}_\pm\not{k}_\pm = (k_\pm)^2 = 0$ because the neutrinos are massless.

In the H^0 rest frame, the momenta of $\tau^\pm$ and $\nu(\bar{\nu})$ are exprresed as

$$p^\mu_\pm = (E, \mp\vec{p}), \tag{3.23}$$
$$k^\mu_\pm = (|\vec{k}_\pm|, \vec{k}_\pm), \tag{3.24}$$

where

$$E = \frac{m_{H^0}}{2}, \tag{3.25}$$

$$|\vec{p}|^2 = \frac{m_{H^0}^2}{4}\left(1 - \frac{4m_\tau^2}{m_{H^0}^2}\right) \equiv \frac{m_{H^0}^2}{4}\beta^2, \tag{3.26}$$

The tensor product is given as

$$\epsilon_{\mu\nu\rho\sigma} p_-^\mu p_+^\nu k_-^\rho k_+^\sigma = 2E(\vec{k}_- \times \vec{k}_+)\cdot\vec{p}. \tag{3.27}$$

Therefore, the amplitude is obtained as

$$\begin{aligned}
&\overline{|\mathcal{M}(H^0 \to \tau^-\tau^+ \to \pi^-\nu\pi^+\bar{\nu})|^2} \\
&\propto \frac{1}{2}(c_s^2 + c_p^2)\left(1 + \beta^2 + (1-\beta^2)\frac{\vec{k}_-\cdot\vec{k}_+}{|\vec{k}_-||\vec{k}_+|} + 2\beta^2\frac{(\vec{p}\cdot\vec{k}_-)(\vec{p}\cdot\vec{k}_+)}{|\vec{k}_-||\vec{k}_+||\vec{p}|^2}\right) \\
&-\frac{1}{2}(c_s^2 - c_p^2)\left(1 - \beta^2 + (1+\beta^2)\frac{\vec{k}_-\cdot\vec{k}_+}{|\vec{k}_-||\vec{k}_+|} - 2\beta^2\frac{(\vec{p}\cdot\vec{k}_-)(\vec{p}\cdot\vec{k}_+)}{|\vec{k}_-||\vec{k}_+||\vec{p}|^2}\right) - 2\sin 2\theta_{\rm CP}\frac{(\vec{k}_-\times\vec{k}_+)\cdot\vec{p}}{|\vec{k}_-||\vec{k}_+||\vec{p}|}
\end{aligned} \tag{3.28}$$

$$= (c_s^2\beta^2 + c_p^2)\left(1 + \frac{\vec{k}_-^{\parallel}\cdot\vec{k}_+^{\parallel}}{|\vec{k}_-||\vec{k}_+|}\right) - (c_s^2\beta^2 - c_p^2)\frac{\vec{k}_-^{\perp}\cdot\vec{k}_+^{\perp}}{|\vec{k}_-||\vec{k}_+|} - 2c_s c_p\beta\frac{(\vec{k}_-^{\perp}\times\vec{k}_+^{\perp})^{\parallel}}{|\vec{k}_-||\vec{k}_+|}. \tag{3.29}$$

From Eq. (3.28), it is clear that the third term is T-odd term while the others are T-even terms[2]. We can see that if the $H^0\tau\tau$ interaction has both CP-even and -odd couplings, then the T-odd (CP-violating) observable appears.

The angles θ_-, ϕ_- and θ_+, ϕ_+ define the angles of the three-momentum of π^- and π^+ in the τ^- and τ^+ rest frame, respectively. The z axis is defined as the flight direction of τ^- in the H^0 rest frame. In Fig.3.2, the relation between the angles $\theta^\pm$ and $\phi^\pm$ and the three-momentum $\vec{q'}_\pm$ of $\pi^\pm$ in the $\tau^\pm$ rest frame is depicted. In the $\tau^\mp$ rest frame, the momenta of $\tau^\mp$ and $\nu(\bar{\nu})$ are denoted by $p'^\mu_\pm$ and $k'^\mu_\pm$ as

$$p'^\mu_\pm = (m_\tau, 0, 0, 0), \tag{3.30}$$

$$k'^\mu_\pm = k'^0_-(1, -\cos\phi_\pm\sin\theta_\pm, -\sin\phi_\pm\sin\theta_\pm, -\cos\theta_\pm), \tag{3.31}$$

where we used $\vec{k'}_\pm = -\vec{q'}_\pm$ and $k'^0_- = |\vec{k'}|$. In the H^0 rest frame, the momenta of $\tau^\pm$ and $\nu(\bar{\nu})$ are given as

$$p^\mu_\pm = (E, 0, 0, \mp|\vec{p}|), \tag{3.32}$$

[2]Under the time reversal transformation, the three-momenta are transformed as $\vec{p} \to -\vec{p}$ and $\vec{k}_\pm \to -\vec{k}_\pm$

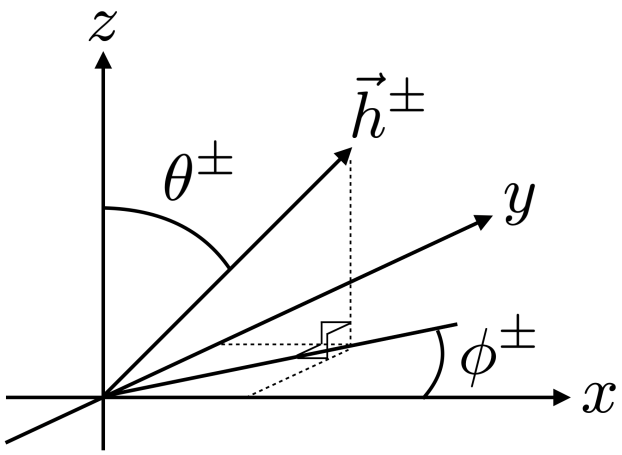


Figure 3.2: The angles $\theta^{\pm}$ and $\phi^{\pm}$ in the $\tau^{\pm}$ rest frame. In the case of $X^{\pm} = \pi^{\pm}$, the polarimeter $\vec{h}^{\pm}$ is proportional to the three-momentum $\vec{q'}_{\pm}$ of $\pi^{\pm}$ in the $\tau^{\pm}$ rest frame. The z axis is defined along with the direction of τ^- in the H^0 rest frame. The figure is given by Ref. [70].

$$k^{\mu}_{\pm} = (\frac{E}{m_\tau} k'^{0}_{\pm} \mp \frac{|\vec{p}|}{m_\tau} k'^{z}_{\pm}, k'^{x}_{\pm}, k'^{y}_{\pm}, \mp \frac{|\vec{p}|}{m_\tau} k'^{0}_{\pm} + \frac{E}{m_\tau} k'^{z}_{\pm}). \tag{3.33}$$

By using Eqs. (3.32) and (3.33), the $\theta_{\pm}$ and $\phi_{\pm}$ dependence of the amplitude is obtained as[85]

$$\overline{|\mathcal{M}(H^0 \to \tau^-\tau^+ \to \pi^-\nu\pi^+\bar{\nu})|^2} \propto 1 + \cos\theta_- \cos\theta_+ - \sin\theta_- \sin\theta_+ \cos(2\theta_{\rm CP} - \Delta\phi), \tag{3.34}$$

where $\beta = 1$ is assumed and $\Delta\phi \equiv \phi^+ - \phi^-$. The angle $\Delta\phi$, which corresponds to the angle between the plane defined by the vectors $\vec{p}_-$ and $\vec{q}_-$ and those defined by the vectors $\vec{p}_+$ and $\vec{q}_+$ in the H^0 rest frame, as depicted in Fig.3.3. By integrating Eq. (3.34) for θ^- and θ^+, the angular distribution of the decay products of H^0 are obtained as follows.

$$\int\int d\cos\theta^- d\cos\theta^+ \ \overline{|\mathcal{M}(H^0_j \to \tau^-\tau^+ \to \pi^-\nu\pi^+\bar{\nu})|^2} \propto 16 - \pi^2 \cos(2\theta_{\rm CP} - \Delta\phi). \tag{3.35}$$

By looking at the shape of the distributions depending on the value of $\theta_{\rm CP}$, we can extract the information of $\theta_{\rm CP}$.

The discussion for the other decay modes of tau leptons, i.e., $X^{\pm} = \rho^{\pm}$ and $a_1^{\pm}$, is more complex. In those cases, the angles $\theta_{\pm}$ and $\phi_{\pm}$ correspond to the angles of the

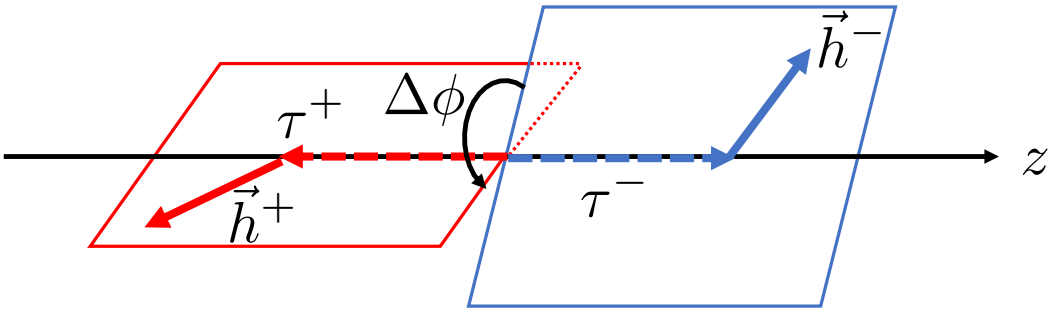


Figure 3.3: The angle $\Delta\phi$ in the H^0 rest frame. In the case of $X^\pm = \pi^\pm$, the polarimeter $\vec{h}^\pm$ is proportional to the three-momentum $\vec{q'}_\pm$ of $\pi^\pm$ in the $\tau^\pm$ rest frame. The z axis is defined along with the direction of τ^- in the H^0 rest frame.

polarimeter $\vec{h}^\pm$ defined by the momenta of the decay products of $\tau^\pm$ in the rest frame of $\tau^\pm$ as follows.

$$\vec{h}^\pm \propto \vec{\Pi}^\pm - \vec{\Pi}^{5\pm}, \tag{3.36}$$

where

$$\Pi^\pm_\mu \equiv 4\mathrm{Re}(J^\pm_\mu k^\pm \cdot J^\pm) - 2k^\pm_\mu J^\pm \cdot J^{\pm *}, \tag{3.37}$$
$$\Pi^{5\pm}_\mu \equiv 2\epsilon_{\mu\nu\rho\sigma}\mathrm{Im}(J^{\pm\nu}J^{\pm *\rho}k^\sigma_\pm). \tag{3.38}$$

In terms of the polarimeter $\vec{h}^\pm$, the amplitude is rewritten as

$$\begin{aligned}\overline{|\mathcal{M}(H^0 \to \tau^-\tau^+ \to X^-\nu X^+\bar{\nu})|^2} \propto 1 &+ \frac{(\vec{h}_- \cdot \vec{p}_-)(\vec{h}_+ \cdot \vec{p}_-)}{|\vec{h}_-||\vec{h}_+||\vec{p}_-|^2} \\ &- \cos 2\theta_{\mathrm{CP}} \frac{(\vec{h}_- \times \vec{p}_-)\cdot(\vec{h}_+ \times \vec{p}_-)}{|\vec{h}_-||\vec{h}_+||\vec{p}_-|^2} \\ &- \sin 2\theta_{\mathrm{CP}} \frac{(\vec{h}_- \times \vec{h}_+)\cdot \vec{p}_-}{|\vec{h}_-||\vec{h}_+||\vec{p}_-|},\end{aligned} \tag{3.39}$$

where the last term is T-odd term while the others are T-even terms because the polarimeter is transformed as $\vec{h}^\pm \to -\vec{h}^\pm$ under the time reversal transformation. From Eq. (3.39), we can see that the T-odd (CP-violating) observable appears when neither $\theta_{\mathrm{CP}} = n\pi$ nor $\theta_{\mathrm{CP}} = n\pi + \pi/2$. The hadronic currents $J^{\pm\mu}$ for $X^\pm = \rho^\pm$ and $a_1^\pm$ are given as follows. For $X^\pm = \rho^\pm$ decaying to $\rho^\pm \to \pi^\pm\pi^0$, the hadronic current $J^{\pm\mu}$ is given as

$$J^{\pm\mu} \propto q^\mu_{\pi^\pm} - q^\mu_{\pi^0}. \tag{3.40}$$

For $X = a_1^{\pm}$ decaying to $a_1^{\pm} \to \pi^{\pm}\pi^0\pi^0$ ($a_1^{\pm} \to \pi^{\pm}\pi^{\pm}\pi^{\mp}$), when ${q_1}^{\mu}$, ${q_2}^{\mu}$ and q_3^{μ} are the momenta of π^0, π^0 and $\pi^{\pm}$ ($\pi^{\pm}$, $\pi^{\pm}$ and $\pi^{\mp}$), the hadronic current $J^{\pm\mu}$ is given as

$$J^{\pm\mu} \propto \left[q_1^{\mu} - q_3^{\mu} - Q^{\mu} \frac{Q \cdot (q_1 - q_3)}{Q^2} \right] F_{\rho}((q_1 + q_3)^2) + (1 \leftrightarrow 2), \tag{3.41}$$

where $Q = q_1 + q_2 + q_3$ and

$$F_{\rho}(Q^2) = \frac{B_{\rho}(Q^2) + \alpha B_{\rho'}(Q^2)}{1 + \alpha}, \tag{3.42}$$

with the Breit-Wigner factor

$$B_V(Q^2) = \frac{m_V^2}{m_V^2 - Q^2 - i\sqrt{Q^2}\Gamma_V(Q^2)}. \tag{3.43}$$

The running width is

$$\Gamma_V(Q^2) = \Gamma_V \frac{\sqrt{Q^2}}{m_V} \frac{g_V(Q^2)}{g_V(m_V^2)}, \tag{3.44}$$

where

$$g_{\rho}(Q^2) = \bar{\beta} \left(\frac{m_{\pi^-}^2}{Q^2}, \frac{m_{\pi^0}^2}{Q^2} \right)^3, \tag{3.45}$$

with

$$\bar{\beta}(a, b) = (1 + a^2 + b^2 - 2a - 2b - 2ab)^{1/2}. \tag{3.46}$$

We take $\alpha = 0.145$[61].

Chapter 4

Aligned two Higgs doublet model

We consider the CP-violating THDM in which the scalar sector consists of two isospin sector doublets $\Phi_{1,2}$ and the other components are the same as the SM, and the Lagrangian respects the SM gauge symmetries. In our model, we assume that the scalar potential $\mathcal{V}$ is aligned to realize the SM-ilke couplings for 125 GeV Higgs boson at tree level, and the Yukawa interaction term $\mathcal{L}_{\rm yukawa}$ is also aligned to remove new contribution to the FCNCs at tree level[1]. In addition, the additional CP-violating phases arise form both of sectors as we confirm below[2]. After that, we discuss the numerical analysis for the EDM satisfying the data, and we consider the simulation of the collider experiment to get the information of the CP violating phase form the angular distribution.

[1]The experimental data indicate that the discovered Higgs boson h^{125} is SM like, i.e., the couplings of h^{125} are the same couplings as the SM Higgs boson within the margin of error. Since the Higgs boson discovery at 2012, therefore, the decoupling scenario, in which the extra particles are decoupled, and the alignment on the Higgs potential (without decoupling) are often considered. In the decoupling scenario, it is not easy to get the large effect of the CP violation. When the alignment of the Higgs potential is slightly broken, the phenomenology of h^{125} becomes rich. The test with precision measurements of h^{125} in such a model have been also being studied. On the other hand, the extra contribution to the FCNCs vanishes if the extra Yukawa interaction is forbidden by a symmetry ,e.g., Z_2 symmetry as mentioned below. In this case, However, the extra CP-violating phases also vanish in the Yukawa sector.

[2]So far, the THDM with CP violation has been discussed in many papers, for example, [15, 16, 17, 18, 19, 20, 21]. The THDM in which the CP-violating phase is introduced by the mixing between the CP-even and -odd states is usually strongly constrained from the EDM data. Therefore, if the THDM with the multiple O(1) CP-violating phases can easily satisfy the EDM data, the EWBG in the THDM will be more notable scenario for BAU.

4.1 Lagrangian

4.1.1 Higgs potential

In any basis for the two isodoublet fields (Φ'_1, Φ'_2), the Higgs potential[87] is given by

$$\begin{aligned}\mathcal{V} =& -\mu'^2_1(\Phi'^\dagger_1\Phi'_1) - \mu'^2_2(\Phi'^\dagger_2\Phi'_2) - \left[\mu'^2_3(\Phi'^\dagger_1\Phi'_2) + h.c.\right] \\ &+ \tfrac{1}{2}\lambda'_1(\Phi'^\dagger_1\Phi'_1)^2 + \tfrac{1}{2}\lambda'_2(\Phi'^\dagger_2\Phi'_2)^2 + \lambda'_3(\Phi'^\dagger_1\Phi'_1)(\Phi'^\dagger_2\Phi'_2) + \lambda'_4(\Phi'^\dagger_2\Phi'_1)(\Phi'^\dagger_1\Phi'_2) \\ &+ \left\{\left[\tfrac{1}{2}\lambda'_5(\Phi'^\dagger_1\Phi'_2) + \lambda'_6(\Phi'^\dagger_1\Phi'_1) + \lambda'_7(\Phi'^\dagger_2\Phi'_2)\right](\Phi'^\dagger_1\Phi'_2) + h.c.\right\}, \end{aligned} \tag{4.1}$$

where $\mu'^2_{1,2}$ and $\lambda'_{1,2,3,4}$ are real, while μ'^2_3 and $\lambda'_{5,6,7}$ are complex. When the doublet fields get the vacuum expectation values (VEVs), $\langle\Phi'_k\rangle = (0, v_k e^{i\xi_k}/\sqrt{2})^T$, we can consider the the following U(2) transformation from (Φ'_1, Φ'_2) to so-called the Higgs basis[88, 89] (Φ_1, Φ_2) without loss of generality.

$$\begin{pmatrix} \Phi_1 \\ \Phi_2 \end{pmatrix} = \begin{pmatrix} \cos\beta & \sin\beta \\ -\sin\beta & \cos\beta \end{pmatrix} \begin{pmatrix} e^{-i\xi_1} & 0 \\ 0 & e^{-i\xi_2} \end{pmatrix} \begin{pmatrix} \Phi'_1 \\ \Phi'_2 \end{pmatrix}, \tag{4.2}$$

where $\tan\beta \equiv v_2/v_1$. The two doublet fields Φ_1 and Φ_2 are parametrized as

$$\Phi_1 = \begin{pmatrix} G^+ \\ \frac{1}{\sqrt{2}}(v + h^0_1 + iG^0) \end{pmatrix}, \quad \Phi_2 = \begin{pmatrix} H^+ \\ \frac{1}{\sqrt{2}}(h^0_2 + ih^0_3) \end{pmatrix}, \tag{4.3}$$

where G^+ and G^0 are the Nambu-Goldstone bosons and $v \equiv \sqrt{v_1^2 + v_2^2} = (\sqrt{2}G_F)^{-1/2}$ with G_F being the Fermi constant. In the Higgs basis, the Higgs potential is rewritten by

$$\begin{aligned}\mathcal{V} =& -\mu^2_1(\Phi^\dagger_1\Phi_1) - \mu^2_2(\Phi^\dagger_2\Phi_2) - \left[\mu^2_3(\Phi^\dagger_1\Phi_2) + h.c.\right] \\ &+ \tfrac{1}{2}\lambda_1(\Phi^\dagger_1\Phi_1)^2 + \tfrac{1}{2}\lambda_2(\Phi^\dagger_2\Phi_2)^2 + \lambda_3(\Phi^\dagger_1\Phi_1)(\Phi^\dagger_2\Phi_2) + \lambda_4(\Phi^\dagger_2\Phi_1)(\Phi^\dagger_1\Phi_2) \\ &+ \left\{\left[\tfrac{1}{2}\lambda_5(\Phi^\dagger_1\Phi_2) + \lambda_6(\Phi^\dagger_1\Phi_1) + \lambda_7(\Phi^\dagger_2\Phi_2)\right](\Phi^\dagger_1\Phi_2) + h.c.\right\}, \end{aligned} \tag{4.4}$$

where $\mu^2_{1,2}$ and $\lambda_{1,2,3,4}$ are real, while μ^2_3 and $\lambda_{5,6,7}$ are complex. These parameters, μ^2_i and λ_i, are expressed by μ'^2_i and λ'_i (see Appendix A). The stationary conditions for the Higgs potential

$$0 = \left.\frac{\partial\mathcal{V}}{\partial h^0_j}\right|_{\substack{\Phi_1=\langle\Phi_1\rangle \\ \Phi_2=\langle\Phi_2\rangle}}, \tag{4.5}$$

lead to

$$\mu_1^2 = \frac{1}{2}\lambda_1 v^2,\ \mu_3^2 = \frac{1}{2}\lambda_6 v^2. \tag{4.6}$$

The remaining dimensionful parameter is redefined as $M^2 \equiv -\mu_2^2$ below. The squared mass of the charged Higgs boson is given by

$$m_{H^\pm}^2 = M^2 + \tfrac{1}{2}\lambda_3 v^2. \tag{4.7}$$

The squared-mass matrix for the neutral Higgs bosons in the basis of (h_1^0, h_2^0, h_3^0) is given by

$$\mathcal{M}_{ij}^2 \equiv \left.\frac{\partial^2 \mathcal{V}}{\partial h_i \partial h_j}\right|_{\substack{\Phi_1=\langle\Phi_1\rangle \\ \Phi_2=\langle\Phi_2\rangle}} = v^2 \begin{pmatrix} \lambda_1 & \mathrm{Re}[\lambda_6] & -\mathrm{Im}[\lambda_6] \\ \mathrm{Re}[\lambda_6] & \frac{M^2}{v^2} + \frac{1}{2}(\lambda_3+\lambda_4+\mathrm{Re}[\lambda_5]) & -\frac{1}{2}\mathrm{Im}[\lambda_5] \\ -\mathrm{Im}[\lambda_6] & -\frac{1}{2}\mathrm{Im}[\lambda_5] & \frac{M^2}{v^2} + \frac{1}{2}(\lambda_3+\lambda_4-\mathrm{Re}[\lambda_5]) \end{pmatrix}_{ij}. \tag{4.8}$$

This is diagonalized by the orthogonal matrix $\mathcal{R}$ as $\mathcal{R}^T\mathcal{M}^2\mathcal{R} = \mathrm{diag}(m_{H_1^0}^2, m_{H_2^0}^2, m_{H_3^0}^2)$. The mass eigenstates of the neutral Higgs bosons are expressed as

$$h_i^0 = \mathcal{R}_{ij} H_j^0. \tag{4.9}$$

In the model, since one of the complex phase of parameters can be absorbed by redefinition of the doublet fields, the Higgs potential has 11 parameters which are $v, M, \lambda_{1,2,3,4}, |\lambda_{5,6,7}|$ and the 2 physical phases. Hereafter, we take $\mathrm{Im}[\lambda_5] = 0$ by using the phase redefinition, $(\Phi_1^\dagger\Phi_2) \to e^{-i\arg[\lambda_5]/2}(\Phi_1^\dagger\Phi_2)$, and we also redefine the other complex parameters as $\mu_3^2 e^{-i\arg[\lambda_5]/2} \to \mu_3^2$, $\lambda_6 e^{-i\arg[\lambda_5]/2} \to \lambda_6$ and $\lambda_7 e^{-i\arg[\lambda_5]/2} \to \lambda_7$.

We assume the following alignment for the Higgs potential[69],

$$\lambda_6 = 0, \tag{4.10}$$

in which the mixing matrix is diagonalized as $\mathcal{R}_{ij} = \delta_{ij}$, so that the neutral Higgs bosons do not mix with each other. Such an alignment can be realized by the twisted custodial symmetry of the Higgs potential, which respects global the $SU(2)_L \times SU(2)_R$ symmetry[90, 68] [3]. Since the CP invariance is also led when the symmetry is completely

[3]Under the $SU(2)_L \times SU(2)_R$ transformation, the Higgs doublets are transformed as $(i\sigma_2\Phi_i^*, \Phi_i) \to U_L(i\sigma_2\Phi_i^*, \Phi_i)U_R^\dagger$. If the $SU(2)_L \times SU(2)_R$ invariance is required, two kinds of the relation among the parameters are given as

$$\text{(I)} \quad \lambda_4 = \lambda_5, \tag{4.11}$$

$$\text{(II)} \quad \lambda_4 = -\lambda_5 \text{ and } \lambda_6 = \lambda_7 = 0, \tag{4.12}$$

where the CP-violating phases are vanished.

imposed, we here simply assume $\lambda_6 = 0$ to investigate an effects of the CP violation from the Higgs potential. The squared masses of the neutral scalars are then given by

$$m^2_{H^0_1} = \lambda_1 v^2, \tag{4.13}$$

$$m^2_{H^0_2} = M^2 + \frac{1}{2}(\lambda_3 + \lambda_4 + \mathrm{Re}[\lambda_5])v^2, \tag{4.14}$$

$$m^2_{H^0_3} = M^2 + \frac{1}{2}(\lambda_3 + \lambda_4 - \mathrm{Re}[\lambda_5])v^2. \tag{4.15}$$

We identify H^0_1 as the discovered Higgs boson with the mass of 125 GeV, and we consider that the other Higgs bosons H^0_2, H^0_3 and $H^\pm$ are heavier. Consequently, there are 7 free parameters which can be chosen as follows

$$m_{H^0_2}, m_{H^0_3}, m_{H^\pm}, M, \lambda_2, |\lambda_7| \text{ and } \theta_7, \tag{4.16}$$

where $\theta_7 \equiv \arg[\lambda_7] \in (-\pi, \pi]$.

4.1.2 Yukawa interaction term

In the weak basis for the fermions which the left-handed quark and lepton doublets are defined as ${Q'}_L$ and ${L'}_L$, and the right-handed up-type quark, down-type quark and charged lepton singlets are defined as ${u'}_R$, ${d'}_R$ and ${e'}_R$, the Yukawa interaction term is given by

$$\mathcal{L}_{\mathrm{yukawa}} = -\sum_{k=1}^{2}\left(\bar{Q'}_L {y'}^{\dagger}_{u,k}\tilde{\Phi'}_k {u'}_R + \bar{Q'}_L {y'}_{d,k}\Phi'_k {d'}_R + \bar{L'}_L {y'}_{e,k}\Phi'_k {e'}_R + h.c.\right) \tag{4.17}$$

$$= -\sum_{k=1}^{2}\left(\bar{Q'}_L y^{\dagger}_{u,k}\tilde{\Phi}_k {u'}_R + \bar{Q'}_L y_{d,k}\Phi_k {d'}_R + \bar{L'}_L y_{e,k}\Phi_k {e'}_R + h.c.\right), \tag{4.18}$$

where $\tilde{\Phi}_k = i\sigma_2\Phi^*_k$ and ${y'}_{f,k}$ and $y_{f,k}$ are the 3×3 complex Yukawa coupling matrices which are related as[69]

$$y_{f,1} = \left({y'}_{f,1}e^{i\xi_1}\right)\cos\beta + \left({y'}_{f,2}e^{i\xi_2}\right)\sin\beta, \tag{4.19}$$

$$y_{f,2} = -\left({y'}_{f,1}e^{i\xi_1}\right)\sin\beta + \left({y'}_{f,2}e^{i\xi_2}\right)\cos\beta. \tag{4.20}$$

The mass eigenstates of the fermions are represented as those without a prime, Eq. (4.18) is then rewritten as

$$\mathcal{L}_{\mathrm{yukawa}} = -\bar{Q}^u_L\left(\sqrt{2}\frac{M_u}{v}\tilde{\Phi}_1 + \rho_u\tilde{\Phi}_2\right)u_R - \bar{Q}^d_L\left(\sqrt{2}\frac{M_d}{v}\Phi_1 + \rho_d\Phi_2\right)d_R$$

Model	ζ_u	ζ_d	ζ_l
Our model	arbitrary complex	arbitrary complex	arbitrary complex
Type-I THDM	$1/\tan\beta$	$1/\tan\beta$	$1/\tan\beta$
Type-II THDM	$1/\tan\beta$	$-\tan\beta$	$-\tan\beta$
Type-X THDM	$1/\tan\beta$	$1/\tan\beta$	$-\tan\beta$
Type-Y THDM	$1/\tan\beta$	$-\tan\beta$	$1/\tan\beta$

Table 4.1: ζ_f factors in the THDMs. The names of the models are referred to Refs. [71, 93].

$$-\bar{L}_L\left(\sqrt{2}\frac{M_e}{v}\Phi_1+\rho_e\Phi_2\right)e_R+h.c., \tag{4.21}$$

where $Q_L^u=(u_L,V_{\rm CKM}d_L)^T$ and $Q_L^d=(V_{\rm CKM}^\dagger u_L,d_L)^T$ with $V_{\rm CKM}$ being the Cabibbo-Kobayashi-Maskawa (CKM) matrix. While M_f are the diagonalized-mass matrices for the fermions, ρ_f are 3×3 complex matrices whose off-diagonal elements generally induce dangerous FCNCs which are strongly constrained by flavor experiments.

In order to remove new contribution to the FCNCs at tree revel, we consider the alignment for the Yukawa sector proposed by Pich and Tuzon[71] as

$$y_{f,2}=\zeta_f\ y_{f,1}, \tag{4.22}$$

where ζ_f are complex values. Thus, $y_{f,1}$ and $y_{f,2}$ are diagonalized at the same time, and then ρ_f are expressed by

$$\rho_u=\frac{\sqrt{2}}{v}M_u\zeta_u^* \tag{4.23}$$

$$\rho_{d,e}=\frac{\sqrt{2}}{v}M_{d,e}\zeta_{d,e}. \tag{4.24}$$

There is another prescription to avoid the FCNCs suggested by Glashow and Weinberg[91], in which an invariance of the Lagrangian under the Z_2 transformation: $\Phi'_1\to\Phi'_1$ and $\Phi'_2\to-\Phi'_2$ forbids one of the Yukawa matrices $y'_{k,f}$. There are four types of Yukawa interactions depending on the Z_2 charge assignment for the right-handed fermions[92, 93]. The ζ_f factors in each model are summarized in Tab. 4.1.

In the basis of the mass eigenstates of the fermions and the Higgs bosons, the Yukawa interaction term is written as

$$\mathcal{L}_{\rm yukawa}\supset-\sum_{f=u,d,e}\left\{\bar{f}_LM_ff_R+\sum_{j=1}^{3}\bar{f}_L\left(\frac{M_f}{v}\kappa_f^j\right)f_RH_j^0+h.c.\right\}$$

$$-\frac{\sqrt{2}}{v}\left\{-\zeta_u \bar{u}_R (M_u^\dagger V_{\rm CKM}) d_L + \zeta_d \bar{u}_L (V_{\rm CKM} M_d) d_R + \zeta_e \bar{\nu}_L M_e e_R\right\} H^+ + h.c., \tag{4.25}$$

where κ_f^j are the coupling factors for the interactions of the neutral Higgs bosons to the fermions which are given as[69]

$$\kappa_f^j = \mathcal{R}_{1j} + \left[\mathcal{R}_{2j} + i(-2I_f)\mathcal{R}_{3j}\right] |\zeta_f| e^{i(-2I_f)\theta_f}, \tag{4.26}$$

where $\theta_f \equiv \arg[\zeta_f] \in (-\pi, \pi]$ and $I_u = 1/2, I_d = I_e = -1/2$. As we mentioned above, due to the alignment of the Higgs potential $\mathcal{R}_{jk} = \delta_{jk}$, κ factors are written as

$$\kappa_f^1 = 1, \tag{4.27}$$
$$\kappa_f^2 = |\zeta_f| e^{i(-2I_f)\theta_f}, \tag{4.28}$$
$$\kappa_f^3 = i(-2I_f)\kappa_f^2. \tag{4.29}$$

We can see that the Yukawa couplings for H_1^0 are not affected by the CP-violating phases at tree-level, while those of $H_{2,3}^0$ have the CP-violating phases.

4.1.3 Kinetic term of the scalar fields

The kinetic term for the scalar doublet fields is given by[69]

$$\mathcal{L}_{\rm kin} = |D_\mu \Phi'_1|^2 + |D_\mu \Phi'_2|^2 = |D_\mu \Phi_1|^2 + |D_\mu \Phi_2|^2, \tag{4.30}$$

where D_μ is the covariant derivative as $D_\mu = \partial_\mu + i g_2 \frac{\sigma^a}{2} W_\mu^a + i g_1 \frac{1}{2} B_\mu$ with g_2 and g_1 being the $\mathrm{SU}(2)_L$ and $\mathrm{U}(1)_Y$ gauge coupling constants, respectively. In the mass eigenstates of the gauge bosons and Higgs bosons, the trilinear Higgs-gauge-gauge type couplings are expressed as

$$\mathcal{L}_{\rm kin} \supset \sum_j^3 \mathcal{R}_{1j} \left(\frac{2m_W^2}{v} W_\mu W^\mu + \frac{m_Z^2}{v} Z_\mu Z^\mu\right) H_j^0, \tag{4.31}$$

where the masses of the gauge bosons are defined as $m_W = g_2 v/2$ and $m_Z = \sqrt{g_2^2 + g_1^2}\, v/2$. When the alignment limit $\mathcal{R}_{jk} = \delta_{jk}$ is taken, the couplings of $H_1^0 VV$ ($V = W,\ Z$) are the same as the SM ones, and those of $H_2^0 VV$ and $H_3^0 VV$ vanish at tree level.

4.1.4 Theoretical and experimental constraints

The perturbative unitarity[94, 95, 96, 97] and the vacuum stability[98, 99] give the constraint on the parameters of the Higgs potential. The electroweak S, T and U

parameters[100, 101] constraining the masses and mixings of the Higgs bosons are also considered. New contributions to the T parameter from the additional Higgs bosons vanish at one-loop level by imposing $m_{H_3} = m_{H^\pm}$ and $\lambda_6 = 0$, because of the custodial symmetry in the Higgs potential[102, 103, 104, 105, 106]. In addition, the constraints from the flavor experiments such as B physics are considered[107]. For the constraint on the mass of charged Higgs bosons and ζ_q in the Yukawa-alignment scenario, we refer to Ref. [108]. For instance, for $m_{H^\pm} = 200$ GeV, we estimate the upper limit of $|\zeta_u^* \zeta_d|$ to be 0.32 (2.4) for $\arg[\zeta_u^* \zeta_d] = 0$ (1) by using the relation of the constrained combination $\zeta_u^* \zeta_d / m_{H^\pm}^2$ for $|\zeta_u| \ll |\zeta_d|$. The EDM experiments constraining new CP-violating effects are discussed in next section.

4.2 Scenario cancelling the electric dipole moment

We have studied about the scenario without the large EDM in our paper[69] which we review in this section.

4.2.1 Constraint from the electric dipole moment data

As we mentioned above, the ACME collaboration using the thorium-monoxide EDM gave the upper limit $|d_e + kC_S| < 1.1 \times 10^{-29}$ e cm at the 90% CL[81]. According to the discussion given in Refs. [47, 45], the value of kC_S is typically two orders of magnitude smaller than the current bound in our benchmark scenarios which are introduced below. Therefore, we neglect this contribution, and we simply consider the bound on the electron EDM as $|d_e| < 1.1 \times 10^{-29}$ e cm (90% CL) in the following discussion. In addition, the nEDM collaboration updated the constraint on the neutron EDM as $|d_n| < 1.8 \times 10^{-26}$ e cm (90% CL)[82] as we also mentioned above. In our analysis, we estimate the neutron EDM by using the following QCD sum rule[46, 109, 110, 111]

$$d_n = 0.79 d_d - 0.20 d_u + e(0.59 d_d^C + 0.30 d_u^C)/g_3, \tag{4.32}$$

where g_3 is the QCD gauge coupling constant. The Weinberg operator and the four-fermi interaction also give contributions to the neutron EDM. According to the discussion given in Refs. [41, 47, 45] (Ref. [45]), the contribution from $C_W (C_{ff'})$ is typically given as two (more than two) orders of magnitude smaller than the current bound in our benchmark scenarios. Thus, we simply apply Eq. (4.32) to our analysis.

Finally, the other EDM data of atoms is satisfied by considering the constraints for the above electron and the neutron EDMs. Hereafter, we concentrate on the contributions from d_f ($f = e$, d and u) and d_q^C ($q = d$ and u).



(4.1-a) Fermion-loop (4.1-b) Higgs boson-loop

Figure 4.1: BZ type diagrams contributing to the electron EDM. The figures are given by Ref. [69].

4.2.2 Destructive interference between the Barr-Zee type contributions

In this model, the dominant contributions to d_f are given by the two-loop BZ type diagrams[84] as we mention above. In the Yukawa-aligned THDM, we have evaluated analytically the each contribution $d_f^V(X)$ ($V = \gamma, Z$ and W) defined in Eqs. (3.15) and (3.16), and he explicit formulae for each contribution to d_f are given in Appendix B. The gauge boson-loop contributions d_e(gauge) are proportional to $\sum_{j=1}^{3} \mathcal{R}_{1j}\mathrm{Im}[\kappa_f^j]$, so that this contribution vanishes by imposing the alignment of the Higgs potential $\mathcal{R}_{ij} = \delta_{ij}$. Because the non-BZ type diagrams at two-loop level with Higgs bosons and gauge bosons mediation are also proportional to $\sum_{j=1}^{3} \mathcal{R}_{1j}\mathrm{Im}[\kappa_f^j]$, according to the discussion given in Refs.[43, 45], they vanish in the alignment limit. In this case, the gauge dependent terms of the d_f also vanish. Consequently, the dominant contributions to d_f are given by the Higgs boson and fermion-loops as shown in Fig. 4.1.

We consider the destructive interference between the contributions from the fermion-loop and Higgs boson-loop. Requiring $d_e \simeq 0$ and a finiteness of each contribution, we get the relation between the CP-violating parameters. When nearly degeneracy of the extra Higgs boson masses and $\theta_d = 0$ are assumed, the relation is given as[69]

$$\left(A^\gamma I^\gamma + A^Z I^Z + A^W I^W\right) |\zeta_u| \sin(\theta_u - \theta_e) \simeq -\left(B^\gamma J^\gamma + B^Z J^Z + B^W J^W\right) |\lambda_7| \sin(\theta_7 - \theta_e), \tag{4.33}$$

where A and B are the constant factors:

$$A^\gamma = \frac{32}{3} \sin^2\theta_W \frac{m_t^2}{v^2}, \tag{4.34}$$

$$A^Z = \frac{1}{3} \frac{(1 - 4\sin^2\theta_W)(3 - 8\sin^2\theta_W)}{\cos^2\theta_W} \frac{m_t^2}{v^2}, \tag{4.35}$$

$$A^W = 3\frac{m_t^2}{v^2}, \tag{4.36}$$

$m_u = 1.29 \times 10^{-3}$,	$m_c = 0.619$,	$m_t = 171.7$	
$m_d = 2.93 \times 10^{-3}$,	$m_s = 0.055$,	$m_b = 2.89$	
$m_e = 0.487 \times 10^{-3}$,	$m_\mu = 0.103$,	$m_\tau = 1.746$	(in GeV)
$\alpha_{\rm em} = 1/127.955$,	$m_Z = 91.1876$ GeV,	$m_W = 80.379$ GeV,	$\alpha_S = 0.1179$
$\lambda = 0.22453$,	$A = 0.836$,	$\bar{\rho} = 0.122$,	$\bar{\eta} = 0.355$

Table 4.2: Input values for the SM parameters at the m_Z scale. The fermion masses at m_Z given in Refs. [112, 113]. The other parameters in the table are taken in Ref. [114]. The Wolfenstein parameters of the CKM matrix λ, A, $\bar{\rho}$ and $\bar{\eta}$ are defined in Ref. [114].

$$B^\gamma = 4\sin^2\theta_W, \tag{4.37}$$

$$B^Z = \frac{1}{2}\frac{(1-4\sin^2\theta_W)}{\cos^2\theta_W}\cos 2\theta_W, \tag{4.38}$$

$$B^W = -\frac{1}{2}, \tag{4.39}$$

and I and J are the loop functions depending on the masses of the extra Higgs bosons:

$$I^V = 2\int_0^1 dz \left[\frac{1}{z} - (1-z)\right] C_{tt}^{V\tilde{H}}(z), \qquad (V = \gamma \text{ and } Z), \tag{4.40}$$

$$I^W = \int_0^1 dz \frac{2-z}{z}\left[\frac{2}{3} - z\right] C_{tb}^{W\tilde{H}}(z), \tag{4.41}$$

$$J^V = 2\int_0^1 dz (1-z) C_{\tilde{H}\tilde{H}}^{V\tilde{H}}(z), \qquad (V = \gamma, Z \text{ and } W), \tag{4.42}$$

where $C_{XY}^{GH}(z)$ are given in Appendix B, and its argument $m_{\tilde{H}}$ denotes the mass of the extra Higgs bosons in the loop. From Eq. (4.33), it is clear that the two independent phases θ_u (or θ_e) and θ_7 can be taken such that the fermion- and the Higgs boson-loop contributions to d_e cancel with each other.

4.2.3 Numerical analysis for the aligned two Higgs doublet model

Hereafter, we show the numerical result reported in our paper[69]. We have numerically calculated the electron EDM with the SM input parameters given in Tab. 4.2. As we mentioned in Sec. 4.1, we assume $m_{H_3^0} = m_{H^\pm}$ to avoid the constraint from the electroweak T parameter in the following analysis. In Fig. 4.2, the contour plot of the electron EDM is shown as a function of $m_{H_2^0}$ and $m_{H^\pm}(= m_{H_3^0})$ with $(\theta_u, \theta_d, \theta_e, \theta_7) = (2, 0, \pi/2, 1)$, $|\lambda_7| = 0.3$, $|\zeta_u| = 0.01$, $|\zeta_d| = 0.1$ and $|\zeta_e| = 0.5$ at the scale m_Z. The green

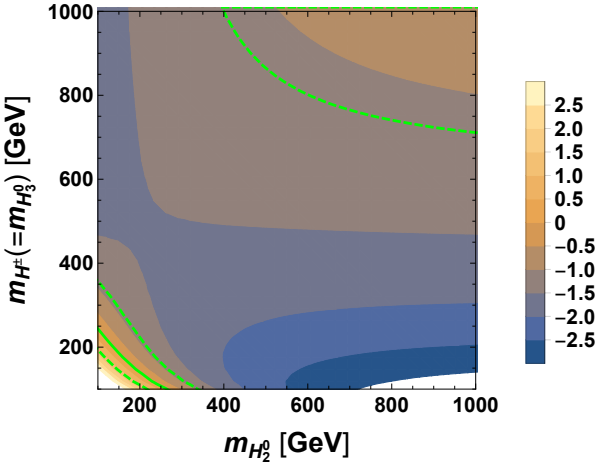


Figure 4.2: Contour plot for the electron EDM d_e in the unit of 10^{-29} e cm as a function of $m_{H_2^0}$ and $m_{H^\pm}(= m_{H_3^0})$ with $(\theta_u, \theta_d, \theta_e, \theta_7) = (2, 0, \pi/2, 1)$, $|\lambda_7| = 0.3$, $|\zeta_u| = 0.01$, $|\zeta_d| = 0.1$ and $|\zeta_e| = 0.5$ at the scale m_Z in the panel. The green solid line denotes $d_e = 0$ and the area between the green dashed lines is the allowed region against the constraint from the electron EDM. The figure is given by Ref. [69].

solid line corresponds to $d_e = 0$ and the green dashed lines corresponds to $|d_e| = 1.1$ as the current bounds of the electron EDM. When the masses of the extra Higgs bosons are $\mathcal{O}(200)$ GeV, d_e is getting close to 0. If one of the extra Higgs boson has much larger mass than that of the others, $|d_e|$ is getting larger because the cancellation becomes weaker. On the other hand, if all the masses are taken to be larger up to about 400 GeV, $|d_e|$ becomes larger because of the same reason. If they are further taken to be larger, $|d_e|$ becomes smaller due to the decoupling behavior of the extra Higgs bosons.

In the left (right) panel of Fig. 4.3, the contour plot of the electron EDM is shown as a function of θ_u and θ_7 in the case with $m_{H_2^0} = 280$, $m_{H^\pm} = 230$, $|\lambda_7| = 0.3$, $|\zeta_u| = 0.01$, $|\zeta_d| = 0.1$, $|\zeta_e| = 0.5$, $\theta_d = 0$ and $\theta_e = 0$ $(\pi/4)$. Similar to Fig. 4.2, the green solid line denotes $d_e = 0$ and the green dashed lines corresponds to $|d_e| = 1.1$ as the current bounds of the electron EDM. The magnitude of the electron EDM $|d_e|$ gets maximal value at around $(\theta_u, \theta_7) = (\pm\pi/2, \pm\pi/2)$ in the left panel. We find that there are regions realizing $d_e \simeq 0$ away from $(\theta_u, \theta_7) = (0, 0)$ due to the destructive interference. In the right panel, the shape of the contour is shifted to the upper-right region from that of the left panel. Similarly, we find the regions realizing $d_e \simeq 0$ away from $(\theta_u, \theta_7) = (0, 0)$. For instance, we get $d_e = -0.95 \times 10^{-29}$ e cm[69] at the point $(\theta_u, \theta_7) = (1.2, -1.8)$ marked by the star in the right panel of Fig. 4.3.

Therefore, we have shown that there are $\mathcal{O}(1)$ CP-violating phases satisfying the

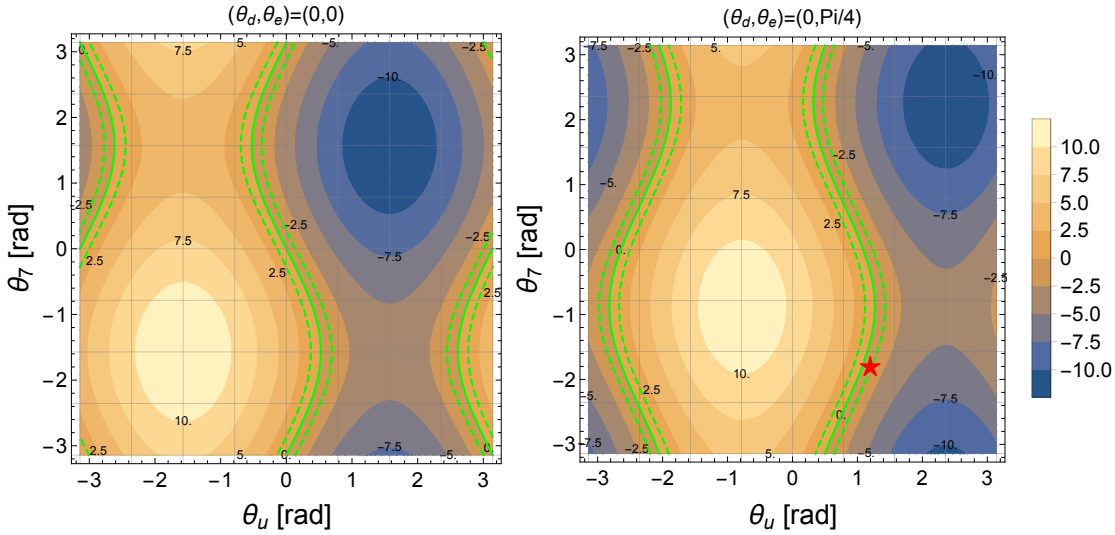


Figure 4.3: Contour plot for the electron EDM d_e in the unit of 10^{-29} e cm as a function of θ_u and θ_7 in the case with $m_{H_2^0} = 280$, $m_{H^\pm} = 230$, $|\lambda_7| = 0.3$, $|\zeta_u| = 0.01$, $|\zeta_d| = 0.1$ and $|\zeta_e| = 0.5$. The left (right) panel corresponds to the case with $\theta_d = 0$ and $\theta_e = 0$ $(\pi/4)$. The green solid lines denote $d_e = 0$ and the area between the green dashed lines is the allowed region against the constraint from the electron EDM. In the right panel, $d_e = -0.95 \times 10^{-29}$ e cm at the point marked by the star $(\theta_u, \theta_7) = (1.2, -1.8)$. The figure is given by Ref. [69].

constraints on d_e and d_n due to the destructive interference. In addition, we have found that to realize the destructive effects, the masses of $\mathcal{O}(100)$ GeV of the additional Higgs bosons are required. We note that in the parameter allowed region of d_e, which we take above, the neutron EDM is typically two orders of magnitude smaller than the current upper limit[69].

4.2.4 Future experiment for the electric dipole moment

Several future experiments for the electron and neutron EDM are planned. For example, the upper bounds on the electron and neutron EDM might be improved to be one order of the magnitude smaller than the current one, such as around 10^{-30} e cm[115] and 10^{-27} e cm[116], respectively If such an improvement for the electron EDM is realized, the widths of the allowed region in Figs. 4.2 and 4.3 are made about 1/10. On the other hand, although the improvement for the neutron EDM can give the upper limit for θ_u, since the predicted value of the neutron EDM is two orders of magnitude smaller than the current bound in our scenario, the allowed region is thus not changed. The sensitivity for the neutron EDM might reach around 10^{-28} e cm level by using spallation neutron sources[117]. Moreover, an experiment for the proton EDM with the accuracy of 10^{-29} e cm level[118] is also planned These experiments might play a complementary role to prove our scenario in the future.

4.3 Renormalization group equation analysis

In order to see the stability of our scenario, we have also studied about the behavior of the destructive cancellation at the high energy by the RGE analysis in our paper[69]. We have discussed the scale dependence of the electron EDM d_e which satisfies the current data at the scale of m_Z by the destructive interference. We have evaluated the running of all the dimensionless couplings of the THDM from the m_Z scale to a high energy scale by using the one-loop β-functions given in Appendix D.

First, we consider the scale dependence of the Yukawa interaction which are aligned at the scale of m_Z. The degree of the alignment can be parametrized as[119]

$$\Delta_q \equiv \mathrm{Tr}[\delta y_q^\dagger \delta y_q], \quad \text{where} \quad \delta y_q \equiv \hat{\rho}_q - \left(\frac{\hat{\rho}_q^{33}}{\hat{M}_q^{33}}\right)\hat{M}_q, \quad (q = u, d). \tag{4.43}$$

We note that Δ_q vanishes when the alignment are realized. In Fig. 4.4, the running behavior of Δ_u (left) and Δ_d (right) is shown. It has seen that both of Δ_q are significantly small up to a high energy scale such as at least about 10^{10} GeV where the Landau pole appears (see the discussion below). The alignment is stable because the source of the

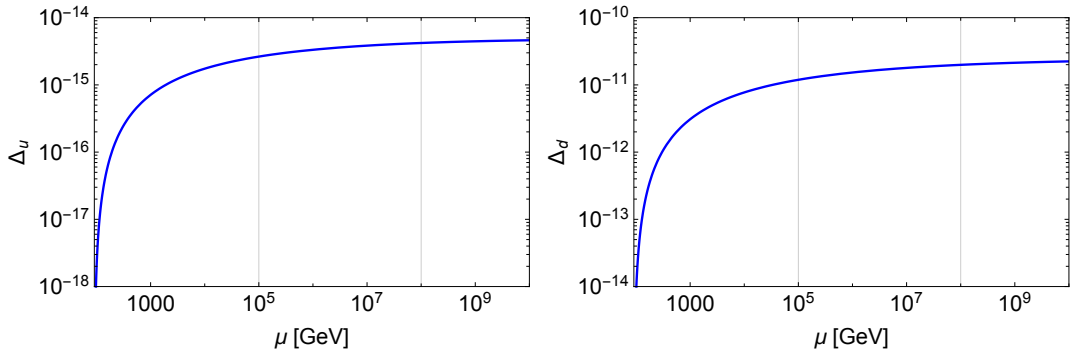


Figure 4.4: RGE running of the parameter defined in Eq. (4.43) from m_Z with the benchmark parameters given in Tab. 4.3. The figures are given by Ref. [69].

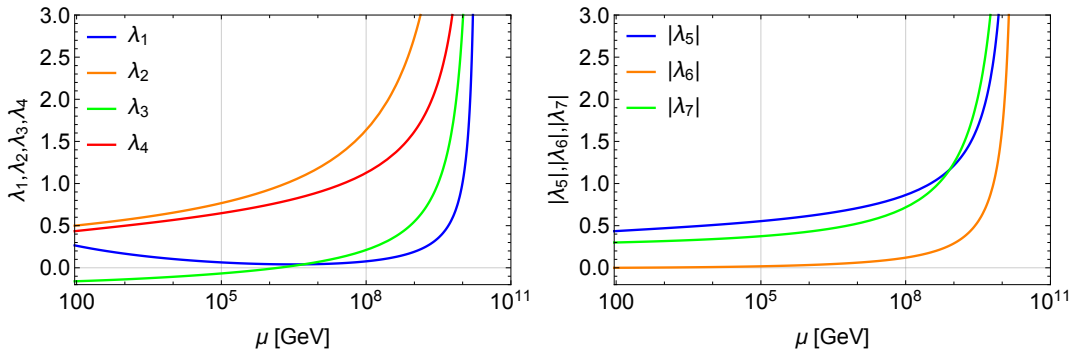


Figure 4.5: RGE-running behavior of the Higgs self couplings from m_Z with the benchmark parameters given in Tab. 4.3. The left (right) panel corresponds to $\lambda_{1\text{-}4}$ ($|\lambda_{5\text{-}7}|$). The figures are given by Ref. [69].

breaking of the alignment mainly arises from the tiny off-diagonal elements of the CKM matrix[69].

Next, we consider the scale dependence of the parameters of the Higgs potential which are aligned at the scale of m_Z. The degree of the alignment can be seen by looking at the running of the λ_6 parameter, see Eq. (4.8). In Fig. 4.5, the scale dependence of all the dimensionless parameters in the Higgs potential is shown. It has seen that the growth of the $|\lambda_6|$ parameter is quite slow for the scale, and it blows up together with all the other couplings at around $\mu = 10^{10}$ GeV which is the scale appearing the Landau pole. Therefore, the alignment of the Higgs potential is stable up to such a high energy scale in our scenario[69].

$M = 240,$	$m_{H_2^0} = 280,$	$m_{H_3^0} = 230,$	$m_{H^\pm} = 230$	(in GeV)
$\|\zeta_u\| = 0.01,$	$\|\zeta_d\| = 0.1,$	$\|\zeta_e\| = 0.5,$	$\|\lambda_7\| = 0.3,$	$\lambda_2 = 0.5$
$\theta_u = 1.2,$	$\theta_d = 0,$	$\theta_e = \pi/4,$	$\theta_7 = -1.8$	(in rad)

Table 4.3: Input values for the THDM at the scale m_Z. The table is given by Ref. [69].

Finally, we discuss the scale dependence of d_e which can be evaluated by

$$\mu\frac{\partial}{\partial\mu}\hat{d}_e(\mu) = \mu\frac{\partial}{\partial\mu}\hat{d}_e(\text{fermion})(\mu) + \mu\frac{\partial}{\partial\mu}\hat{d}_e(\text{Higgs})(\mu) + \mu\frac{\partial}{\partial\mu}\hat{d}_e(\text{gauge})(\mu), \qquad (4.44)$$

where the contribution from the gauge boson loop $\hat{d}_e(\text{gauge})$, which vanishes at m_Z scale, appears at higher energy scales, because of the breaking of the alignment of theHiggs potential. In addition, the SM-like Higgs boson H_1^0 is no longer the pure CP-even state at higher energy scales, so that a H_1^0 contribution to $\hat{d}_e$ appears as well as H_2^0 and H_3^0. In Fig. 4.6, the scale dependence of $\hat{d}_e$ and the contributions $\hat{d}_e(X)$ (X=fermion, Higgs and gauge) are shown, where subdominant contributions from non-BZ type diagrams is neglected. It has seen that the cancellation between $\hat{d}_e(\text{fermion})$ and $\hat{d}_e(\text{Higgs})$ is kept up to a higher energy scales. However, due to the growth of $\hat{d}_e(\text{gauge})$, the total value is getting larger, and it exceeds $|d_e| = 1.747 \times 10^{-16}$ GeV^{-1}, which is the current bounds given at low energy scale, at around $\mu = 10^8$ GeV[69]. The value of $\hat{d}_e$ at the high energy scale is not the value constrained by experiments. However, it would be viable to see the stability of the relation between the parameters for the destructive cancellation at the m_Z scale [4] .

4.4 Collider signals

In this section, we discuss the test of the scenario cancelling the EDM at future lepton collider. In our scenario, the alignment limit of the Higgs potential $\mathcal{R}_{ij} = \delta_{ij}$ are assumed, so that the couplings of the SM-like Higgs boson H_1 are the same as those of the SM Higgs boson at tree level. Thus, the phenomenology of the extra Higgs bosons can be important to test our scenario.

[4]There is the study about the stability of the alignment of the Higgs potential from high energy at which the twisted custodial symmetry imposed[68]. However, in this case, the twisted custodial symmetry respect the CP conservation of the Higgs potential.

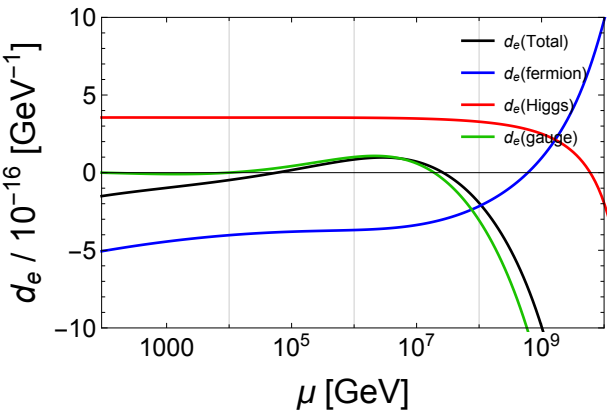


Figure 4.6: RGE running of the electron EDM from m_Z with the benchmark parameters given in Tab. 4.3. The figure is given by Ref. [69].

4.4.1 Production of the extra Higgs bosons

Proton proton collider

As we discussed above, we consider the alignment scenario in which the vertices H_2^0VV and H_3^0VV $(V = W, Z)$ vanish at tree level. On the other hand, for the charged Higgs bosons, the $H^\pm W^\mp Z$ vertex generally does not appear at tree level in THDMs [120, 121, 122], because we can define the Higgs basis, see Eqs. (4.2) and (4.3). In addition, because of the $U(1)_{\rm em}$ invariance, the $H^\pm W^\mp \gamma$ vertex does not appear at tree level in any kind of extension of the Higgs sector. Therefore, the extra Higgs bosons can be produced via the Yukawa interactions such as $gg \to H_j^0$ (gluon fusion), $gg \to t\bar{t}H_j^0$ (top quark associated production), $gg \to b\bar{b}H_j^0$ (bottom quark associated production) and $gb \to H^\pm t$ (gluon-bottom fusion) where $j = 2, 3$. They are also produced by the following pair production processes with the s-channel gauge boson mediations as $q\bar{q} \to Z^* \to H_2^0 H_3^0$, $q\bar{q}' \to W^* \to H^\pm H_j^0$ and $q\bar{q} \to Z^*/\gamma^* \to H^+H^-$.

For the the neutral Higgs bosons, the cross section is mainly given from the gluon fusion process. We refer the LHC Higgs Cross Section Working Group [123] at N3LO in QCD. As we discussed in our paper[69], the cross section of top (bottom) quark associated production are quantitatively small in the scenario with the extra Higgs bosons of $\mathcal{O}$ (200) GeV and $\zeta_u = 0.01$ and $\zeta_d = 0.1$. According to [123], $\sigma^{\rm SM}_{t\bar{t}h}$ ($\sigma^{\rm SM}_{b\bar{b}h}$) is given about 120 (100) fb at NLO in QCD for $m_h = 200$ GeV and $\sqrt{s} = 13$ TeV where $\sigma^{\rm SM}_{t\bar{t}h}$ ($\sigma^{\rm SM}_{b\bar{b}h}$) is the cross section for $gg \to t\bar{t}h$ ($gg \to b\bar{b}h$) in the SM. In our scenario, the cross section estimated as $\sigma^{\rm SM}_{t\bar{t}h} \times |\zeta_u|^2$ ($\sigma^{\rm SM}_{b\bar{b}h} \times |\zeta_d|^2$) is negligibly small because of the small coupling $|\zeta_u| = 0.01$ ($|\zeta_d| = 0.1$). The cross sections for the gluon fusion and the bottom quark associated processes with the varying mass of the extra Higgs boson are

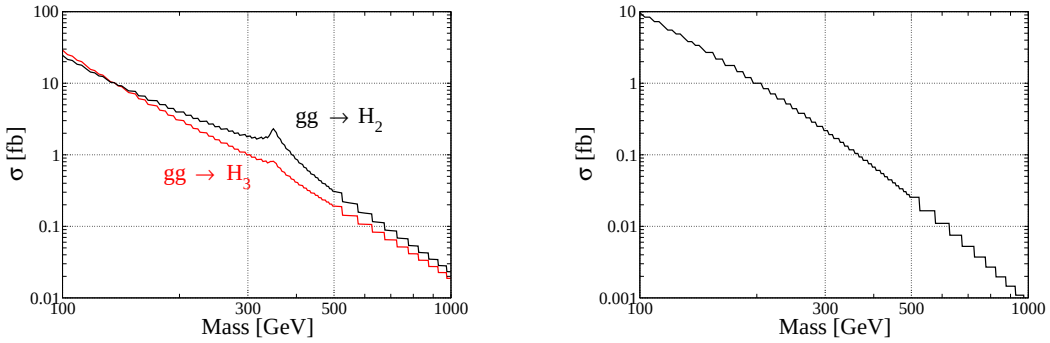


Figure 4.7: Cross section for $gg \to \phi^0$ (left) and $gg \to b\bar{b}\phi^0$ (right) at $\sqrt{s} = 13$ TeV ($\phi^0 = H_2$ or H_3) with $|\zeta_u| = 0.01$, $|\zeta_d| = 0.1$, $\theta_u = 1.2$ and $\theta_d = 0$. The figures are given by Ref. [69].

shown in Fig. 4.7. It is seen that the cross section of the gluon fusion process is typically one order of magnitude larger than that of the bottom quark associated process.

As we also discussed in our paper[69], the charged Higgs boson is produced by the top decay $t \to H^{\pm} b$ in the scenarios with $m_{H^{\pm}} < m_t$ which have already been highly constrained by the current LHC data [124, 125]. In our scenarios with $m_{H^{\pm}} > m_t$, the charged Higgs boson is produced by the gluon-bottom fusion process whose cross section with the varying $m_{H^{\pm}}$ is shown in Fig. 4.8. NLO corrections in QCD have been discussed in Refs. [126, 127].

Finally, we consider the pair production processes. Since thees cross sections are determined by the gauge coupling, these production processes are important even when the values of the Yukawa coupling parameters ζ_f are small. The cross sections with the varying masses of the extra Higgs bosons is shown in Fig. 4.9. We can see that these cross sections can be larger than those given by the single production processes in the wide range of the mass region in our scenario.

Electron positron collider

As we have discussed above, since the couplings of $H_j^0 VV$ ($j = 2, 3$) vanish at tree level due to the alignment of the Higgs potential, the extra Higgs boson is not produced via the Higgs-strahlung process and the vector boson fusion at the electron positron collider. Therefore, the pair production of the additional Higgs bosons is important to test our scenario. The following processes are considered.

$$e^+ e^- \to H_2^0 H_3^0, \tag{4.45}$$

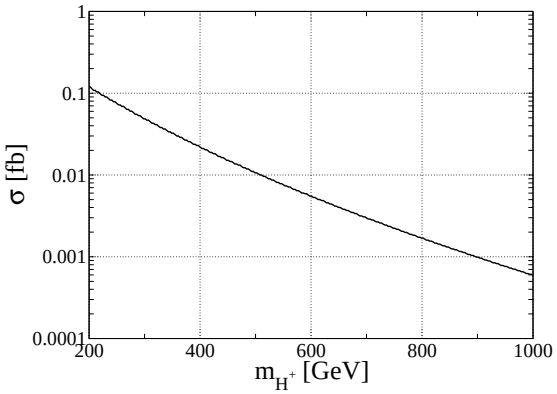


Figure 4.8: Cross section for $gb \to H^- t$ at $\sqrt{s} = 13$ TeV with $|\zeta_u| = 0.01$, $|\zeta_d| = 0.1$, $\theta_u = 1.2$ and $\theta_d = 0$. The figure is given by Ref. [69].

$$e^+e^- \to \nu\bar{\nu}H_2^0 H_3^0, \tag{4.46}$$

whose diagrams are shown in Fig. 4.10. The cross sections as a function of the collision energy $\sqrt{s}$ are shown in Fig. 4.11. It is seen that the cross section of $e^+e^- \to \nu\bar{\nu}H_2^0 H_3^0$ is more than three order of the magnitude smaller than that of $e^+e^- \to H_2^0 H_3^0$[70]. Therefor, we focus on $e^+e^- \to H_2^0 H_3^0$ as promising process to test the CP violation.

4.4.2 Decay of the extra Higgs bosons

We discuss the branching ratios of the extra Higgs bosons. Since our scenario is assumed the alignment such as $\mathcal{R}_{jk} = \delta_{jk}$, the extra Higgs bosons are mainly decay into a fermion pair. If it is kinematically allowed, they can also decay into a (off-shell) gauge boson and another Higgs boson. In addition, although there are loop-induced decay processes such as $H_{2,3}^0 \to \gamma\gamma, Z\gamma, gg$ and $H^\pm \to W^\pm Z, W^\pm\gamma$, except for the $H_{2,3}^0 \to gg$, the branching ratios of them are negligibly small; i.e., $BR(H_{2,3}^0 \to \gamma\gamma/Z\gamma)$ and $BR(H^\pm \to W^\pm Z, W^\pm\gamma)$[122] are typically smaller than $\mathcal{O}(10^{-4})$.

In Fig. 4.12, we show the branching ratios of H_2^0 (left), H_3^0 (center) and $H^\pm$ (right) as a function of the extra-Higgs-boson mass with $m_{H_2^0} - 50\,\text{GeV} = m_{H_3^0} = m_{H^\pm}$, $|\zeta_u| = 0.01$, $|\zeta_d| = 0.1$, $|\zeta_e| = 0.5$, $|\lambda_7| = 0.3$, $\theta_u = 1.2$, $\theta_d = 0$, $\theta_e = 0.79$ and $\theta_7 = -1.8$[70]. For H_3^0, the dominant decay modes are $\tau^+\tau^-$ and $b\bar{b}$ ($t\bar{t}$) with their branching ratios to be about 50 (80) % when the mass of H_3^0 is smaller (larger) than $2m_t$. On the other hand, H_2^0 mainly decays into $Z^* H_3^0$ and $W^{\pm *} H^\mp$ due to the mass difference, while the branching ratios of $H_2^0 \to \tau^+\tau^-$ and $b\bar{b}$ can be $\mathcal{O}(10)\%$ for $m_{H_2^0} < 2m_t$. For $H^\pm$, the main decay

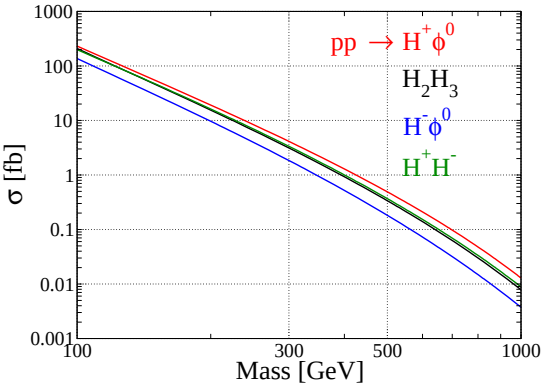


Figure 4.9: Cross sections for the pair production processes at $\sqrt{s} = 13$ TeV with $m_{H^\pm} = m_{H_2} = m_{H_3}$. The figure is given by Ref. [69].

mode is $\tau\nu$ (tb) if $m_{H^\pm}$ is smaller (larger) than the top mass.

$H^0_{2,3} \to \tau\tau$ is important from the viewpoint of the test of the CP violation as we discuss below. The decays of the heavy scalars into τ leptons have been looked for at the LHC. If the heavy scalars have the mass 200 GeV, the observed upper limit for the gluon-fusion cross-section is given by $O(100)$ fb[128] which is roughly two orders of magnitude larger than our cross section. Therefore, we can safely avoid the constraint from the current LHC data.

4.4.3 Angular distribution

If the extra Higgs bosons are produced, the CP-violating phases can be measured from their decay products at collider experiments in this scenario[69]. In our scenario, the CP-violating phases from the Yukawa interaction affect angular distributions of such decay products. On the other hand, the effect of the CP-violating phases of the Higgs potential do not directly appear in the decays of the extra Higgs bosons into fermions. However, if we can measure the CP-violating effect in the angular distributions, it indirectly proves the existence of the CP-violating phases in the Higgs potential because of the necessity of the cancellation of the EDM as discussed in Sec. 4.2.

In our model, the $H^0_j\tau\tau$ interaction is given as

$$\mathcal{L}_{H^0_j\tau\tau} = -\frac{m_\tau}{v}\bar{\tau}\left[\mathrm{Re}(\kappa^j_e) + i\mathrm{Im}(\kappa^j_e)\gamma_5\right]\tau H^0_j, \tag{4.47}$$

thus, the $\Delta\phi$ distributions for $H^0_{2,3}$, which are the angular distributions of the decay

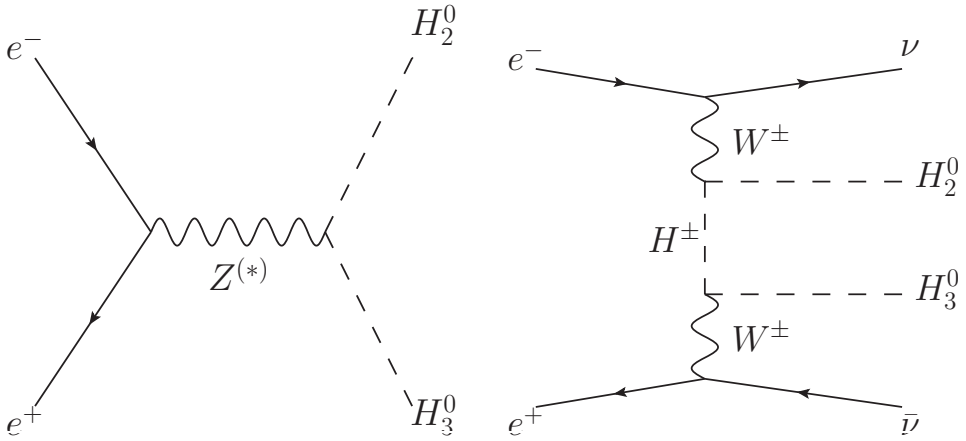


Figure 4.10: Feynman diagrams of the pair production of the heavy Higgs bosons. The figures are given by Ref. [70].

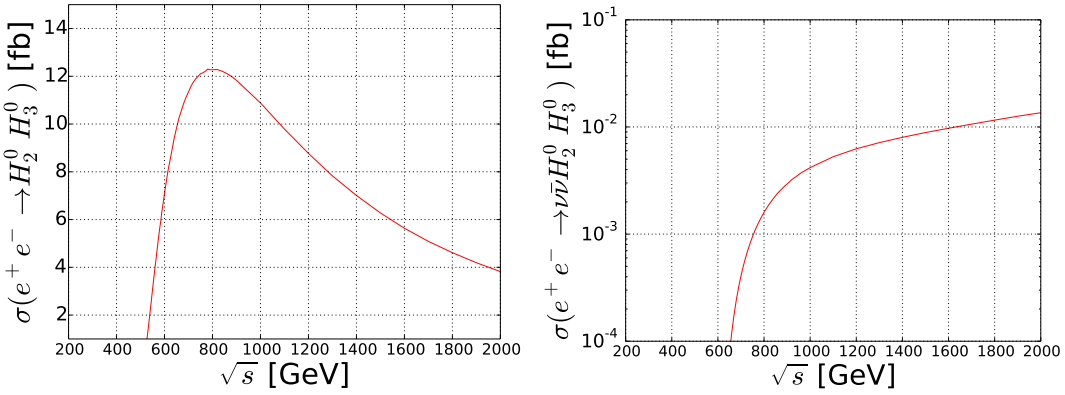


Figure 4.11: Cross section of $e^+e^- \to H_2^0 H_3^0$ ($e^+e^- \to \nu\bar{\nu} H_2^0 H_3^0$) at $\sqrt{s} = 500$, 750 and 1000 GeV for the scenario with $(\theta_u, \theta_d, \theta_e, \theta_7) = (1.2, 0, \pi/4, 0)$, $|\lambda_7| = 0.3$, $|\zeta_u| = 0.01$, $|\zeta_d| = 0.1$ and $|\zeta_e| = 1$ We take $m_{H_2} = m_{H_3} = m_{H^\pm} = M$ in the left (right) panel. The figures are given by Ref. [70].

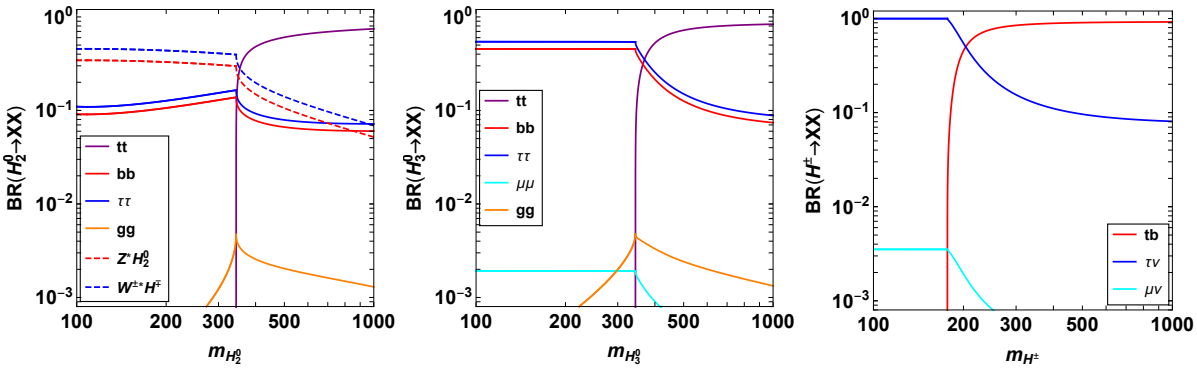


Figure 4.12: Branching ratios of H_2^0 (left), H_3^0 (center) and $H^{\pm}$ (right) as the function of the extra-Higgs-boson mass with $m_{H_2^0} - 50$ GeV $= m_{H_3^0} = m_{H^{\pm}}$, $|\zeta_u| = 0.01$, $|\zeta_d| = 0.1$, $|\zeta_e| = 0.5$, $|\lambda_7| = 0.3$, $\theta_u = 1.2$, $\theta_d = 0$. $\theta_e = 0.79$ and $\theta_7 = -1.8$. The figures are given by Ref. [70].

products of tau leptons produced by $H_{2,3}^0 \to \tau^+\tau^-$ given by Eq.(3.35), are obtained as[69]

$$\int\int d\cos\theta^- d\cos\theta^+ \; \overline{|\mathcal{M}(H_2^0 \to \tau^-\tau^+ \to X^-\nu X^+\bar{\nu})|^2} \propto 16 - \pi^2\cos(2\theta_\tau - \Delta\phi), \tag{4.48}$$

$$\int\int d\cos\theta^- d\cos\theta^+ \; \overline{|\mathcal{M}(H_3^0 \to \tau^-\tau^+ \to X^-\nu X^+\bar{\nu})|^2} \propto 16 - \pi^2\cos(2\theta_\tau - \Delta\phi + \pi). \tag{4.49}$$

The normalized distribution for the decay of H_2^0 (H_3^0) can be plotted in the left (right) panel of Fig. 4.13. It is clear that the $\Delta\phi$ distributions are depend on the value of θ_e. In the next section, we perform the signal and background simulation in order to investigate whether we can extract the information of the CP violation in our scenario from the $\Delta\phi$ distributions at future colliders.

The reconstruction method of the momenta of the tau leptons in the hadronic decays which contains one neutrino has been proposed in Ref. [129]. By using the information of the production vertex of the tau lepton, the impact parameters of the decay products of the tau leptons and the transverse momentum on the $\tau^+\tau^-$ system, the momenta of the tau leptons can be fully reconstructed. In Ref. [63], they focus on the Higgs-strahlung process ($e^+e^- \to Zh^{SM}$) with the decay of Z into electrons, muons and hadrons with the consideration of the detection of the all the Z decay products.

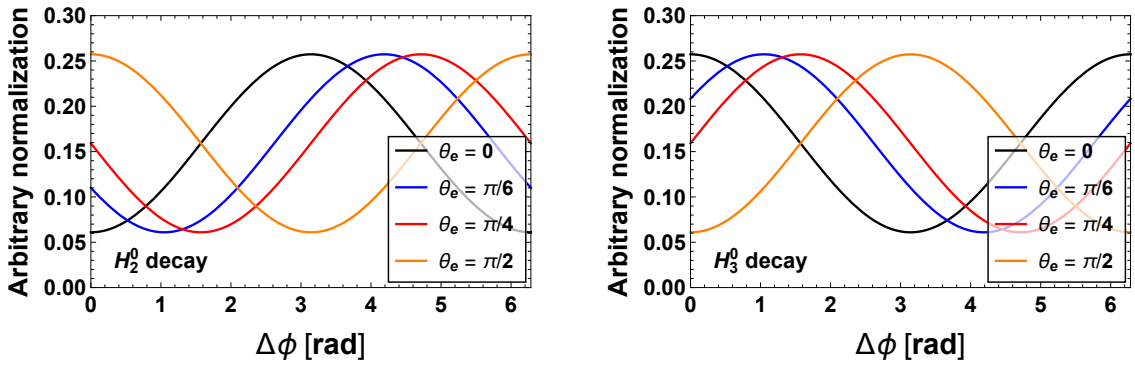


Figure 4.13: Analytical prediction. Normalized $\Delta\phi$ distributions for $H_j^0 \to \tau^-\tau^+ \to X^-\nu X^+\bar{\nu}$ with j =2 (left) and 3 (right). The figures are given by Ref. [70].

4.5 Simulation studies at future lepton colliders

In this section, we discuss the testability of the scenario cancelling the EDM, which are discussed in our paper[69], at future lepton colliders. In particular, we investigate the feasibility of measuring the effect of the CP-violating phases at the ILC.

By taking into account the decay property of the additional Higgs bosons and the reconstruction of the azimuthal angle $\Delta\phi$, the $e^+e^- \to b\bar{b}\tau^+\tau^-$ process is useful to test the CP-violating phase. We set the benchmark point given in Tab. 4.3. This benchmark point is marked as the star in the right panel of Fig. 4.3. Assuming the expected performance of the ILC[27, 28], we take the beam polarization that -80% for the electron beam and $+30\%$ for the positron beam[5], by which the cross section of $e^+e^- \to H_2^0 H_3^0$ is enhanced. The center mass of the energy $\sqrt{s}$ is assumed to be 800 GeV, where the cross section of $e^+e^- \to H_2^0 H_3^0$ is maximized. Then we obtain the cross section of $e^+e^- \to H_2^0 H_3^0$ to be 12.3 fb and the decay rates of $H_2^0(H_3^0) \to \tau^+\tau^-$ and $H_2^0(H_3^0) \to b\bar{b}$ to be 11.8% (54.2%) and 9.92% (45.5%), respectively. The total decay width of $H_2^0(H_3^0)$ is given as 1.23×10^{-3} (2.20×10^{-4}) GeV.

We consider two types of the background processes[70]. The first one has exactly the same final state as that of the signal process, which arises from the pair production of the neutral (off-shell) gauge bosons (Fig. 4.14-a), the Higgs-strahlung process (Fig. 4.14-b) and the Drell-Yan processes (Fig. 4.14-c). The other one comes from the $t\bar{t}$ production with the top decay: $t \to bW \to b\tau\nu$ (Fig. 4.14-d).

We perform the simulation study using MadGraph5[75] for generating the $e^+e^- \to b\bar{b}\tau^+\tau^-(\nu\bar{\nu})$ events which are passed to TauDecay[61] in order to consider the hadronic

[5]The beam polarization is expressed as $(N_R - N_L)/(N_R + N_L)$, where N_R and N_L are number of the right-handed and left-handed particles, respectively[130].

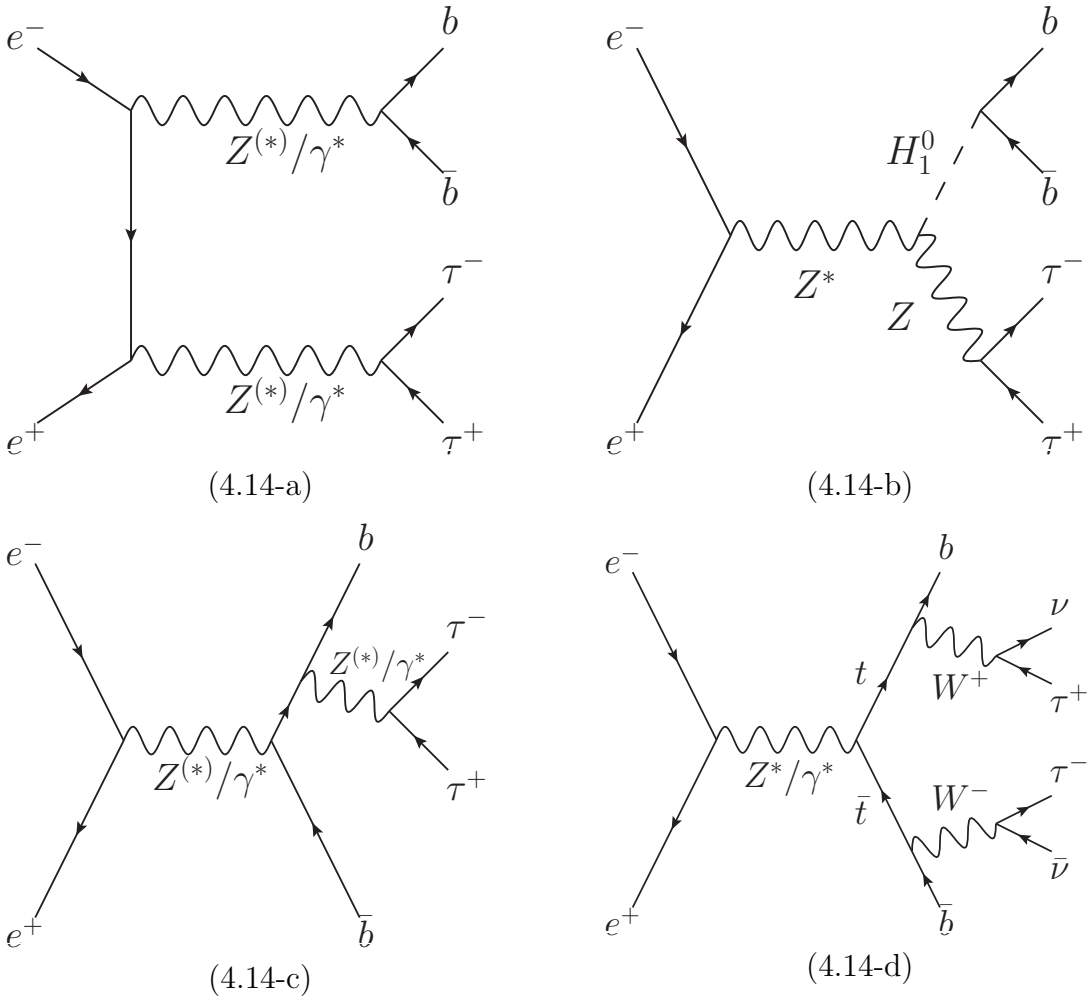


Figure 4.14: Typical Feynman diagrams of the background processes. The figures are given by Ref. [70].

decays of the tau leptons. In our simulation, we consider hadronic decays of the tau leptons, i.e., $\tau^\pm \to \pi^\pm\nu$, $\tau^\pm \to \rho^\pm\nu \to \pi^\pm\pi^0\nu$, $\tau^\pm \to a_1^\pm\nu \to \pi^\pm\pi^0\pi^0\nu$ and $\tau^\pm \to a_1^\pm\nu \to \pi^\pm\pi^\pm\pi^\mp\nu$. The branching ratios of these decays are given as 10.8%, 25.5%, 9.26% and 8.99%, respectively[3] [6]. In addition, we assume the efficiency for the identification of a bottom quark jet to be 70%, in which the mis-identification rate of jets from other quarks and gluons is estimated to be less than O(1)%[132]. For the decay mode of the tau leptons, we also take the efficiency for the identification of π, ρ and a_1 mesons as 89.3%, 75.2% and 64.3%, respectively[133]. Although $a_1^\pm$ has mainly two decay modes: $a_1^\pm \to \pi^\pm\pi^0\pi^0$ and $a_1^\pm \to \pi^\pm\pi^\pm\pi^\mp$. For both of the decay modes, we take the identification efficiency of the former presented in Ref. [133].

Since the energy resolution of jets $\Delta E/E$ is expected to be $0.17/\sqrt{E}$ at the ILC[134], we consider a larger bin size such as 10 GeV for jet energies as a conservative choice for $E = \mathcal{O}(100)$ GeV. We do not perform the detector level simulation.

In Fig. 4.15, the $b\bar{b}$ invariant mass $m_{b\bar{b}}$ distributions for $e^+e^- \to b\bar{b}\tau^+\tau^-$ and $e^+e^- \to b\bar{b}\tau^+\tau^-\nu_\tau\bar{\nu}_\tau$ with the tau leptons decaying into π, ρ and a_1 are shown. The black, green and blue histogram are the distributions given by the signal events, the background from the $t\bar{t}$ production and background $b\bar{b}\tau^+\tau^-$, respectively. It is seen that the background event can be reduced by the cut $|m_{b\bar{b}} - m_{H_3^0(H_2^0)}| \leq 10$ GeV which extracts the signal events containing the decay of H_2^0 (H_3^0) into $\tau^+\tau^-$. After applying the cuts of $|m_{b\bar{b}} - m_{H_3^0}| \leq 10$ GeV and $|m_{b\bar{b}} - m_{H_2^0}| \leq 10$ GeV, the invariant mass $m_{\text{pions+missing}}$ distribution for all the pions produced by the decays of tau leptons and missing momentum, is shown in Fig. 4.16. That corresponds to the invariant mass distribution of $\tau^+\tau^-$ which can be reconstructed by all the visible particles of the final state and the information of the initial state of the e^+e^- collision. In addition to the cuts of $m_{b\bar{b}}$, by applying the similar cuts for that invariant mass such as $|m_{\text{pions+missing}} - m_{H_2^0(H_3^0)}| \leq 10$ GeV, most of the background events can be cut. The numbers of the events before and after applying the kinematic cuts for the signal and the background processes of $e^+e^- \to b\bar{b}\tau^+\tau^-$ and $e^+e^- \to b\bar{b}\tau^+\tau^-\nu\bar{\nu}$ are summarized in Tab. 4.4. By using the two cuts for $m_{b\bar{b}}$ and $m_{\text{pions+missing}}$, we can neglect the background events[70].

Since the $\Delta\phi$ distributions of $H_2^0 \to \tau^+\tau^-$ and $H_3^0 \to \tau^+\tau^-$ are different from each other as discussed in Sec. 4.4.3, two events should be separated by the appropriate condition in order to make plots of the $\Delta\phi$ distributions for each decay. As we mentioned above, for extracting the events containing $H_2^0(H_3^0) \to \tau^+\tau^-$, we introduce the kinematic cut which imposes $|m_{b\bar{b}} - m_{H_3^0(H_2^0)}| \leq 10$ GeV on the invariant mass $m_{b\bar{b}}$ and also $|m_{\text{pions+missing}} - m_{H_2^0(H_3^0)}| \leq 10$ GeV on the invariant mass $m_{\text{pions+missing}}$ at the same time.

[6] There are the leptonic decays of the tau leptons, i.e., $\tau^\pm \to l^\pm\nu\bar{\nu}$. However, since two neutrinos are produced per tau decay, the momentum reconstruction method which is proposed in Ref.[129] cannot be simply applied to this decay modes. In Ref.[131], in addition to $\tau^\pm \to \pi^\pm\nu$ and $\tau^\pm \to \rho^\pm\nu$, such leptonic tau decay modes are discussed with the other observable which is different from our $\Delta\phi$.

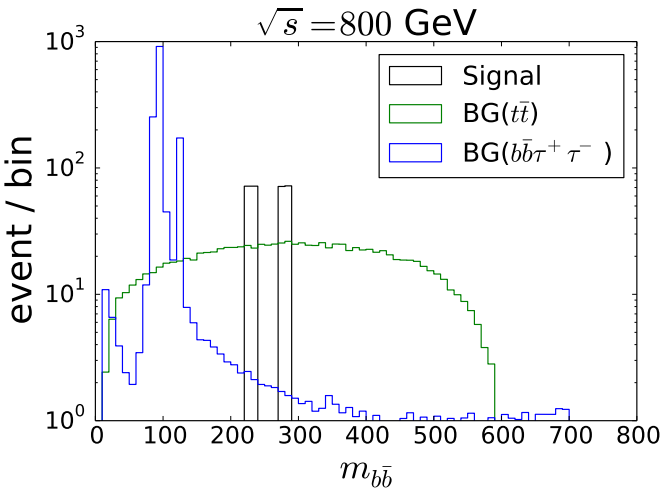


Figure 4.15: $b\bar{b}$ invariant mass $m_{b\bar{b}}$ distribution for the benchmark point given in Tab. 4.3. $\sqrt{s}$ = 800 GeV and $\mathcal{L}$ = 3000 /fb are assumed. The figure is given by Ref. [70].

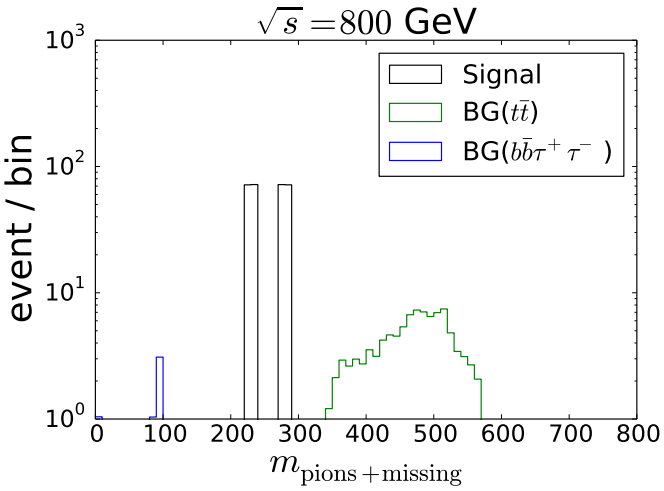


Figure 4.16: Invariant mass distribution of all pions produced by tau decay and missing momentum for the benchmark point given in Tab. 4.3 after the cuts of $b\bar{b}$ invariant mass such as $|m_{b\bar{b}} - m_{H_3^0}| \leq 10$ GeV and $|m_{b\bar{b}} - m_{H_2^0}| \leq 10$ GeV. $\sqrt{s} = 800$ GeV and $\mathcal{L} = 3000$ /fb are assumed. The figure is given by Ref. [70].

	$t\bar{t}$	$b\bar{b}\tau^+\tau^-$	(ZZ)	(ZH_1^0)	$(Z\gamma^*)$	$(\gamma^*\gamma^*)$	$H_2^0H_3^0$	$S/\sqrt{S+B}$
No cut	6093	10080	(4205)	(1248)	(3662)	(179)	1867	13.90
$\lvert m_{bb} - m_{H^0_{3/2}}\rvert \leq 10$ GeV	272/308	23/24	(0/0)	(0/0)	(2/2)	(4/5)	934/933	26.64/26.23
$\lvert m_{\text{pions+missing}} - m_{H^0_{2/3}}\rvert \leq 10$ GeV	0/0	0/0	(0/0)	(0/0)	(0/0)	(0/0)	934/933	30.56/30.55
Combined values after $m_{b\bar{b}}$ cut	580	47	(0)	(0)	(4)	(9)	1867	37.28
Combined values after two cuts	0	0	(0)	(0)	(0)	(0)	1867	43.21

Table 4.4: Numbers of the events of the signal and the background of $e^+e^- \to b\bar{b}\tau^+\tau^-$ and $e^+e^- \to b\bar{b}\tau^+\tau^-\nu\bar{\nu}$ for the benchmark point given in Tab. 4.3 with $\sqrt{s} = 800$ GeV and $\mathcal{L} = 3000$ /fb. The efficiency for the identification of the bottom as 70% is considered. The values in parentheses are the numbers of partial event of $e^+e^- \to b\bar{b}\tau^+\tau^-$. The values of the left (right) side of the slashes are the numbers of the event after the cut $|m_{b\bar{b}} - m_{H_3^0}| \leq 10$ GeV ($|m_{b\bar{b}} - m_{H_2^0}| \leq 10$ GeV) in the second line. In the third line, the slashes in a similar manner for the additional cut $|m_{\text{pions+missing}} - m_{H_2^0}| \leq 10$ GeV and $|m_{\text{pions+missing}} - m_{H_3^0}| \leq 10$ GeV. The forth line corresponds to the combined number of the events which are exhibited in the second line. The last line corresponds to the combined number of the event after the two cuts. The table given by Ref. [70].

After applying this invariant-mass selection, we make a plot of the $\Delta\phi$ distributions for $H_2^0 \to \tau^+\tau^-$ and $H_3^0 \to \tau^+\tau^-$. As we can see in Eqs. (4.48) and (4.49), the normalized $\Delta\phi$ distributions for $H_2^0 \to \tau^+\tau^-$ and $H_3^0 \to \tau^+\tau^-$ have the relation in which one is shifted from the other by π radian along the horizontal axis. Therefore, by combining both of the $\Delta\phi$ distributions with the consideration of this relation, the significance to know whether θ_e is finite or not can be enhanced[70]. We make the combined plot of $\Delta\phi$ distributions in Fig. 4.17. The red and black lines correspond to the scenario with $\theta_e = \pi/4$ and 0, and the bars for each of the bins correspond to the 1σ error. From this figure, at the third (seventh) bin from left in which $\Delta\phi$ is about 1.8-2.7 (5.4-6.3), it is seen that the data of the black histogram is 6.0 (4.0) σ away from these of the red histogram.

Next, we survey the parameter region in which we can get the significance on the $\Delta\phi$ distribution. We focus on the third bin of the $\Delta\phi$ distribution, and the significance is expressed as $(N^i_{\theta_e=45^\circ} - N^i_{\theta_e=0^\circ})/\sqrt{N^i_{\theta_e=45^\circ}}$, where $N^i_{\theta_e=45^\circ}$ ($N^i_{\theta_e=0^\circ}$) is number of the signal event with $\theta_e = 45^\circ$ (0°) in the i'th bin. The numbers of the signal event for any scenarios are estimated from these of the benchmark point by the production cross section and the branching ratios of the additional Higgs bosons. We note that the stability of the EDM cancellation at a high energy for any scenarios is not always realized when the scenario away from the benchmark point discussed in Ref. [69].

We perform the scan for the coupling strength $|\zeta_e| \in (0, 2]$ and the additional Higgs masses $m_{H_2^0} \in (100, 500]$ with the fixed mass difference $m_{H_3^0} = m_{H_2^0} - 50$ GeV. The

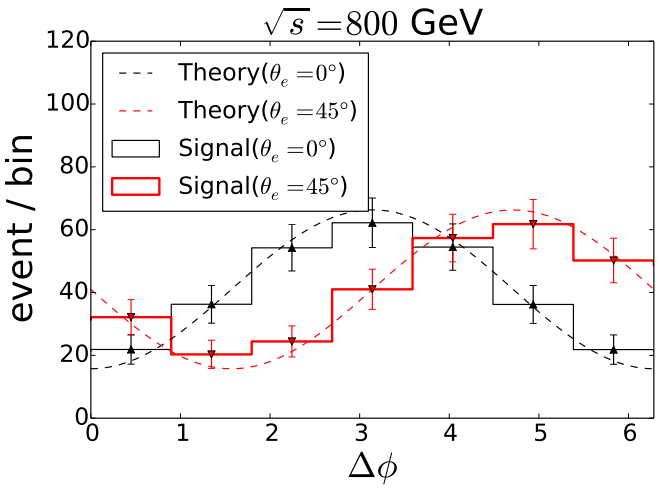


Figure 4.17: $\Delta\phi$ distribution for benchmark in our paper[69]. $m_{H_2^0} = 280$, $m_{H_3^0} = m_{H^\pm} = 230$, $\sqrt{s} = 800$ GeV and $\mathcal{L} = 3000$ /fb are assumed. The signal events are compared with the theoretical prediction (dashed line). The bars for each of the bins correspond to the 1σ error. For the third bin, the 5σ error bar of the red histogram cannot reach the black histogram. The figure is given by Ref. [70].

other parameters are taken to be the same as the benchmark point of Ref. [69]. On the other hand, we also investigate the excluded region against for the electron EDM data which are not allowed even if we take any value of $\theta_7 \in (-\pi, \pi]$ with $|\lambda_7| = 0.01$, 0.1, 0.3, 0.5 and 0.7, where θ_7 and $|\lambda_7|$ does not give large effects to the $\Delta\phi$ distribution,

In Fig. 4.18, the contour plot of the significance on the $\Delta\phi$ distribution is denoted by the solid lines, and the excluded regions against for the electron EDM data denoted by the color shaded regions above the dashed lines. The point marked by the star corresponds to the benchmark point when $\lambda_7 = 0.3$ and $\theta_e = -1.8$. In the area of the left side of the pink (cyan, black and purple) solid line, we can get more than 1 (2, 5 and 8) σ significance on the $\Delta\phi$ distribution for $\sqrt{s} = 800$ GeV. It is seen that the significance is enhanced in the parameter space with lighter masses and about $|\zeta_e| = 0.5$ because the number of the evens of $e^+e^- \to \tau^+\tau^- b\bar{b}$ increases. When the additional Higgs bosons are heavier than $2m_t$, the $H_j^0 \to t\bar{t}$ cannel is opened, and the significance is small due to the decrease of the cross section of $e^+e^- \to \tau^+\tau^- b\bar{b}$. The color shaded region above the blue (yellow, green and red) dashed line denotes the excluded region against for the electron EDM data which are not allowed even if we take any value of $\theta_7 \in (-\pi, \pi]$ when $|\lambda_7|$ are fixed as 0.01 (0.1, 0.3 and 0.5). The color shaded regions are piled up in the order of blue, yellow, green and red. It is seen that the cancellation

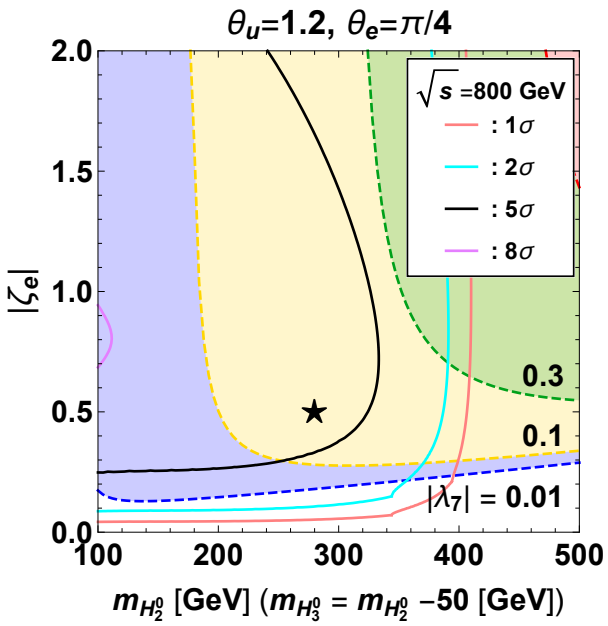


Figure 4.18: Contour plot of the significance on the $\Delta\phi$ distribution and the excluded region against for the electron EDM data for $\theta_e = \pi/4$. The solid lines denote the contours for the significance on the $\Delta\phi$ distribution. The point marked by the star corresponds to the benchmark point when $\lambda_7 = 0.3$ and $\theta_e = -1.8$. The blue (yellow, green and red) shaded region above the blue (yellow, green and red) dashed line denotes the excluded region against for the electron EDM data which are not allowed even if we take any value of $\theta_7 \in (-\pi, \pi]$ when $|\lambda_7|$ are fixed as 0.01, 0.1, 0.3 and 0.5. The color shaded regions are piled up in the order of blue, yellow, green and red. The figure is given by Ref. [70].

works well for the wide regions for $|\zeta_e|$ in which the electron EDM is satisfied, when $|\lambda_7| = 0.1$ (0.3, 0.5) and $m_{H_2^0}$ is smaller than about 200 (320, 460) GeV. On the other hand, if the coupling strength $|\lambda_7|$ is smaller or the masses are larger, the cancellation does not work due to the unbalance of the two contributions between the fermion loops and the Higgs boson loops on the BZ diagrams, so that the allowed regions remain in which the small value of the overall factor $|\zeta_e|$ on the electron EDM. We note that if the electron EDM bound is improved by one order of magnitude, the height of the dashed lines are made about 1/10, so that the parameter in which the cancellation does not work well are surveyed. It is seen the remaining parameter regions in which the cancellation works well can be tested from the $\Delta\phi$ distribution[70].

In Fig. 4.19, for other energy $\sqrt{s} = 250$, 500, 750, 1000 and 1250 GeV, the parameter

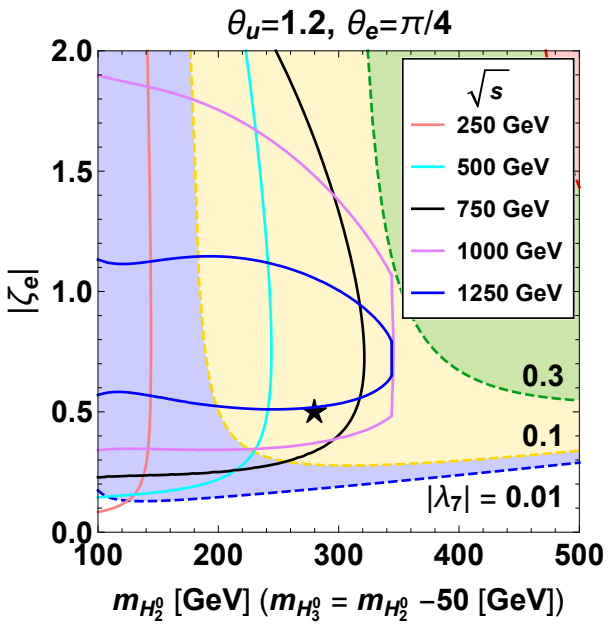


Figure 4.19: $\sqrt{s}$ dependence of the significance on the $\Delta\phi$ distribution and the excluded region against for the electron EDM data for $\theta_e = \pi/4$. In the areas of the left side of the solid lines, we can get the 5 σ significance on the $\Delta\phi$ distribution for $\sqrt{s} = 250$, 500, 750, 1000 and 1250 GeV. The point marked by the star corresponds to the benchmark point when $\lambda_7 = 0.3$ and $\theta_e = -1.8$. The color shaded regions and the dashed lines are the same as those in Fig. 4.18. The figure is given by Ref. [70].

regions in which the significance can get to be more than 5 σ on the $\Delta\phi$ distribution are exhibited as the areas of the left side of the pink, cyan, black, purple and blue solid lines, respectively. At the point marked by the star, the parameters are taken to be the same as the benchmark point when $\lambda_7 = 0.3$ and $\theta_e = -1.8$. The color shaded regions are the same as those in Fig. 4.18. Since the decay cannel $H_j^0 \to t\bar{t}$ $(j = 2, 3)$ opens when the additional Higgs bosons have masses larger than $2m_t$, the significance quickly decreases due to the dominance of this cannel on the decay of H_j^0. For $m_{H^0_{2,3}} < 2m_t$, the test of CP violation by using the $\Delta\phi$ distributions can play a complement role to the future EDM experiments when $\lambda_7 \leq 3$[70].

In Fig. 4.20, the excluded regions against for the electron EDM data are shown by the θ_e-$m_{H_2^0}$ axes with $|\zeta_e| = 0.5$. In the left (right) panel, we take $m_{H_3^0} = m_{H^\pm} = m_{H_2^0} - 50$ GeV and $\theta_e = \pi/4$ ($m_{H_3^0} = m_{H^\pm} = m_{H_2^0} + 50$ GeV and $\theta_e = 3\pi/4$). The blue (yellow, green, red and purple) shaded areas with blue (yellow, green red and purple) dashed lines as the boundary are the excluded region against for the electron EDM data even

if we take any value of $\theta_7 \in (-\pi, \pi]$ when $|\lambda_7|$ are fixed as 0.01 (0.1, 0.3, 0.5 and 0.7). The color shaded regions are piled up in the order of blue, yellow, green, red and purple. When $|\lambda_7|$ is smaller or the masses of extra Higgs bosons are heavier, the balance between the fermion-loop contributions and the Higgs boson-loop contributions to the electron EDM on the BZ diagrams is lost. Since the fermion-loop contributions to the electron EDM then become dominant, the cancellation cannot work for any value of θ_7, and θ_e should be about θ_u to satisfy the EDM data. In the left (right) panel of Fig. 4.20, the points marked by the black (white) star corresponds to the benchmark (other) scenario with $m_{H_2^0} = 280$ (230) GeV, $m_{H_3^0} = m_{H^\pm} = 230$ (280) GeV and $\theta_e = \pi/4$ ($3\pi/4$). From the $\Delta\phi$ distributions, it is not clear whether the benchmark scenario with $m_{H_2^0} = 280$ GeV, $m_{H_3^0} = 230$ GeV and $\theta_e = \pi/4$ or another scenario with $m_{H_2^0} = 230$ GeV, $m_{H_3^0} = 280$ GeV and $\theta_e = 3\pi/4$. However, from Fig. 4.20, when the coupling strength $|\lambda_7|$ is fixed as 0.3, it is seen that the benchmark point marked by the black star in the left panel satisfies the current electron EDM data, while the parameter set marked by the white star in the right panel is excluded by the EDM data. By considering EDM data, one can be rejected[70].

Finally, we mention the testability of the CP property in our scenarios at the LHC. In this scenario, the neutral Higgs bosons are produced from the gluon-fusion process $gg \to H^0_{2,3}$ and the bottom quark associated production $gg \to H^0_{2,3} b\bar{b}$. However, these production cross sections are very small, typically a few fb level in our benchmark point, due to the small values of the Yukawa couplings, i.e., $\zeta_u = 0.01$ and $\theta_d = 0.1$[69]. This is two orders of magnitude smaller than the upper limit for the gluon-fusion cross-section which is given by the LHC data if it is assumed that the heavy scalars have the mass of 200 GeV[128]. There are pair production processes such as $pp \to H^0_2 H^0_3$, $H^0_{2,3} H^\pm$ and H^+H^-, and their cross sections are $\mathcal{O}(10)$ fb[69]. On the other hand, the cross section of the $t\bar{t}$ production as the main background are measured by LHC at $\sqrt{s} = 13$ TeV as about 10^6 fb[135]. Thus, it is difficult to get the enough significance to see the $\Delta\phi$ distribution. In addition, since the initial state cannot be known at the parton level, the reconstruction method for the tau leptons used in our analysis cannot be simply applied.

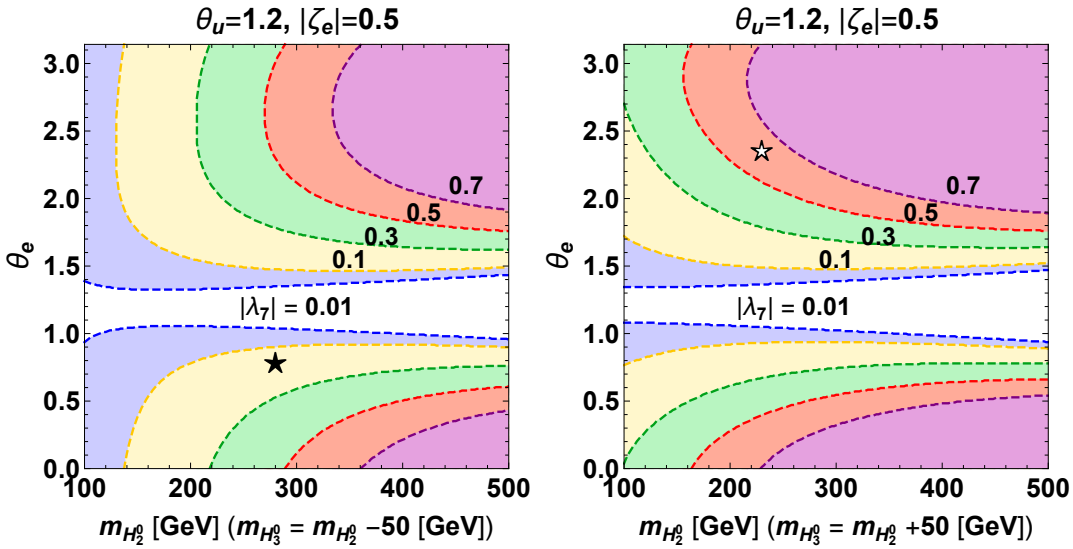


Figure 4.20: The excluded region against for the electron EDM data with $|\zeta_e| = 0.5$. The color shaded regions denote the excluded region against for the electron EDM data which are not allowed even if we take the scan for $\theta_7 \in (-\pi, \pi]$ when $|\lambda_7| = 0.01$, 0.1, 0.3, 0.5 and 0.7. The color shaded regions are piled up in the order of blue, yellow, green, red and purple as $|\lambda_7|$ grows larger. In the left (right) panel of Fig. 4.20, the points marked by the black (white) star corresponds to the benchmark (other) scenario with $m_{H_2^0} = 280$ (230) GeV, $m_{H_3^0} = m_{H^\pm} = 230$ (280) GeV and $\theta_e = \pi/4$ ($3\pi/4$). The figures are given by Ref. [70].

Chapter 5

Summary

5.1 Conclusion

We have discussed the aligned scenario of the CP violating THDM in which the Yukawa alignment is assumed to avoid the FCNCs at tree-level and the alignment in the Higgs potential is also assumed to realize that the coupling constants for the 125 GeV Higgs boson are the same as those of the SM at tree-level. In our paper[69], we have found the non-trivial parameter regions in which the electron EDM can be satisfied by considering the destructive interference between the Barr-Zee type contributions even if the CP violating phases have O(1). This is main results of our paper[69]. We have also found that there are the scenarios with both the alignment in the Yukawa interaction and that in the Higgs potential which can be stable up to a high energy scale such as 10^8 GeV, by analyzing the scale dependence of the dimensionless couplings with the RGEs at one-loop level.

In addition, in the paper[70], for such a EDM suppressing scenario with O(1) phases, we have investigated how to test the CP violation at the high energy collider experiment. In our scenario, since the alignment in the Higgs potential is imposed, the phenomenology of the extra Higgs bosons is important. In particular, we have considered the processes containing the decays of the extra neutral Higgs bosons into a pair of tau leptons. In order to know the feasibility to extract the information of the CP violating phase which appears on the behavior of the decay products of tau leptons, we have performed the simulation of the production and the decays of the extra bosons at the ILC with several energy of $\sqrt{s}$ and $\mathcal{L} = 3\ ab^{-1}$. As the result of the analysis with the consideration of the event numbers of the signal and the background processes, we have found that the scenario with finite θ_e may be distinguished from the scenario with $\theta_e = 0$ at future experiments on the ILC even if the EDM is not measured. This is main results of our paper[70]. In addition, we have found that the EDM experiments

and the test of the angular distribution complement each other in the search for the parameters of the CP-violating model.

5.2 Future prospects

In addition to what has been discussed in the thesis, there are other ways to test CP violation.For example, the precision measurement of the couplings of ZZZ, ZWW[50, 51] and $h^{125}ff$[52, 53, 54] can give the information of the presence of the CP phases at collider experiments. It is also important to consider them in order to test the model in more detail. We mention the study for the test of the CP violating phase of the Higgs potential which are discussed in Ref. [136]. According to Ref. [136], when the alignment of the Higgs potential is even slightly broken, the decay mode $h_3 \to h_2 h_1$ can play a role on the measurement of the CP-violating phase corresponding to θ_7 in our model. We also mention that the couplings of $H_2^0 H_2^0 H_3^0$ and $H_3^0 H_3^0 H_3^0$ are given as $-\frac{1}{2} v \mathrm{Im}[\lambda_7]$ in our model. Therefore, if the alignment of the Higgs potential is respected, by surveying these interaction and combining our study in this thesis, the information of λ_7 and θ_7 might be gotten at future experiments.

Our final goal is to give an explanation for BAU. Therefore, we should be study about the possibility of the EWBG to create the enough abundance of the baryon number in our model. According to the discussion in Ref. [18], even if the vacuum expectation values of the Higgs doublets are taken to be $(\langle\Phi_1^0\rangle, \langle\Phi_2^0\rangle) = (v/\sqrt{2}, 0)$ at the zero temperature, they can be $(\langle\Phi_1^0\rangle, \langle\Phi_2^0\rangle) = (v_1', v_2')/\sqrt{2}$ at the finite temperature. If the such a phase transition can be realized, the top quark mass can be complex via ζ_u in the process of the EWPT, and the baryon asymmetry of the Universe may be then generated by new CP violating source. In order to know whether BAU can be explained in our scenario while the experimental data are satisfied at the same time, we have to perform the analysis for the electroweak phase transition and B number creation at the finite temperature. We also mention that the possibility of the loss of the alignment on the scalar potential at finite temperature. In this case, both vacuum expectation values can be also finite. It is also important to survey the effect to BAU of the deviation from the alignment at finite temperature.

5.3 My contributions in the original papers

Finally, I would like to state my contributions in the original papers[69, 70]. For the detail of the model discussed in Refs. [69, 70], after the rough discussion with my collaborators about the original idea for the model cancelling the EDM, I have proposed

the concrete model which has the multiple CP-violating phases with two kinds of the alignment. I have provided to my collaborators the first results of the analysis, i.e.,

- the analytical and numerical calculations of the BZ type contribution to the electron and the neutron EDM.
- the analytical and numerical calculations of the RGE running of all the dimensionless couplings of the general THDM.
- the signal and background simulation for the production and decay of the additional Higgs bosons.
- the analysis for the invariant mass distribution and the kinematical cuts of the signal and background events.
- the analysis for the angular distribution for the decay products of the tau leptons on $H^0_{2,3} \to \tau^+\tau^-$.

I have written the first draft of the paper for the publication of our studies.

Appendix A

Parameters of the scalar potential: relations between two bases

The relations between the potential parameters on the original basis and the Higgs basis given in Eqs. (4.1) and (4.4)are expressed as follows[89]

$$\mu_1^2 = +\mu'^2_1 c_\beta^2 + \mu'^2_2 s_\beta^2 + 2\mathrm{Re}[\mu'^2_3 e^{i\xi}] c_\beta s_\beta, \tag{A.1}$$

$$\mu_2^2 = +\mu'^2_1 s_\beta^2 + \mu'^2_2 c_\beta^2 - 2\mathrm{Re}[\mu'^2_3 e^{i\xi}] c_\beta s_\beta, \tag{A.2}$$

$$\mu_3^2 = -(\mu'^2_1 - \mu'^2_2) c_\beta s_\beta + \mathrm{Re}[\mu'^2_3 e^{i\xi}](c_\beta^2 - s_\beta^2) + i\mathrm{Im}[\mu'^2_3 e^{i\xi}], \tag{A.3}$$

$$\lambda_1 = +\lambda'_1 c_\beta^4 + \lambda'_2 s_\beta^4 + 2\lambda'_{345} c_\beta^2 s_\beta^2 + 4\left(\mathrm{Re}[\lambda'_6 e^{i\xi}] c_\beta^2 + \mathrm{Re}[\lambda'_7 e^{i\xi}] s_\beta^2\right) c_\beta s_\beta, \tag{A.4}$$

$$\lambda_2 = +\lambda'_1 s_\beta^4 + \lambda'_2 c_\beta^4 + 2\lambda'_{345} c_\beta^2 s_\beta^2 - 4\left(\mathrm{Re}[\lambda'_6 e^{i\xi}] s_\beta^2 + \mathrm{Re}[\lambda'_7 e^{i\xi}] c_\beta^2\right) c_\beta s_\beta, \tag{A.5}$$

$$\lambda_3 = +\lambda'_3 + (\lambda'_1 + \lambda'_2 - 2\lambda'_{345}) c_\beta^2 s_\beta^2 - 2\left(\mathrm{Re}[\lambda'_6 e^{i\xi}] - \mathrm{Re}[\lambda'_7 e^{i\xi}]\right)(c_\beta^2 - s_\beta^2) c_\beta s_\beta, \tag{A.6}$$

$$\lambda_4 = +\lambda'_4 + (\lambda'_1 + \lambda'_2 - 2\lambda'_{345}) c_\beta^2 s_\beta^2 - 2\left(\mathrm{Re}[\lambda'_6 e^{i\xi}] - \mathrm{Re}[\lambda'_7 e^{i\xi}]\right)(c_\beta^2 - s_\beta^2) c_\beta s_\beta, \tag{A.7}$$

$$\begin{aligned}\lambda_5 = &+\mathrm{Re}[\lambda'_5 e^{2i\xi}] + (\lambda'_1 + \lambda'_2 - 2\lambda'_{345}) c_\beta^2 s_\beta^2 - 2\left(\mathrm{Re}[\lambda'_6 e^{i\xi}] - \mathrm{Re}[\lambda'_7 e^{i\xi}]\right)(c_\beta^2 - s_\beta^2) c_\beta s_\beta \\ &+ i\left[\mathrm{Im}[\lambda'_5 e^{2i\xi}](c_\beta^2 - s_\beta^2) - 2\left(\mathrm{Im}[\lambda'_6 e^{i\xi}] - \mathrm{Im}[\lambda'_7 e^{i\xi}]\right) c_\beta s_\beta\right],\end{aligned} \tag{A.8}$$

$$\begin{aligned}\lambda_6 = &-\left[\lambda'_1 c_\beta^2 - \lambda'_2 s_\beta^2 - \lambda'_{345}(c_\beta^2 - s_\beta^2)\right] c_\beta s_\beta + \mathrm{Re}[\lambda'_6 e^{i\xi}] c_\beta^2 (c_\beta^2 - 3s_\beta^2) - \mathrm{Re}[\lambda'_7 e^{i\xi}] s_\beta^2 (s_\beta^2 - 3c_\beta^2) \\ &+ i\left(\mathrm{Im}[\lambda'_5 e^{2i\xi}] c_\beta s_\beta + \mathrm{Im}[\lambda'_6 e^{i\xi}] c_\beta^2 + \mathrm{Im}[\lambda'_7 e^{i\xi}] s_\beta^2\right),\end{aligned} \tag{A.9}$$

$$\begin{aligned}\lambda_7 = &-\left[\lambda'_1 s_\beta^2 - \lambda'_2 c_\beta^2 + \lambda'_{345}(c_\beta^2 - s_\beta^2)\right] c_\beta s_\beta - \mathrm{Re}[\lambda'_6 e^{i\xi}] s_\beta^2 (s_\beta^2 - 3c_\beta^2) + \mathrm{Re}[\lambda'_7 e^{i\xi}] c_\beta^2 (c_\beta^2 - 3s_\beta^2) \\ &- i\left(\mathrm{Im}[\lambda'_5 e^{2i\xi}] c_\beta s_\beta - \mathrm{Im}[\lambda'_6 e^{i\xi}] s_\beta^2 - \mathrm{Im}[\lambda'_7 e^{i\xi}] c_\beta^2\right),\end{aligned} \tag{A.10}$$

where $\xi \equiv \xi_2 - \xi_1$, $c_\beta = \cos\beta$, $s_\beta = \sin\beta$ and $\lambda'_{345} \equiv \lambda'_3 + \lambda'_4 + \mathrm{Re}[\lambda'_5 e^{2i\xi}]$.

Appendix B

Exact formulae of the Barr-Zee type contributions

We here list the Barr-Zee type contributions to the EDM (CEDM) for a fermion (quark) d_f^γ, d_f^Z and d_f^W (d_q^C) given in Eqs. (3.15) and (3.16) (Eq. (4.32)).The fermion-loop contributions to the EDM are

$$d_f^V(f') = \frac{em_f}{(16\pi^2)^2} 8 g_{Vff}^v g_{Vf'f'}^v Q_{f'} N_C \frac{m_{f'}^2}{v^2} \times \sum_j^3 \int_0^1 dz \left\{ \mathrm{Im}[\kappa_f^j]\mathrm{Re}[\kappa_{f'}^j] \left(\frac{1}{z} - 2(1-z) \right) + \mathrm{Re}[\kappa_f^j]\mathrm{Im}[\kappa_{f'}^j] \frac{1}{z} \right\} C_{f'f'}^{VH_j^0}(z), \tag{B.1}$$

$$d^W_{f(I_f=-\frac{1}{2})}(tb) = \frac{eg_2^2 m_f}{(16\pi^2)^2} N_C \int_0^1 dz \left\{ \frac{m_t^2}{v^2}\mathrm{Im}[\zeta_f^*\zeta_u]\frac{2-z}{z} + \frac{m_b^2}{v^2}\mathrm{Im}[\zeta_f^*\zeta_d] \right\} [Q_t(1-z) + Q_b z] C_{tb}^{WH^\pm}(z), \tag{B.2}$$

$$d^W_{f(I_f=+\frac{1}{2})}(tb) = \frac{eg_2^2 m_f}{(16\pi^2)^2} N_C \int_0^1 dz \left\{ \frac{m_t^2}{v^2}\mathrm{Im}[\zeta_f\zeta_u^*] + \frac{m_b^2}{v^2}\mathrm{Im}[\zeta_f\zeta_d^*]\frac{1+z}{1-z} \right\} [Q_t(1-z) + Q_b z] C_{tb}^{WH^\pm}(z), \tag{B.3}$$

the Higgs boson-loop contributions to EDM are

$$d_f^V(H^\pm) = \frac{em_f}{(16\pi^2)^2} 4 g_{Vff}^v (i g_{H^+H^-V}) \sum_j^3 \mathrm{Im}[\kappa_f^j] \frac{g_{H^\pm H^\mp H_j^0}}{v} \int_0^1 dz (1-z) C_{H^\pm H^\pm}^{VH_j^0}(z), \tag{B.4}$$

$$d_f^W(H^\pm H^0) = \frac{eg_2^2 m_f}{(16\pi^2)^2} \frac{1}{2} \sum_j^3 \mathrm{Im}[\kappa_f^j] \frac{g_{H^\pm H^\mp H_j^0}}{v} \int_0^1 dz (1-z) C_{H^\pm H_j^0}^{WH^\pm}(z), \tag{B.5}$$

the gauge-loop contributions to EDM are

$$d_f^V(W) = \frac{em_f}{(16\pi^2)^2} 8 g_{Vff}^v (i g_{WWV}) \frac{m_W^2}{v^2} \sum_j^3 \mathcal{R}_{1j} \mathrm{Im}[\kappa_f^j] \\ \times \int_0^1 dz \left[\left\{ \left(6 - \frac{m_V^2}{m_W^2}\right) + \left(1 - \frac{m_V^2}{2m_W^2}\right) \frac{m_{H_j^0}^2}{m_W^2} \right\} \frac{(1-z)}{2} - \left(4 - \frac{m_V^2}{m_W^2}\right) \frac{1}{z} \right] C_{WW}^{VH_j^0}(z), \tag{B.6}$$

$$d_f^W(WH^0) = \frac{eg_2^2 m_f}{(16\pi^2)^2} \frac{1}{2} \frac{m_W^2}{v^2} \sum_j^3 \mathcal{R}_{1j} \mathrm{Im}[\kappa_f^j] \int_0^1 dz \left\{ \frac{4-z}{z} - \frac{m_{H^\pm}^2 - m_{H_j^0}^2}{m_W^2} \right\} (1-z) C_{WH_j^0}^{WH^\pm}(z), \tag{B.7}$$

and the quark-loop contributions to CEDM are

$$d_q^C(q') = \frac{m_q}{(16\pi^2)^2} 4 g_3^3 \frac{m_{q'}^2}{v^2} \sum_j^3 \int_0^1 dz \left\{ \mathrm{Im}[\kappa_q^j] \mathrm{Re}[\kappa_{q'}^j] \left(\frac{1}{z} - 2(1-z) \right) + \mathrm{Re}[\kappa_q^j] \mathrm{Im}[\kappa_{q'}^j] \frac{1}{z} \right\} C_{q'q'}^{gH_j^0}(z), \tag{B.8}$$

where $V = \gamma$, Z and N_C is the color factor. The coupling constants are given by $g_{\gamma ff}^v = eQ_f$, $g_{Zff}^v = g_z(I_f/2 - Q_f s_W^2)$, $g_{H^+H^-\gamma} = -ie$, $g_{H^+H^-Z} = -ig_Z c_{2W}/2$, $g_{H^\pm H^\mp H_j^0} = (\lambda_3 \mathcal{R}_{1j} + \mathrm{Re}[\lambda_7]\mathcal{R}_{2j} - \mathrm{Im}[\lambda_7]\mathcal{R}_{3j})v$, $g_{WWA} = -ie$ and $g_{WWZ} = -ig_Z c_W^2$, where Q_f are the electric charges of the fermion, $g_Z = \sqrt{g_1^2 + g_2^2}$, $s_W = \sin\theta_W$, $c_W = \cos\theta_W$ and $c_{2W} = \cos 2\theta_W$.

$$C_{XY}^{GH}(z) = C_0 \left(0, 0; m_G^2, m_H^2, \frac{(1-z)m_X^2 + z m_Y^2}{z(1-z)}\right), \tag{B.9}$$

and where C_0 is the Passarino-Veltman function[137],

$$C_0(0,0;m_1^2,m_2^2,m_3^2) = \frac{1}{m_1^2 - m_2^2} \left\{ \frac{m_1^2}{m_1^2 - m_3^2} \log\left(\frac{m_3^2}{m_1^2}\right) - \frac{m_2^2}{m_2^2 - m_3^2} \log\left(\frac{m_3^2}{m_2^2}\right) \right\}. \tag{B.10}$$

We confirmed the consistency of our results with Refs. [43, 44, 45, 46, 47, 48].

Appendix C

Decay of the heavy Higgs bosons

We here list the partial decay width of the extra Higgs bosonsin Sec. 4.4.2. We refer to Refs. [59, 138, 139, 56].

$$\Gamma(H_i^0 \to f\bar{f}) = \frac{N_C G_F m_{H_i^0} m_f^2}{4\sqrt{2}\pi}\left(1-\frac{4m_f^2}{m_{H_i^0}^2}\right)^{3/2}\left[(\mathrm{Re}[\kappa_f^i])^2+(\mathrm{Im}[\kappa_f^i])^2\left(1-\frac{4m_f^2}{m_{H_i^0}^2}\right)^{-1}\right], \tag{C.1}$$

$$\Gamma(H_i^0 \to gg) = \frac{G_F \alpha_s^2(m_{H_i^0}) m_{H_i^0}^3}{64\sqrt{2}\pi^3}\left[\left|\sum_q \mathrm{Re}[\kappa_q^i] A_{1/2}^H(\tau_q^i)\right|^2+\left|\sum_q \mathrm{Im}[\kappa_q^i] A_{1/2}^A(\tau_q^i)\right|^2\right], \tag{C.2}$$

$$\Gamma(H_i^0 \to \phi V^*) = \frac{9G_\mu^2 m_V^4}{8\pi^3}\delta_V' m_{H_i^0} g_{H_i^0\varphi V}^2\, G\left(\frac{m_\varphi^2}{m_{H_i^0}^2}, \frac{m_V^2}{m_{H_i^0}^2}\right), \tag{C.3}$$

$$\begin{aligned}\Gamma(H^+ \to ff') = {} & \frac{N_C}{16\pi m_{H^\pm}^3}\left[\left(m_{H^\pm}^2-m_f^2-m_{f'}^2\right)^2-4m_f^2 m_{f'}^2\right]^{1/2} \\ & \times\left[\left(m_{H^\pm}^2-m_f^2-m_{f'}^2\right)\left(|y_f^+|^2+|y_{f'}^+|^2\right)-4m_f m_{f'}\mathrm{Re}[y_f^{+*}y_{f'}^+]\right],\end{aligned} \tag{C.4}$$

where $\tau_X^i = m_{H_i^0}^2/4m_X^2$, $\delta_Z' = \frac{7}{12}-\frac{10}{9}\sin^2\theta_W+\frac{40}{27}\sin^4\theta_W$, $\delta_W' = 1$ and $\phi = H_{j\neq i}^0(H^\pm)$ for $V^* = Z^*(W^*)$. The couplings y_f^+ and $y_{f'}^+$ are given by $\mathcal{L} \supset (\bar{f}_R y_f^+ f_L' + \bar{f}_L y_{f'}^+ f_R')H^+ + h.c.$. The functions $A(\tau)$ are given by

$$A_{1/2}^H(\tau) = 2[\tau+(\tau-1)f(\tau)]\tau^{-2}, \tag{C.5}$$

$$A_{1/2}^A(\tau) = 2\tau^{-1}f(\tau), \tag{C.6}$$

and where

$$f(\tau) = \begin{cases} \arcsin^2 \sqrt{\tau}, & \text{for} \quad \tau \leq 1, \\ -\frac{1}{4}\left[\log \frac{1+\sqrt{1-\tau^{-1}}}{1-\sqrt{1-\tau^{-1}}} - i\pi\right]^2, & \text{for} \quad \tau > 1. \end{cases} \tag{C.7}$$

In terms of $\lambda(x,y) = -1 + 2x + 2y - (x-y)^2$ with $x = m_X^2/m_{H_i^0}^2$, the function $G(x,y)$ is given by

$$\begin{aligned} G(x,y) = \frac{1}{4}\Bigg\{ & 2(-1+y-x)\sqrt{\lambda(x,y)}\left[\frac{\pi}{2} + \arctan\left(\frac{y(1-y+x)-\lambda(x,y)}{(1-x)\sqrt{\lambda(x,y)}}\right)\right] \\ & + (\lambda(x,y) - 2x)\log x + \frac{1}{3}(1-x)\left[5(1+x) - 4y - \frac{2}{y}\lambda(x,y)\right]\Bigg\}. \end{aligned} \tag{C.8}$$

Appendix D

Beta functions

We here list the beta functions of the dimensionless coupling constants of general THDM up to one-loop level given.The couplings are expressed in any basis of the fermions and the scalar doublet fields given in Eqs. (4.1) and (4.18).The beta functions of the gauge coupling constants are given as

$$16\pi^2\beta_{g_3} = \left(-11 + \frac{4}{3}n_g\right) g_3^3, \tag{D.1}$$

$$16\pi^2\beta_{g_2} = \left(-\frac{22}{3} + \frac{4}{3}n_g + \frac{1}{6}n_d\right) g_2^3, \tag{D.2}$$

$$16\pi^2\beta_{g_1} = \left(\frac{20}{9}n_g + \frac{1}{6}n_d\right) g_1^3, \tag{D.3}$$

where n_g is the number of the generation of the fermions and n_d is the number of scalar doublets. The beta functions of the Yukawa-coupling matrices are given as

$$\begin{aligned} 16\pi^2\beta_{y_{u,k}} =& -2\sum_l^2 (y_{u,l}y_{d,k}y_{d,l}^\dagger) + \frac{1}{2}\sum_l^2 y_{u,k}[(y_{u,l}^\dagger y_{u,l}) + (y_{d,l}y_{d,l}^\dagger)] + \sum_l^2 (y_{u,l}y_{u,l}^\dagger)y_{u,k} \\ &+ \sum_l^2 \mathrm{Tr}[yy]_{lk} y_{u,l} - (8g_3^2 + \frac{9}{4}g_2^2 + \frac{17}{12}g_1^2)y_{u,k}, \end{aligned} \tag{D.4}$$

$$\begin{aligned} 16\pi^2\beta_{y_{d,k}} =& -2\sum_l^2 (y_{u,l}^\dagger y_{u,k}y_{d,l}) + \frac{1}{2}\sum_l^2 [(y_{u,l}^\dagger y_{u,l}) + (y_{d,l}y_{d,l}^\dagger)]y_{d,k} + \sum_l^2 y_{d,k}(y_{d,l}^\dagger y_{d,l}) \\ &+ \sum_l^2 \mathrm{Tr}[yy]_{lk} y_{d,l} - (8g_3^2 + \frac{9}{4}g_2^2 + \frac{5}{12}g_1^2)y_{d,k}, \end{aligned} \tag{D.5}$$

$$16\pi^2\beta_{y_{e,k}} =\frac{1}{2}\sum_{l}^{2}(y_{e,l}y_{e,l}^{\dagger})y_{e,k}+\sum_{l}^{2}y_{e,k}(y_{e,l}^{\dagger}y_{e,l})+\sum_{l}^{2}\mathrm{Tr}[yy]_{lk}y_{e,l}-(\frac{9}{4}g_2^2+\frac{15}{4}g_1^2)y_{e,k}, \tag{D.6}$$

where

$$\mathrm{Tr}[yy]_{lk}=\mathrm{Tr}[N_C\left(y_{u,l}^{\dagger}y_{u,k}+y_{d,l}^{\dagger}y_{d,k}\right)+y_{e,l}^{\dagger}y_{e,k}]. \tag{D.7}$$

The beta functions of the scalar self-couplings are given as

$$\begin{aligned}
16\pi^2\beta_{\lambda_1} =& \,2\left\{6\lambda_1^2+2\lambda_3^2+2\lambda_3\lambda_4+\lambda_4^2+|\lambda_5|^2+12|\lambda_6|^2\right\}\\
&-4\left\{N_C\left(\mathrm{Tr}\left[y_{u,1}y_{u,1}^{\dagger}y_{u,1}y_{u,1}^{\dagger}\right]+\mathrm{Tr}\left[y_{d,1}y_{d,1}^{\dagger}y_{d,1}y_{d,1}^{\dagger}\right]\right)+\mathrm{Tr}\left[y_{e,1}y_{e,1}^{\dagger}y_{e,1}y_{e,1}^{\dagger}\right]\right\}\\
&+4\mathrm{Tr}[yy]_{11}\lambda_1+2\mathrm{Tr}[yy]_{21}(\lambda_6+\lambda_6^*)+\frac{3}{4}(3g_2^4+g_1^4+2g_2^2g_1^2)-3(3g_2^2+g_1^2)\lambda_1,
\end{aligned} \tag{D.8}$$

$$\begin{aligned}
16\pi^2\beta_{\lambda_2} =& \,2\left\{6\lambda_2^2+2\lambda_3^2+2\lambda_3\lambda_4+\lambda_4^2+|\lambda_5|^2+12|\lambda_7|^2\right\}\\
&-4\left\{N_C\left(\mathrm{Tr}\left[y_{u,2}y_{u,2}^{\dagger}y_{u,2}y_{u,2}^{\dagger}\right]+\mathrm{Tr}\left[y_{d,2}y_{d,2}^{\dagger}y_{d,2}y_{d,2}^{\dagger}\right]\right)+\mathrm{Tr}\left[y_{e,2}y_{e,2}^{\dagger}y_{e,2}y_{e,2}^{\dagger}\right]\right\}\\
&+4\mathrm{Tr}[yy]_{22}\lambda_2+2\mathrm{Tr}[yy]_{12}(\lambda_7+\lambda_7^*)+\frac{3}{4}(3g_2^4+g_1^4+2g_2^2g_1^2)-3(3g_2^2+g_1^2)\lambda_2,
\end{aligned} \tag{D.9}$$

$$\begin{aligned}
16\pi^2\beta_{\lambda_3} =& \,2\left\{(\lambda_1+\lambda_2)(3\lambda_3+\lambda_4)+2\lambda_3^2+\lambda_4^2+|\lambda_5|^2+2|\lambda_6|^2+2|\lambda_7|^2+4(\lambda_6\lambda_7^*+\lambda_6^*\lambda_7)\right\}\\
&-4\left\{N_C\left(\mathrm{Tr}\left[y_{u,1}y_{d,2}y_{d,2}^{\dagger}y_{u,1}^{\dagger}\right]+\mathrm{Tr}\left[y_{u,2}y_{d,1}y_{d,1}^{\dagger}y_{u,2}^{\dagger}\right]-\mathrm{Tr}\left[y_{u,1}y_{d,2}y_{d,1}^{\dagger}y_{u,2}^{\dagger}\right]-\mathrm{Tr}\left[y_{u,2}y_{d,1}y_{d,2}^{\dagger}y_{u,1}^{\dagger}\right]\right)\right.\\
&\qquad\left.+N_C\left(\mathrm{Tr}\left[y_{u,2}y_{u,1}^{\dagger}y_{u,1}y_{u,2}^{\dagger}\right]+\mathrm{Tr}\left[y_{d,2}y_{d,2}^{\dagger}y_{d,1}y_{d,1}^{\dagger}\right]\right)+\mathrm{Tr}\left[y_{e,2}y_{e,2}^{\dagger}y_{e,1}y_{e,1}^{\dagger}\right]\right\}\\
&+2(\mathrm{Tr}[yy]_{11}+\mathrm{Tr}[yy]_{22})\lambda_3+\mathrm{Tr}[yy]_{12}(\lambda_6+\lambda_6^*)+\mathrm{Tr}[yy]_{21}(\lambda_7+\lambda_7^*)\\
&+\frac{3}{4}(3g_2^4+g_1^4-2g_2^2g_1^2)-3(3g_2^2+g_1^2)\lambda_3,
\end{aligned} \tag{D.10}$$

$$\begin{aligned}
16\pi^2\beta_{\lambda_4} =& \,2\left\{(\lambda_1+\lambda_2+4\lambda_3)\lambda_4+2\lambda_4^2+4|\lambda_5|^2+5|\lambda_6|^2+5|\lambda_7|^2+(\lambda_6\lambda_7^*+\lambda_6^*\lambda_7)\right\}\\
&-4\left\{N_C\left(\mathrm{Tr}\left[y_{u,2}y_{d,1}y_{d,2}^{\dagger}y_{u,1}^{\dagger}\right]+\mathrm{Tr}\left[y_{u,1}y_{d,2}y_{d,1}^{\dagger}y_{u,2}^{\dagger}\right]-\mathrm{Tr}\left[y_{u,2}y_{d,1}y_{d,1}^{\dagger}y_{u,2}^{\dagger}\right]-\mathrm{Tr}\left[y_{u,1}y_{d,2}y_{d,2}^{\dagger}y_{u,1}^{\dagger}\right]\right)\right.\\
&\qquad\left.+N_C\left(\mathrm{Tr}\left[y_{u,2}y_{u,1}^{\dagger}y_{u,1}y_{u,2}^{\dagger}\right]+\mathrm{Tr}\left[y_{d,2}y_{d,2}^{\dagger}y_{d,1}y_{d,1}^{\dagger}\right]\right)+\mathrm{Tr}\left[y_{e,2}y_{e,2}^{\dagger}y_{e,1}y_{e,1}^{\dagger}\right]\right\}\\
&+2(\mathrm{Tr}[yy]_{11}+\mathrm{Tr}[yy]_{22})\lambda_4+\mathrm{Tr}[yy]_{12}(\lambda_6+\lambda_6^*)+\mathrm{Tr}[yy]_{21}(\lambda_7+\lambda_7^*)\\
&+3g_2^2g_1^2-3(3g_2^2+g_1^2)\lambda_4,
\end{aligned} \tag{D.11}$$

$$\begin{aligned}
16\pi^2\beta_{\lambda_5} =& \,2\left\{(\lambda_1+\lambda_2+4\lambda_3+6\lambda_4)\lambda_5+5\lambda_6^2+5\lambda_7^2+2\lambda_6\lambda_7\right\}\\
&-4\left\{N_C\left(\mathrm{Tr}\left[y_{u,2}y_{u,1}^{\dagger}y_{u,2}y_{u,1}^{\dagger}\right]+\mathrm{Tr}\left[y_{d,2}y_{d,1}^{\dagger}y_{d,2}y_{d,1}^{\dagger}\right]\right)+\mathrm{Tr}\left[y_{e,2}y_{e,1}^{\dagger}y_{e,2}y_{e,1}^{\dagger}\right]\right\}\\
&+2(\mathrm{Tr}[yy]_{11}+\mathrm{Tr}[yy]_{22})\lambda_5+2\mathrm{Tr}[yy]_{12}\lambda_6+2\mathrm{Tr}[yy]_{21}\lambda_7-3(3g_2^2+g_1^2)\lambda_5,
\end{aligned} \tag{D.12}$$

$$
\begin{aligned}
16\pi^2\beta_{\lambda_6} = {} & 2\left\{(6\lambda_1+3\lambda_3+4\lambda_4)\lambda_6+(3\lambda_3+2\lambda_4)\lambda_7+\lambda_5(5\lambda_6^*+\lambda_7^*)\right\} \\
& -4\left\{N_C\left(\mathrm{Tr}\left[y_{u,1}y_{u,1}^\dagger y_{u,2}y_{u,1}^\dagger\right]+\mathrm{Tr}\left[y_{d,1}y_{d,1}^\dagger y_{d,2}y_{d,1}^\dagger\right]\right)+\mathrm{Tr}\left[y_{e,1}y_{e,1}^\dagger y_{e,2}y_{e,1}^\dagger\right]\right\} \\
& +(3\mathrm{Tr}[yy]_{11}+\mathrm{Tr}[yy]_{22})\lambda_6+\mathrm{Tr}[yy]_{12}\lambda_1+\mathrm{Tr}[yy]_{21}(\lambda_3+\lambda_4+\lambda_5)-3(3g_2^2+g_1^2)\lambda_6,
\end{aligned}
\tag{D.13}
$$

$$
\begin{aligned}
16\pi^2\beta_{\lambda_7} = {} & 2\left\{(6\lambda_2+3\lambda_3+4\lambda_4)\lambda_7+(3\lambda_3+2\lambda_4)\lambda_6+\lambda_5(\lambda_6^*+5\lambda_7^*)\right\} \\
& -4\left\{N_C\left(\mathrm{Tr}\left[y_{u,2}y_{u,2}^\dagger y_{u,2}y_{u,1}^\dagger\right]+\mathrm{Tr}\left[y_{d,2}y_{d,2}^\dagger y_{d,2}y_{d,1}^\dagger\right]\right)+\mathrm{Tr}\left[y_{e,2}y_{e,2}^\dagger y_{e,2}y_{e,1}^\dagger\right]\right\} \\
& +(\mathrm{Tr}[yy]_{11}+3\mathrm{Tr}[yy]_{22})\lambda_7+\mathrm{Tr}[yy]_{21}\lambda_2+\mathrm{Tr}[yy]_{12}(\lambda_3+\lambda_4+\lambda_5)-3(3g_2^2+g_1^2)\lambda_7.
\end{aligned}
\tag{D.14}
$$

We confirmed the consistency of our results with Ref. [140, 119, 113].

Appendix E

Other scenarios

In this section, we also consider other scenarios. Here, in order to concentrate on the discussion of the testability of the CP violation, the stability of the EDM cancellation at a high energy for these scenarios is not always considered. We take the following input parameters,

$$|\zeta_u| = 0.01, \quad |\zeta_d| = 0.1, \quad |\zeta_e| = 1, \quad |\lambda_7| = 0.3, \quad \lambda_2 = 0.5, \quad \theta_u = 1, \quad \theta_d = 0, \tag{E.1}$$

and, for the mass parameters, we consider three parameter sets called Benchmark 1, 2 and 3.

$$\text{Benchmark 1}: \quad m_{H_2^0} = 150, \quad m_{H_3^0} = 170, \quad m_{H^+} = 170, \quad M = 120, \tag{E.2}$$

$$\text{Benchmark 2}: \quad m_{H_2^0} = 200, \quad m_{H_3^0} = 220, \quad m_{H^+} = 220, \quad M = 180, \tag{E.3}$$

$$\text{Benchmark 3}: \quad m_{H_2^0} = 230, \quad m_{H_3^0} = 250, \quad m_{H^+} = 250, \quad M = 210 \quad \text{in GeV}, \tag{E.4}$$

The remaining parameters θ_e and θ_7 are not fixed in order to see the testability of the various scenario with difference magnitude of CP-violating phases in the following analysis. The one of the phase θ_7 is chosen to suppress the electron EDM in the scenario. The center-of-mass energy $\sqrt{s}$ of the simulation for Benchmark 1, 2 and 3 is chosen so that the cross section of $e^+e^- \to H_2H_3$ is maximized as 500, 650 and 750 GeV, respectively.

We perform the simulation with the varying $\theta_e \in [0, \pi/4]$ for Benchmark 1, 2 and 3, where θ_7 is taken as the appropriate value so that the cancelling mechanism works and the electron EDM satisfies the current constraint. In Figs. E.1, E.2 and E.3, the combined plots of $\Delta\phi$ distributions for H_2 and H_3 decays of the scenario with the finite θ_e which can be distinguished from the scenario with $\theta_e = 0$ are shown for Benchmark

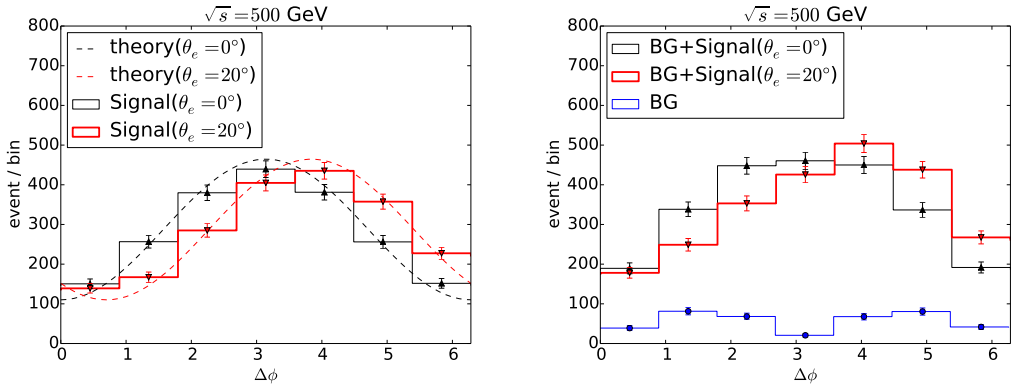


Figure E.1: $\Delta\phi$ distribution with consideration of H_2^0 and H_3^0 decay for benchmark 1 with $\sqrt{s} = 500$ GeV and $L = 3000$ /fb. The electron EDM $d_e = -0.17 \times 10^{-29}$ e cm when the phase $\theta_e = 0.35$ and $\theta_7 = -1.8$ rad. Left: the signal compared with the theoretical prediction (dashed line). Right: the signal and background.

1, 2 and 3, respectively. In the left panel, the combined plot of $\Delta\phi$ distributions of the signal events generated by the simulation and the analytical curve of Eq. (4.48) normalized by the number of the generated signal events are plotted for the consistency check. In the right panel, the combined plot of $\Delta\phi$ distributions of the signal events and the background events generated by the simulation. The red and black lines are correspond to the scenario with and without the finite θ_e in the left and right panel. From Figs. E.1, it is seen the 5σ error bar of the red histogram cannot reach the black histogram at the 3rd bin. Therefor, we consider that the scenario with finite θ_e can be distinguished from the scenario with $\theta_e = 0$ for Benchmark 1. We can consider the same discussion in Figs. E.2 and E.3.

Next, we survey the parameter region in which we can get the significance on the $\Delta\phi$ distribution for the finite θ_e by scanning the coupling strength $|\zeta_e| \in (0, 2]$ and the additional Higgs masses $m_{H_2^0} \in (100, 500]$ with the fixed mass difference $m_{H_3^0} = m_{H_2^0} + 20$. In addition, we investigate the excluded region against for the electron EDM data which are not allowed even if we take the scan for $\theta_7 \in (-\pi, \pi]$ with $|\lambda_7| = 0.01$, 0.1, 0.3, 0.5 and 0.7.

In Fig. E.4, for $\theta_e = 0.35$ (left panel) and 0.65 (right panel), the contours for the significance on the $\Delta\phi$ distribution are denoted by the solid lines, and the excluded region against for the electron EDM data denoted by the color shaded region above the dashed lines. The points marked by the star correspond to the benchmark 1 (left) and 3 (right). In the left side region of the red (cyan, black, purple and blue) solid line, we can get the 1 (2, 5, 8 and 10) σ significance on the $\Delta\phi$ distribution for $\sqrt{s} = 500$ (750) GeV

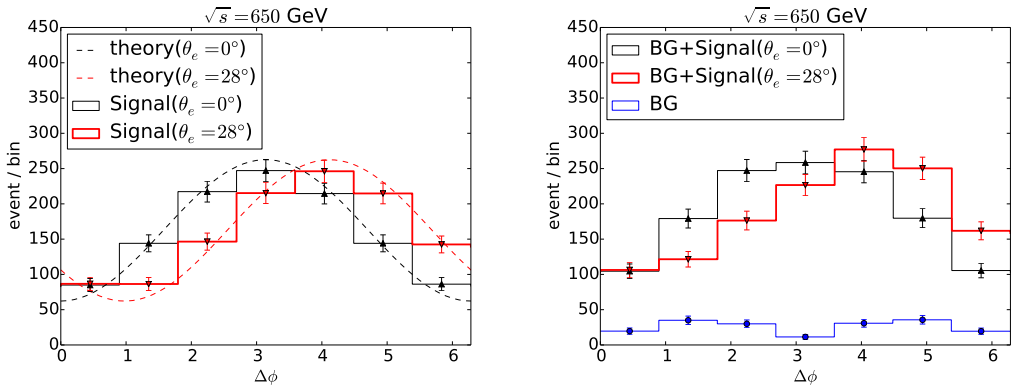


Figure E.2: $\Delta\phi$ distribution with consideration of H_2^0 and H_3^0 decay for benchmark 2 with $\sqrt{s} = 650$ GeV and $L = 3000$ /fb. The electron EDM $d_e = -0.72 \times 10^{-29}$ e cm when the phase $\theta_e = 0.49$ and $\theta_7 = -1.5$ rad. Left: the signal compared with the theoretical prediction (dashed line). Right: the signal and background.

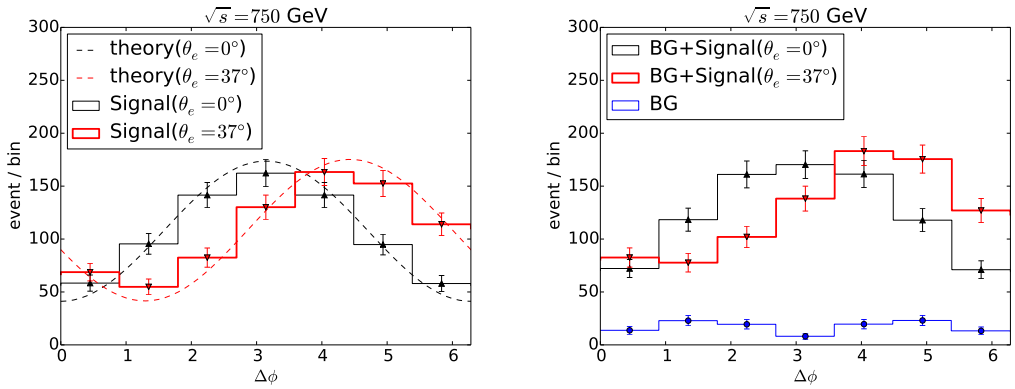


Figure E.3: $\Delta\phi$ distribution with consideration of H_2^0 and H_3^0 decay for benchmark 3 with $\sqrt{s} = 750$ GeV and $L = 3000$ /fb. The electron EDM $d_e = -0.062 \times 10^{-29}$ e cm when the phase $\theta_e = 0.65$ and $\theta_7 = -1.5$ rad. Left: the signal compared with the theoretical prediction (dashed line). Right: the signal and background.

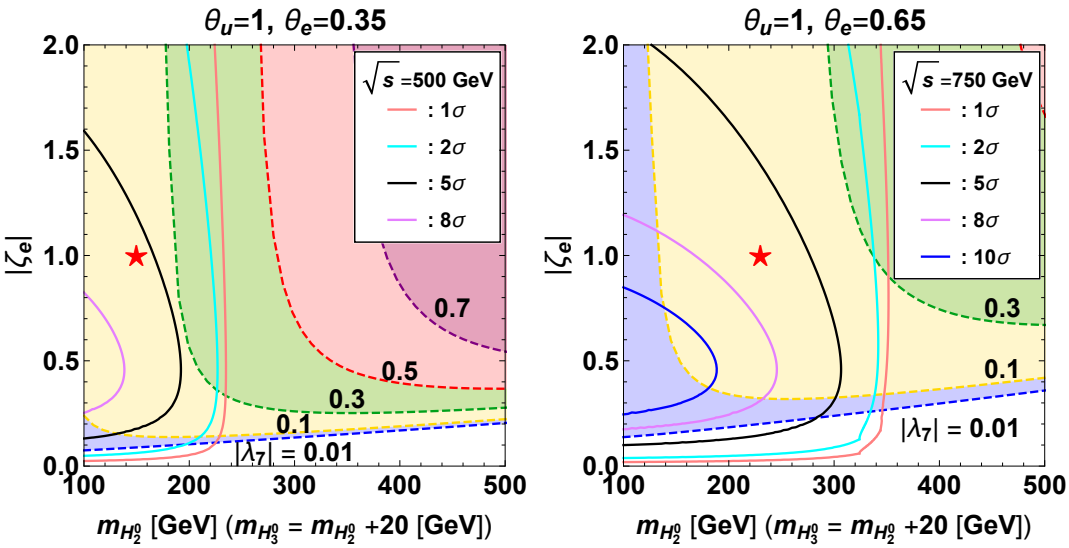


Figure E.4: Contour plot of the significance on the $\Delta\phi$ distribution and the excluded region against for the electron EDM data for $\theta_e = 0.35$ (left) and 0.65 (right). The solid lines denote the contours for the significance on the $\Delta\phi$ distribution. The points marked by the star correspond to the benchmark 1 (left) and 3 (right). The color shaded region above the dashed lines denote the excluded region against for the electron EDM data which are not allowed even if we take the scan for $\theta_7 \in (-\pi, \pi]$ when $|\lambda_7| = 0.01$, 0.1, 0.3, 0.5 and 0.7.

in the left (right) panel. It is seen that the significance is enhance in the parameter space with lighter masses and about $|\zeta_e| = 0.5$ because the number of the evens of $e^+e^- \to \tau^+\tau^- b\bar{b}$ increase. When the masses are heavier than $2m_t$, the $H_j^0 \to t\bar{t}$ mode becomes dominant and the cross section of $e^+e^- \to \tau^+\tau^- b\bar{b}$ are quickly decreased. The color shaded region above the blue (yellow, green red and purple) dashed lines denote the excluded region against for the electron EDM data which are not allowed even if we take the scan for $\theta_7 \in (-\pi, \pi]$ when $|\lambda_7| = 0.01$, 0.1 (0.3, 0.5 and 0.7). It is seen that the cancellation works well, when $|\lambda_7| = 0.5$ (0.3) and around $m_{H_2^0} = 200$ because there are he wide region for $|\zeta_e|$ in which EDM is satisfied.

In Fig. E.5, for $\theta_e = 0.35$ (left) and 0.65 (right), we can get the 5 σ significance on the $\Delta\phi$ distribution for $\sqrt{s} = 250$ (500, 750, 1000 and 1250) GeV in the left side region of the red (cyan, black, purple and bleu) solid lines, and color shaded region above the dashed lines denote the same as Fig. E.4 Since the decay cannel $H_j^0 \to t\bar{t}$ $(j = 2, 3)$ open when the additional Higgs masses have about $2m_t$, the significance are quickly decreased due to the dominance of it cannel on the decay of H_j^0.

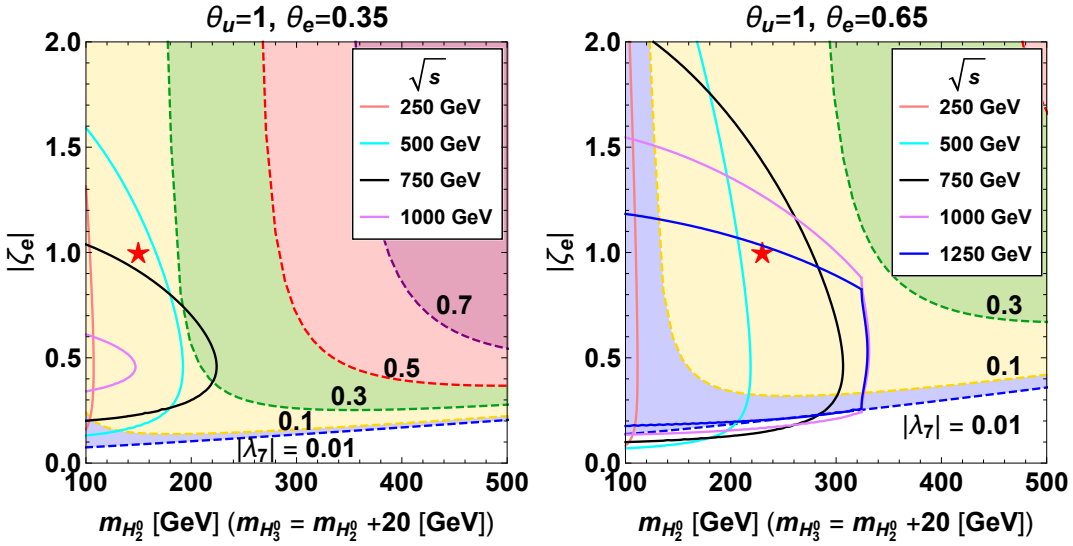


Figure E.5: Contour plot of the $\sqrt{s}$ dependence of the significance on the $\Delta\phi$ distribution and the excluded region against for the electron EDM data for $\theta_e = 0.35$ (eft) and 0.65 (right). In the left side region of the solid lines, we can get the 5 σ significance on the $\Delta\phi$ distribution for $\sqrt{s} = 250$, 500, 750, 1000 and 1250 GeV. The points marked by the star correspond to the benchmark 1 (left) and 3 (right). The color shaded region are the same as it in Figure 4.18

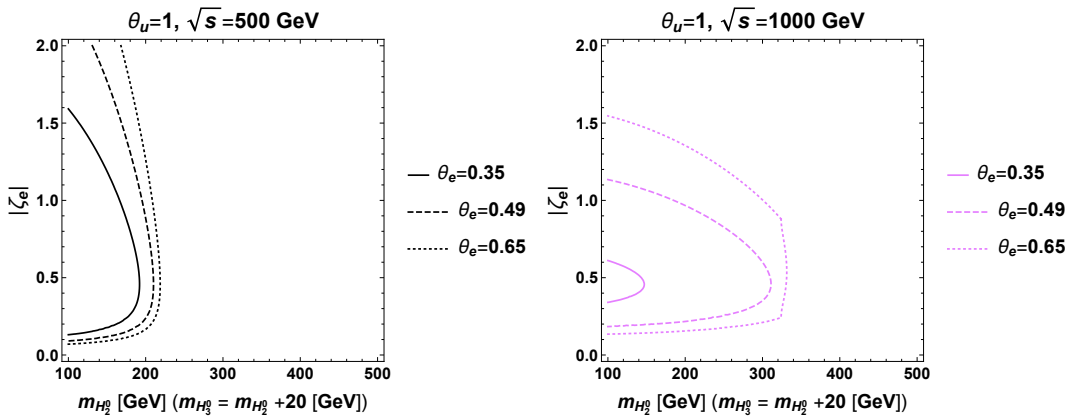


Figure E.6: In the left side region of the solid, dashed and dotted line, we can get the 5 σ significance on the $\Delta\phi$ distribution with $\sqrt{s} = 500$ (left) and 1000 (right) for $\theta_e = 0.35$, 0.49 and 0.65, respectively.

In Fig. E.6, we exhibited the region in which we can get the 5 σ significance on the $\Delta\phi$ distribution for $\theta_e = 0.35$, 0.49 and 0.65 with $\sqrt{s} = 500$ (left) and 1000 GeV (right). This figure show that when the masses and $|\zeta_e|$ are values in the left side region of the dashed lines, the discrepancy between the finite θ_e and $\theta_e = 0$ on the $\Delta\phi$ distribution might be measured $\theta_e \geq 0.49$.

In Fig. E.7, the excluded region against for the electron EDM data is shown as the color shaded region above the dashed lines by the θ_e-$m_{H_2^0}$ axes. When $|\lambda_7|$ is smaller or the masses of extra Higgs bosons are heavier, θ_e should be about θ_u to satisfy the EDM data because the cancellation cannot work for any value of θ_7. The points marked by the star correspond to the Benchmark 1 ($\theta_e = 0.35$), 2 ($\theta_e = 0.49$) and 3 ($\theta_e = 0.65$). It is not known whether the angular distribution of the decay products of H_2^0 or those of H_3^0 with shifted by $\pi/2$. By considering the information of this figure, one can be rejected.

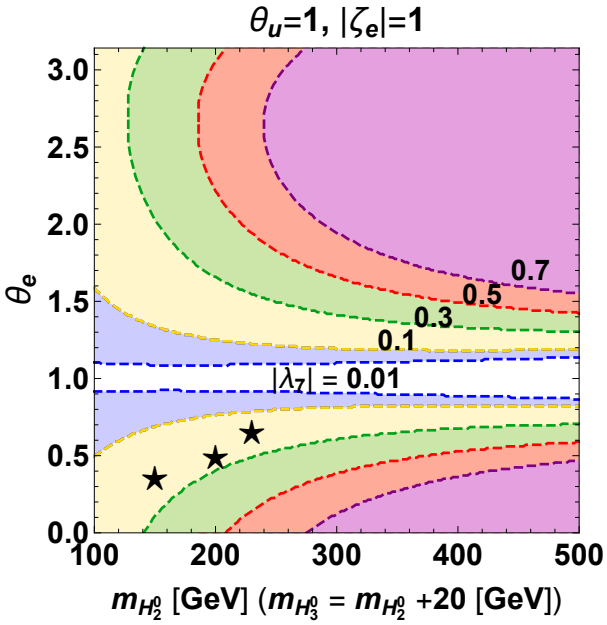


Figure E.7: The excluded region against for the electron EDM data with $|\zeta_e| = 1$. The color shaded regions denote the excluded region against for the electron EDM data which are not allowed even if we take the scan for $\theta_7 \in (-\pi, \pi]$ when $|\lambda_7| = 0.01$, 0.1, 0.3, 0.5 and 0.7. The color shaded regions are piled up as $|\lambda_7|$ grows larger. The points marked by the star correspond to the benchmark 1 ($\theta_e = 0.35$), 2 ($\theta_e = 0.49$) and 3 ($\theta_e = 0.65$).

Appendix F

Description for a spin of fermions

F.1 Notation and convention

The indices of the four-vector (Lorentz vector) are denoted by the Greek alphabet, e.g., $\mu = 0, 1, 2, 3$, while the indices of the three-vector (spatial vector) are denoted by the Roman alphabet, e.g., $i = 1, 2, 3$. The four-vector is described by $x^\mu = (x^0, \vec{x})$. The metric is $g_{\mu\nu} = g^{\mu\nu} = \mathrm{diag}(+1, -1, -1, -1)$. The dot product for the four-vectors is $p \cdot x = p_\mu x^\mu = p^0 x^0 - \vec{p} \cdot \vec{x}$, and $p^2 = p \cdot p$ The derivative operator is $\partial_\mu = (\partial/\partial t, \vec{\nabla})$. The convention for the Levi-Civita symbol $\epsilon^{\mu\nu\rho\sigma}$ is $\epsilon^{0123} = +1$. The Feynman slash is $\not{p} = \gamma_\mu p^\mu$, where the gamma matrices satisfy

$$\{\gamma^\mu, \gamma^\nu\} = 2g^{\mu\nu}. \tag{F.1}$$

The commutator of the gamma matrices is

$$\sigma^{\mu\nu} = \frac{i}{2}\left[\gamma^\mu, \gamma^\nu\right]. \tag{F.2}$$

The gamma 5 matrix is

$$\gamma^5 = i\gamma^0\gamma^1\gamma^2\gamma^3 = -\frac{i}{4!}\epsilon_{\mu\nu\rho\sigma}\gamma^\mu\gamma^\nu\gamma^\rho\gamma^\sigma = \gamma_5. \tag{F.3}$$

The projection matrices are

$$P_R = \frac{1+\gamma^5}{2}, \tag{F.4}$$

$$P_L = \frac{1-\gamma^5}{2}. \tag{F.5}$$

In the Dirac representation, the gamma matrices are given as

$$\gamma_D^0 = \begin{pmatrix} 1 & 0 \\ 0 & -1 \end{pmatrix}, \quad \gamma_D^i = \begin{pmatrix} 0 & \sigma^i \\ -\sigma^i & 0 \end{pmatrix}, \quad \gamma_D^5 = \begin{pmatrix} 0 & 1 \\ 1 & 0 \end{pmatrix}. \tag{F.6}$$

where σ^i is the Pauli matrix. In the Weyl representation, those are given as

$$\gamma_W^0 = \begin{pmatrix} 0 & 1 \\ 1 & 0 \end{pmatrix}, \quad \gamma_W^i = \begin{pmatrix} 0 & -\sigma^i \\ \sigma^i & 0 \end{pmatrix}, \quad \gamma_W^5 = \begin{pmatrix} 1 & 0 \\ 0 & -1 \end{pmatrix}. \tag{F.7}$$

F.2 Solution of the Dirac equation

A general form of a solution for the Dirac equation $(i\not{\partial} - m)\psi(x) = 0$ is given as

$$\psi(x) = \int \frac{d^3\vec{k}}{\sqrt{(2\pi)^3 2E}} \left\{ a_+(\vec{k}) e^{-ik\cdot x} + a_-^\dagger(\vec{k}) e^{+ik\cdot x} \right\}, \tag{F.8}$$

where $E = \sqrt{|\vec{k}|^2 + m}$, and $a_+(\vec{k})$ and $a_-^\dagger(\vec{k})$, which have four indices of spinor, satisfy

$$(\not{k} - m) a_+(\vec{k}) = 0, \tag{F.9}$$

$$(-\not{k} - m) a_-^\dagger(\vec{k}) = 0. \tag{F.10}$$

The ranks of $(\not{k} - m)$ and $(-\not{k} - m)$ are 2, so that there are $4 - 2 = 2$ independent solutions for $a_+(\vec{k})$ and $a_-^\dagger(\vec{k})$, respectively. Using the label $s = \pm$, $a_+(\vec{k})$ and $a_-^\dagger(\vec{k})$ can be expressed as

$$a_+(\vec{k}) = \sum_{s=\pm} b(\vec{k}, s) u(\vec{k}, s), \tag{F.11}$$

$$a_-^\dagger(\vec{k}) = \sum_{s=\pm} d^\dagger(\vec{k}, s) v(\vec{k}, s), \tag{F.12}$$

where the coefficients $b(\vec{k}, s)$ and $d^\dagger(\vec{k}, s)$ play the role as the operator. The spinors $u(\vec{k}, s)$ and $v(\vec{k}, s)$ satisfy

$$(\not{k} - m) u(\vec{k}, s) = 0, \qquad (\iff \bar{u}(\vec{k}, s)(\not{k} - m) = 0\ ), \tag{F.13}$$

$$(-\not{k} - m) v(\vec{k}, s) = 0, \qquad (\iff \bar{v}(\vec{k}, s)(-\not{k} - m) = 0\ ), \tag{F.14}$$

where the Dirac conjugate is $\bar{u}(\vec{k}, s) = u^\dagger(\vec{k}, s)\gamma^0$.

By the charge conjugation of $u(\vec{k},s)$ satisfying the Eq.(F.13), when $v(\vec{k},s)$ are given as

$$v(\vec{k},s) = C\bar{u}^T(\vec{k},s), \tag{F.15}$$

the Eq.(F.14) is automatically satisfied[1]. In addition, when $u(\vec{k},s)$ have the following orthonormality

$$\bar{u}(\vec{k},s)u(\vec{k},s') = 2m\delta_{ss'}, \tag{F.18}$$

the following relations are derived as

$$\bar{v}(\vec{k},s)v(\vec{k},s') = -2m\delta_{ss'}, \tag{F.19}$$
$$\bar{u}(\vec{k},s)v(\vec{k},s') = \bar{v}(\vec{k},s)u(\vec{k},s') = 0, \tag{F.20}$$
$$u^\dagger(\vec{k},s)u(\vec{k},s') = v^\dagger(\vec{k},s)v(\vec{k},s') = 2E\delta_{ss'}, \tag{F.21}$$
$$u^\dagger(\vec{k},s)v(-\vec{k},s') = v^\dagger(-\vec{k},s)u(\vec{k},s') = 0, \tag{F.22}$$
$$\bar{u}(\vec{k},s)\gamma^\mu u(\vec{k},s') = \bar{v}(\vec{k},s)\gamma^\mu v(\vec{k},s') = 2k^\mu\delta_{ss'}. \tag{F.23}$$

The set of $\left\{u(\vec{k},s), s=\pm\right\}$ is complete set for the eigenspace of $\not{k}u(\vec{k},s) = mu(\vec{k},s)$ and the set of $\left\{v(\vec{k},s), s=\pm\right\}$ is complete set for the eigenspace of $\not{k}v(\vec{k},s) = -mv(\vec{k},s)$. Therefore, the completeness relation for the four-spinor space is given as

$$\frac{1}{2m}\sum_{s=\pm}\left\{u(\vec{k},s)\bar{u}(\vec{k},s) - v(\vec{k},s)\bar{v}(\vec{k},s)\right\} = 1. \tag{F.24}$$

For the eigenspace of $\not{k}u(\vec{k},s) = mu(\vec{k},s)$ and $\not{k}v(\vec{k},s) = -mv(\vec{k},s)$, the completeness relations (the projection operators) are respectively given as

$$\sum_{s=\pm}u(\vec{k},s)\bar{u}(\vec{k},s) = \not{k} + m, \tag{F.25}$$

[1]The charge conjugate matrix C satisfies

$$C(\gamma^\mu)^T C^{-1} = -\gamma^\mu \tag{F.16}$$

By the Dirac or Weyl representation, C is expressed as

$$C_D = i\gamma_D^2\gamma_D^0 \quad \text{or} \quad C_W = i\gamma_W^2\gamma_W^0. \tag{F.17}$$

$$\sum_{s=\pm} v(\vec{k},s)\bar{v}(\vec{k},s) = \not{K} - m. \tag{F.26}$$

The expressions without the summation of s depend on what the eigenvalue s is.

(I) When the eigenvalue s is twice the helicity, $u(\vec{k},s)$ and $v(\vec{k},s)$ satisfy

$$2\frac{\vec{S}\cdot\vec{k}}{|\vec{k}|}\ u(\vec{k},s) = s\ u(\vec{k},s), \quad (s=\pm 1), \tag{F.27}$$

$$2\frac{\vec{S}\cdot\vec{k}}{|\vec{k}|}\ v(\vec{k},s) = -s\ v(\vec{k},s), \quad (s=\pm 1), \tag{F.28}$$

where $[\vec{S}\cdot\vec{k}, \not{K}] = 0$ and

$$\vec{S} = \frac{i}{2}(\gamma^2\gamma^3, \gamma^3\gamma^1, \gamma^1\gamma^2). \tag{F.29}$$

The projection operators for the helicity eigenstates are given as

$$u(\vec{k},s)\bar{u}(\vec{k},s) = (\not{K}+m)\left(1 + s\ \frac{2\vec{S}\cdot\vec{k}}{|\vec{k}|}\right)\frac{1}{2}, \tag{F.30}$$

$$v(\vec{k},s)\bar{v}(\vec{k},s) = (\not{K}-m)\left(1 - s\ \frac{2\vec{S}\cdot\vec{k}}{|\vec{k}|}\right)\frac{1}{2}. \tag{F.31}$$

(II) We introduce the Pauli-Lubanski vector which defined as

$$W^\mu = -\frac{1}{4m}\epsilon^{\mu\nu\rho\sigma}\sigma_{\nu\rho}k_\sigma \tag{F.32}$$

and we consider the product as

$$e\cdot W = -\frac{1}{2m}\gamma^5 \not{e}\not{K}, \tag{F.33}$$

where the four vector e is characterized as

$$e^2 = -1, \tag{F.34}$$

$$e\cdot k = 0. \tag{F.35}$$

Since $[\gamma^5\not{e}, \not{K}] = 0$, we consider that s is the eigenvalue of $-2e\cdot W$. The spinors $u(\vec{k},s)$ and $v(\vec{k},s)$ then satisfy

$$-2e\cdot W\ u(\vec{k},s) = s\ u(\vec{k},s), \quad (s=\pm 1), \tag{F.36}$$

$$-2e\cdot W\ v(\vec{k},s) = -s\ v(\vec{k},s), \quad (s=\pm 1). \tag{F.37}$$

The projection operators for the eigenstates are given as

$$u(\vec{k},s)\bar{u}(\vec{k},s) = (\not{k}+m)\left(1+s\ \gamma^5\not{e}\right)\frac{1}{2}, \tag{F.38}$$

$$v(\vec{k},s)\bar{v}(\vec{k},s) = (\not{k}-m)\left(1+s\ \gamma^5\not{e}\right)\frac{1}{2}. \tag{F.39}$$

If $e=\vec{k}/|\vec{k}|$ the eigenvalue s corresponds to twice the helicity.

Bibliography

[1] Georges Aad et al. Observation of a new particle in the search for the Standard Model Higgs boson with the ATLAS detector at the LHC. *Phys. Lett. B*, 716:1–29, 2012.

[2] Serguei Chatrchyan et al. Observation of a New Boson at a Mass of 125 GeV with the CMS Experiment at the LHC. *Phys. Lett. B*, 716:30–61, 2012.

[3] P.A. Zyla et al. Review of Particle Physics. *PTEP*, 2020(8):083C01, 2020.

[4] A.D. Sakharov. Violation of CP Invariance, C asymmetry, and baryon asymmetry of the universe. *Sov. Phys. Usp.*, 34(5):392–393, 1991.

[5] Motohiko Yoshimura. Unified Gauge Theories and the Baryon Number of the Universe. *Phys. Rev. Lett.*, 41:281–284, 1978. [Erratum: Phys.Rev.Lett. 42, 746 (1979)].

[6] Steven Weinberg. Cosmological Production of Baryons. *Phys. Rev. Lett.*, 42:850–853, 1979.

[7] M. Fukugita and T. Yanagida. Baryogenesis Without Grand Unification. *Phys. Lett. B*, 174:45–47, 1986.

[8] V.A. Kuzmin, V.A. Rubakov, and M.E. Shaposhnikov. On the Anomalous Electroweak Baryon Number Nonconservation in the Early Universe. *Phys. Lett. B*, 155:36, 1985.

[9] Makoto Kobayashi and Toshihide Maskawa. CP Violation in the Renormalizable Theory of Weak Interaction. *Prog. Theor. Phys.*, 49:652–657, 1973.

[10] Patrick Huet and Eric Sather. Electroweak baryogenesis and standard model CP violation. *Phys. Rev. D*, 51:379–394, 1995.

[11] K. Kajantie, M. Laine, K. Rummukainen, and Mikhail E. Shaposhnikov. Is there a hot electroweak phase transition at m(H) larger or equal to m(W)? *Phys. Rev. Lett.*, 77:2887–2890, 1996.

[12] Jose R. Espinosa, Ben Gripaios, Thomas Konstandin, and Francesco Riva. Electroweak Baryogenesis in Non-minimal Composite Higgs Models. *JCAP*, 01:012, 2012.

[13] James M. Cline and Kimmo Kainulainen. Electroweak baryogenesis and dark matter from a singlet Higgs. *JCAP*, 01:012, 2013.

[14] Bohdan Grzadkowski and Da Huang. Spontaneous CP-Violating Electroweak Baryogenesis and Dark Matter from a Complex Singlet Scalar. *JHEP*, 08:135, 2018.

[15] Neil Turok and John Zadrozny. Electroweak baryogenesis in the two doublet model. *Nucl. Phys. B*, 358:471–493, 1991.

[16] James M. Cline, Kimmo Kainulainen, and Axel P. Vischer. Dynamics of two Higgs doublet CP violation and baryogenesis at the electroweak phase transition. *Phys. Rev. D*, 54:2451–2472, 1996.

[17] Lars Fromme, Stephan J. Huber, and Michael Seniuch. Baryogenesis in the two-Higgs doublet model. *JHEP*, 11:038, 2006.

[18] James M. Cline, Kimmo Kainulainen, and Michael Trott. Electroweak Baryogenesis in Two Higgs Doublet Models and B meson anomalies. *JHEP*, 11:089, 2011.

[19] Jing Shu and Yue Zhang. Impact of a CP Violating Higgs Sector: From LHC to Baryogenesis. *Phys. Rev. Lett.*, 111(9):091801, 2013.

[20] Kaori Fuyuto, Wei-Shu Hou, and Eibun Senaha. Electroweak baryogenesis driven by extra top Yukawa couplings. *Phys. Lett. B*, 776:402–406, 2018.

[21] Tanmoy Modak and Eibun Senaha. Electroweak baryogenesis via bottom transport. *Phys. Rev. D*, 99(11):115022, 2019.

[22] Hiren H. Patel and Michael J. Ramsey-Musolf. Stepping Into Electroweak Symmetry Breaking: Phase Transitions and Higgs Phenomenology. *Phys. Rev. D*, 88:035013, 2013.

[23] Cheng-Wei Chiang and Toshifumi Yamada. Electroweak phase transition in Georgi–Machacek model. *Phys. Lett. B*, 735:295–300, 2014.

[24] Christophe Grojean, Geraldine Servant, and James D. Wells. First-order electroweak phase transition in the standard model with a low cutoff. *Phys. Rev. D*, 71:036001, 2005.

[25] Shinya Kanemura, Yasuhiro Okada, and Eibun Senaha. Electroweak baryogenesis and quantum corrections to the triple Higgs boson coupling. *Phys. Lett. B*, 606:361–366, 2005.

[26] M. Cepeda et al. Report from Working Group 2: Higgs Physics at the HL-LHC and HE-LHC. *CERN Yellow Rep. Monogr.*, 7:221–584, 2019.

[27] Keisuke Fujii et al. Physics Case for the International Linear Collider. 6 2015.

[28] Keisuke Fujii et al. Physics Case for the 250 GeV Stage of the International Linear Collider. 10 2017.

[29] Pau Amaro-Seoane et al. Laser Interferometer Space Antenna. 2 2017.

[30] Naoki Seto, Seiji Kawamura, and Takashi Nakamura. Possibility of direct measurement of the acceleration of the universe using 0.1-Hz band laser interferometer gravitational wave antenna in space. *Phys. Rev. Lett.*, 87:221103, 2001.

[31] Vincent Corbin and Neil J. Cornish. Detecting the cosmic gravitational wave background with the big bang observer. *Class. Quant. Grav.*, 23:2435–2446, 2006.

[32] Christophe Grojean and Geraldine Servant. Gravitational Waves from Phase Transitions at the Electroweak Scale and Beyond. *Phys. Rev. D*, 75:043507, 2007.

[33] Jose Ramon Espinosa and Mariano Quiros. Novel Effects in Electroweak Breaking from a Hidden Sector. *Phys. Rev. D*, 76:076004, 2007.

[34] J.R. Espinosa, T. Konstandin, J.M. No, and M. Quiros. Some Cosmological Implications of Hidden Sectors. *Phys. Rev. D*, 78:123528, 2008.

[35] Jose R. Espinosa, Thomas Konstandin, Jose M. No, and Geraldine Servant. Energy Budget of Cosmological First-order Phase Transitions. *JCAP*, 06:028, 2010.

[36] Mark Hindmarsh, Stephan J. Huber, Kari Rummukainen, and David J. Weir. Numerical simulations of acoustically generated gravitational waves at a first order phase transition. *Phys. Rev. D*, 92(12):123009, 2015.

[37] Mitsuru Kakizaki, Shinya Kanemura, and Toshinori Matsui. Gravitational waves as a probe of extended scalar sectors with the first order electroweak phase transition. *Phys. Rev. D*, 92(11):115007, 2015.

[38] Katsuya Hashino, Mitsuru Kakizaki, Shinya Kanemura, and Toshinori Matsui. Synergy between measurements of gravitational waves and the triple-Higgs coupling in probing the first-order electroweak phase transition. *Phys. Rev. D*, 94(1):015005, 2016.

[39] Katsuya Hashino, Ryusuke Jinno, Mitsuru Kakizaki, Shinya Kanemura, Tomo Takahashi, and Masahiro Takimoto. Selecting models of first-order phase transitions using the synergy between collider and gravitational-wave experiments. *Phys. Rev. D*, 99(7):075011, 2019.

[40] Ruiyu Zhou and Ligong Bian. Baryon asymmetry and detectable Gravitational Waves from Electroweak phase transition. 1 2020.

[41] Werner Bernreuther and Mahiko Suzuki. The electric dipole moment of the electron. *Rev. Mod. Phys.*, 63:313–340, 1991. [Erratum: Rev.Mod.Phys. 64, 633 (1992)].

[42] Takeshi Fukuyama. Searching for New Physics beyond the Standard Model in Electric Dipole Moment. *Int. J. Mod. Phys. A*, 27:1230015, 2012.

[43] R.G. Leigh, S. Paban, and R.M. Xu. Electric dipole moment of electron. *Nucl. Phys. B*, 352:45–58, 1991.

[44] David Bowser-Chao, Darwin Chang, and Wai-Yee Keung. Electron electric dipole moment from CP violation in the charged Higgs sector. *Phys. Rev. Lett.*, 79:1988–1991, 1997.

[45] Martin Jung and Antonio Pich. Electric Dipole Moments in Two-Higgs-Doublet Models. *JHEP*, 04:076, 2014.

[46] Tomohiro Abe, Junji Hisano, Teppei Kitahara, and Kohsaku Tobioka. Gauge invariant Barr-Zee type contributions to fermionic EDMs in the two-Higgs doublet models. *JHEP*, 01:106, 2014. [Erratum: JHEP 04, 161 (2016)].

[47] Kingman Cheung, Jae Sik Lee, Eibun Senaha, and Po-Yan Tseng. Confronting Higgcision with Electric Dipole Moments. *JHEP*, 06:149, 2014.

[48] Kingman Cheung, Adil Jueid, Ying-Nan Mao, and Stefano Moretti. Two-Higgs-doublet model with soft CP violation confronting electric dipole moments and colliders. *Phys. Rev. D*, 102(7):075029, 2020.

[49] Daniel Egana-Ugrinovic and Scott Thomas. Higgs Boson Contributions to the Electron Electric Dipole Moment. 10 2018.

[50] Celine Degrande. A basis of dimension-eight operators for anomalous neutral triple gauge boson interactions. *JHEP*, 02:101, 2014.

[51] B. Grzadkowski, O.M. Ogreid, and P. Osland. CP-Violation in the ZZZ and ZWW vertices at e^+e^- colliders in Two-Higgs-Doublet Models. *JHEP*, 05:025, 2016. [Erratum: JHEP 11, 002 (2017)].

[52] A. Barroso, P.M. Ferreira, Rui Santos, and Joao P. Silva. Probing the scalar-pseudoscalar mixing in the 125 GeV Higgs particle with current data. *Phys. Rev. D*, 86:015022, 2012.

[53] Joachim Brod, Ulrich Haisch, and Jure Zupan. Constraints on CP-violating Higgs couplings to the third generation. *JHEP*, 11:180, 2013.

[54] Mayumi Aoki, Katsuya Hashino, Daiki Kaneko, Shinya Kanemura, and Mitsunori Kubota. Probing CP violating Higgs sectors via the precision measurement of coupling constants. *PTEP*, 2019(5):053B02, 2019.

[55] Eri Asakawa, S.Y. Choi, Kaoru Hagiwara, and Jae Sik Lee. Measuring the Higgs CP property through top quark pair production at photon linear colliders. *Phys. Rev. D*, 62:115005, 2000.

[56] Ekaterina Christova, Helmut Eberl, Walter Majerotto, and Sabine Kraml. CP violation in charged Higgs decays in the MSSM with complex parameters. *Nucl. Phys. B*, 647(1-2):359–360, 2002.

[57] Yi Chen, Adam Falkowski, Ian Low, and Roberto Vega-Morales. New Observables for CP Violation in Higgs Decays. *Phys. Rev. D*, 90(11):113006, 2014.

[58] Xuan Chen, Gang Li, and Xia Wan. Probe CP violation in $H \to \gamma Z$ through forward-backward asymmetry. *Phys. Rev. D*, 96(5):055023, 2017.

[59] Ligong Bian, Ning Chen, and Yongchao Zhang. CP violation effects in the diphoton spectrum of heavy scalars. *Phys. Rev. D*, 96(9):095008, 2017.

[60] Johann Heinrich Kuhn and F. Wagner. Semileptonic Decays of the tau Lepton. *Nucl. Phys. B*, 236:16–34, 1984.

[61] Kaoru Hagiwara, Tong Li, Kentarou Mawatari, and Junya Nakamura. TauDecay: a library to simulate polarized tau decays via FeynRules and MadGraph5. *Eur. Phys. J. C*, 73:2489, 2013.

[62] Roni Harnik, Adam Martin, Takemichi Okui, Reinard Primulando, and Felix Yu. Measuring CP Violation in $h \to \tau^+\tau^-$ at Colliders. *Phys. Rev. D*, 88(7):076009, 2013.

[63] D. Jeans and G.W. Wilson. Measuring the CP state of tau lepton pairs from Higgs decay at the ILC. *Phys. Rev. D*, 98(1):013007, 2018.

[64] S. Bar-Shalom, D. Atwood, G. Eilam, R.R. Mendel, and A. Soni. Large tree level CP violation in $e^+e^- \to t\bar{t}H^0$ in the two Higgs doublet model. *Phys. Rev. D*, 53:1162–1167, 1996.

[65] Kaoru Hagiwara, Hiroshi Yokoya, and Ya-Juan Zheng. Probing the CP properties of top Yukawa coupling at an e^+e^- collider. *JHEP*, 02:180, 2018.

[66] P. Niezurawski, A.F. Zarnecki, and M. Krawczyk. Model-independent determination of CP violation from angular distributions in Higgs boson decays to WW and ZZ at the photon collider. *Acta Phys. Polon. B*, 36:833–844, 2005.

[67] Fady Bishara, Yuval Grossman, Roni Harnik, Dean J. Robinson, Jing Shu, and Jure Zupan. Probing CP Violation in $h \to \gamma\gamma$ with Converted Photons. *JHEP*, 04:084, 2014.

[68] Masashi Aiko and Shinya Kanemura. New scenario for aligned Higgs couplings originated from the twisted custodial symmetry at high energies. 9 2020.

[69] Shinya Kanemura, Mitsunori Kubota, and Kei Yagyu. Aligned CP-violating Higgs sector canceling the electric dipole moment. *JHEP*, 08:026, 2020.

[70] Shinya Kanemura, Mitsunori Kubota, and Kei Yagyu. Testing aligned CP-violating Higgs sector at future lepton colliders. 1 2021.

[71] Antonio Pich and Paula Tuzon. Yukawa Alignment in the Two-Higgs-Doublet Model. *Phys. Rev. D*, 80:091702, 2009.

[72] Albert M Sirunyan et al. Combined measurements of Higgs boson couplings in proton–proton collisions at $\sqrt{s} = 13\,\text{TeV}$. *Eur. Phys. J. C*, 79(5):421, 2019.

[73] Georges Aad et al. Combined measurements of Higgs boson production and decay using up to 80 fb^{-1} of proton-proton collision data at $\sqrt{s} = 13$ TeV collected with the ATLAS experiment. *Phys. Rev. D*, 101(1):012002, 2020.

[74] Kaori Fuyuto, Wei-Shu Hou, and Eibun Senaha. Cancellation mechanism for the electron electric dipole moment connected with the baryon asymmetry of the Universe. *Phys. Rev. D*, 101(1):011901, 2020.

[75] Johan Alwall, Michel Herquet, Fabio Maltoni, Olivier Mattelaer, and Tim Stelzer. MadGraph 5 : Going Beyond. *JHEP*, 06:128, 2011.

[76] Andrew G. Cohen, D.B. Kaplan, and A.E. Nelson. Progress in electroweak baryogenesis. *Ann. Rev. Nucl. Part. Sci.*, 43:27–70, 1993.

[77] David E. Morrissey and Michael J. Ramsey-Musolf. Electroweak baryogenesis. *New J. Phys.*, 14:125003, 2012.

[78] N.S. Manton. Topology in the Weinberg-Salam Theory. *Phys. Rev. D*, 28:2019, 1983.

[79] Frans R. Klinkhamer and N.S. Manton. A Saddle Point Solution in the Weinberg-Salam Theory. *Phys. Rev. D*, 30:2212, 1984.

[80] C. Jarlskog. Commutator of the Quark Mass Matrices in the Standard Electroweak Model and a Measure of Maximal CP Violation. *Phys. Rev. Lett.*, 55:1039, 1985.

[81] V. Andreev et al. Improved limit on the electric dipole moment of the electron. *Nature*, 562(7727):355–360, 2018.

[82] C. Abel et al. Measurement of the permanent electric dipole moment of the neutron. *Phys. Rev. Lett.*, 124(8):081803, 2020.

[83] Maxim Pospelov and Adam Ritz. Electric dipole moments as probes of new physics. *Annals Phys.*, 318:119–169, 2005.

[84] Stephen M. Barr and A. Zee. Electric Dipole Moment of the Electron and of the Neutron. *Phys. Rev. Lett.*, 65:21–24, 1990. [Erratum: Phys.Rev.Lett. 65, 2920 (1990)].

[85] B. Grzadkowski and J.F. Gunion. Using decay angle correlations to detect CP violation in the neutral Higgs sector. *Phys. Lett. B*, 350:218–224, 1995.

[86] Stanislaw Jadach, Johann H. Kuhn, and Zbigniew Was. TAUOLA: A Library of Monte Carlo programs to simulate decays of polarized tau leptons. *Comput. Phys. Commun.*, 64:275–299, 1990.

[87] T.D. Lee. A Theory of Spontaneous T Violation. *Phys. Rev. D*, 8:1226–1239, 1973.

[88] F.J. Botella and Joao P. Silva. Jarlskog - like invariants for theories with scalars and fermions. *Phys. Rev. D*, 51:3870–3875, 1995.

[89] Sacha Davidson and Howard E. Haber. Basis-independent methods for the two-Higgs-doublet model. *Phys. Rev. D*, 72:035004, 2005. [Erratum: Phys.Rev.D 72, 099902 (2005)].

[90] J. M. Gerard and M. Herquet. A Twisted custodial symmetry in the two-Higgs-doublet model. *Phys. Rev. Lett.*, 98:251802, 2007.

[91] Sheldon L. Glashow and Steven Weinberg. Natural Conservation Laws for Neutral Currents. *Phys. Rev. D*, 15:1958, 1977.

[92] Vernon D. Barger, J.L. Hewett, and R.J.N. Phillips. New Constraints on the Charged Higgs Sector in Two Higgs Doublet Models. *Phys. Rev. D*, 41:3421–3441, 1990.

[93] Mayumi Aoki, Shinya Kanemura, Koji Tsumura, and Kei Yagyu. Models of Yukawa interaction in the two Higgs doublet model, and their collider phenomenology. *Phys. Rev. D*, 80:015017, 2009.

[94] I.F. Ginzburg and I.P. Ivanov. Tree-level unitarity constraints in the most general 2HDM. *Phys. Rev. D*, 72:115010, 2005.

[95] Shinya Kanemura, Takahiro Kubota, and Eiichi Takasugi. Lee-Quigg-Thacker bounds for Higgs boson masses in a two doublet model. *Phys. Lett. B*, 313:155–160, 1993.

[96] Andrew G. Akeroyd, Abdesslam Arhrib, and El-Mokhtar Naimi. Note on tree level unitarity in the general two Higgs doublet model. *Phys. Lett. B*, 490:119–124, 2000.

[97] Shinya Kanemura and Kei Yagyu. Unitarity bound in the most general two Higgs doublet model. *Phys. Lett. B*, 751:289–296, 2015.

[98] Shuquan Nie and Marc Sher. Vacuum stability bounds in the two Higgs doublet model. *Phys. Lett. B*, 449:89–92, 1999.

[99] Shinya Kanemura, Takashi Kasai, and Yasuhiro Okada. Mass bounds of the lightest CP even Higgs boson in the two Higgs doublet model. *Phys. Lett. B*, 471:182–190, 1999.

[100] Michael E. Peskin and Tatsu Takeuchi. A New constraint on a strongly interacting Higgs sector. *Phys. Rev. Lett.*, 65:964–967, 1990.

[101] Michael E. Peskin and Tatsu Takeuchi. Estimation of oblique electroweak corrections. *Phys. Rev. D*, 46:381–409, 1992.

[102] Alex Pomarol and Roberto Vega. Constraints on CP violation in the Higgs sector from the rho parameter. *Nucl. Phys. B*, 413:3–15, 1994.

[103] Howard E. Haber and Alex Pomarol. Constraints from global symmetries on radiative corrections to the Higgs sector. *Phys. Lett. B*, 302:435–441, 1993.

[104] B. Grzadkowski, M. Maniatis, and Jose Wudka. The bilinear formalism and the custodial symmetry in the two-Higgs-doublet model. *JHEP*, 11:030, 2011.

[105] Howard E. Haber and Deva O'Neil. Basis-independent methods for the two-Higgs-doublet model III: The CP-conserving limit, custodial symmetry, and the oblique parameters S, T, U. *Phys. Rev. D*, 83:055017, 2011.

[106] Shinya Kanemura, Yasuhiro Okada, Hiroyuki Taniguchi, and Koji Tsumura. Indirect bounds on heavy scalar masses of the two-Higgs-doublet model in light of recent Higgs boson searches. *Phys. Lett. B*, 704:303–307, 2011.

[107] Farvah Mahmoudi and Oscar Stal. Flavor constraints on the two-Higgs-doublet model with general Yukawa couplings. *Phys. Rev. D*, 81:035016, 2010.

[108] Martin Jung, Antonio Pich, and Paula Tuzon. The B -> Xs gamma Rate and CP Asymmetry within the Aligned Two-Higgs-Doublet Model. *Phys. Rev. D*, 83:074011, 2011.

[109] Maxim Pospelov and Adam Ritz. Neutron EDM from electric and chromoelectric dipole moments of quarks. *Phys. Rev. D*, 63:073015, 2001.

[110] Junji Hisano, Jeong Yong Lee, Natsumi Nagata, and Yasuhiro Shimizu. Reevaluation of Neutron Electric Dipole Moment with QCD Sum Rules. *Phys. Rev. D*, 85:114044, 2012.

[111] Kaori Fuyuto, Junji Hisano, Natsumi Nagata, and Koji Tsumura. QCD Corrections to Quark (Chromo)Electric Dipole Moments in High-scale Supersymmetry. *JHEP*, 12:010, 2013.

[112] Zhi-zhong Xing, He Zhang, and Shun Zhou. Updated Values of Running Quark and Lepton Masses. *Phys. Rev. D*, 77:113016, 2008.

[113] Johan Bijnens, Jie Lu, and Johan Rathsman. Constraining General Two Higgs Doublet Models by the Evolution of Yukawa Couplings. *JHEP*, 05:118, 2012.

[114] M. Tanabashi et al. Review of Particle Physics. *Phys. Rev. D*, 98(3):030001, 2018.

[115] D. Kawall. Searching for the electron EDM in a storage ring. *J. Phys. Conf. Ser.*, 295:012031, 2011.

[116] Ruediger Picker. How the minuscule can contribute to the big picture: the neutron electric dipole moment project at TRIUMF. *JPS Conf. Proc.*, 13:010005, 2017.

[117] K.K.H. Leung et al. The neutron electric dipole moment experiment at the Spallation Neutron Source. *EPJ Web Conf.*, 219:02005, 2019.

[118] V. Anastassopoulos et al. A Storage Ring Experiment to Detect a Proton Electric Dipole Moment. *Rev. Sci. Instrum.*, 87(11):115116, 2016.

[119] Stefania Gori, Howard E. Haber, and Edward Santos. High scale flavor alignment in two-Higgs doublet models and its phenomenology. *JHEP*, 06:110, 2017.

[120] J.A. Grifols and A. Mendez. The $WZH^{\pm}$ Coupling in $SU(2) \times U(1)$ Gauge Models. *Phys. Rev. D*, 22:1725, 1980.

[121] Michel Capdequi Peyranere, Howard E. Haber, and Paulo Irulegui. $H^{\pm} \to W^{\pm}\gamma$ and $H^{\pm} \to W^{\pm}Z$ in two Higgs doublet models. 1. The Large fermion mass limit. *Phys. Rev. D*, 44:191–201, 1991.

[122] Shinya Kanemura. Enhancement of loop induced $H^{\pm}W^{\mp}Z^0$ vertex in two Higgs doublet model. *Phys. Rev. D*, 61:095001, 2000.

[123] *LHC Higgs Cross Section Working Group.*

[124] *Search for charged Higgs bosons with the* $\mathrm{H}^{\pm} \to \tau^{\pm}\nu_{\tau}$ *decay channel in the fully hadronic final state at* $\sqrt{s} = 13$ TeV, 10 2016.

[125] Morad Aaboud et al. Search for charged Higgs bosons decaying via $H^{\pm} \to \tau^{\pm}\nu_{\tau}$ in the τ+jets and τ+lepton final states with 36 fb^{-1} of pp collision data recorded at $\sqrt{s} = 13$ TeV with the ATLAS experiment. *JHEP*, 09:139, 2018.

[126] Tilman Plehn. Charged Higgs boson production in bottom gluon fusion. *Phys. Rev. D*, 67:014018, 2003.

[127] Edmond L. Berger, Tao Han, Jing Jiang, and Tilman Plehn. Associated production of a top quark and a charged Higgs boson. *Phys. Rev. D*, 71:115012, 2005.

[128] Georges Aad et al. Search for heavy Higgs bosons decaying into two tau leptons with the ATLAS detector using pp collisions at $\sqrt{s} = 13$ TeV. *Phys. Rev. Lett.*, 125(5):051801, 2020.

[129] Daniel Jeans. Tau lepton reconstruction at collider experiments using impact parameters. *Nucl. Instrum. Meth. A*, 810:51–58, 2016.

[130] Keisuke Fujii et al. The role of positron polarization for the inital 250 GeV stage of the International Linear Collider. 1 2018.

[131] Xin Chen and Yongcheng Wu. Search for CP violation effects in the $h \to \tau\tau$ decay with e^+e^- colliders. *Eur. Phys. J. C*, 77(10):697, 2017.

[132] Taikan Suehara and Tomohiko Tanabe. LCFIPlus: A Framework for Jet Analysis in Linear Collider Studies. *Nucl. Instrum. Meth. A*, 808:109–116, 2016.

[133] Daniel Jeans and Keita Yumino. ILD benchmark: a study of $e^-e^+ \to \tau^-\tau^+$ at 500 GeV. 12 2019.

[134] Halina Abramowicz et al. The International Linear Collider Technical Design Report - Volume 4: Detectors. 6 2013.

[135] Georges Aad et al. Measurement of the $t\bar{t}$ production cross-section in the lepton+jets channel at $\sqrt{s} = 13$ TeV with the ATLAS experiment. *Phys. Lett. B*, 810:135797, 2020.

[136] Ian Low, Nausheen R. Shah, and Xiao-Ping Wang. Higgs Alignment and Novel CP-Violating Observables in 2HDM. 12 2020.

[137] G. Passarino and M.J.G. Veltman. One Loop Corrections for e+ e- Annihilation Into mu+ mu- in the Weinberg Model. *Nucl. Phys. B*, 160:151–207, 1979.

[138] Abdelhak Djouadi. The Anatomy of electro-weak symmetry breaking. I: The Higgs boson in the standard model. *Phys. Rept.*, 457:1–216, 2008.

[139] Abdelhak Djouadi. The Anatomy of electro-weak symmetry breaking. II. The Higgs bosons in the minimal supersymmetric model. *Phys. Rept.*, 459:1–241, 2008.

[140] G.C. Branco, P.M. Ferreira, L. Lavoura, M.N. Rebelo, Marc Sher, and Joao P. Silva. Theory and phenomenology of two-Higgs-doublet models. *Phys. Rept.*, 516:1–102, 2012.